Dytran 2022.2

Theory Guide

HEXAGON

Americas
5161 California Ave. Suite 200
University Research Park, Irvine, CA 92617
Telephone:(714) 540-8900
Toll Free Number: 1 855 672 7638
Email: americas.contact@mscsoftware.com

Europe, Middle East, Africa
Am Moosfeld 13
81829 Munich, Germany
Telephone: (49) 89 431 98 70
Email: europe@mscsoftware.com

Japan
Shinjuku First West 8F
23-7 Nishi Shinjuku
1-Chome, Shinjuku-Ku
Tokyo 160-0023, JAPAN
Telephone: (81) (3)-6911-1200
Email: MSCJ.Market@mscsoftware.com

Asia-Pacific
100 Beach Road
#16-05 Shaw Tower
Singapore 189702
Telephone: 65-6272-0082
Email: APAC.Contact@mscsoftware.com

Worldwide Web
www.hexagon.com

Support
https://simcompanion.hexagon.com/

Disclaimer

DT:V2022.2:Z:Z:Z:DC-TEO-PDF

Documentation Feedback

At Hexagon, we strive to produce the highest quality documentation and welcome your feedback. If you have comments or suggestions about our documentation, please write to us.

Please include the following information with your feedback:

- Document name
- Release/Version number
- Chapter/Section name
- Topic title (for Online Help)
- Brief description of the content (for example, incomplete/incorrect information, grammatical errors, information that requires clarification or more details and so on.)
- Your suggestions for correcting/improving documentation

You may also provide your feedback about Hexagon documentation by taking a short 5-minute survey.

Note:	The above mentioned e-mail address is only for providing documentation specific feedback. If you have any technical problems, issues, or queries, please contact Technical Support.

Contents

Dytran Theory Manual

4 Models

1 Implicit and Explicit Methods

Overview

A detailed theory of Dytran® is outside the scope of this section. However, it is important to understand the basics of the solution technique, since it is critical to many aspects of the code and is completely different from the usual finite element programs with which you may be familiar. If you are already familiar with explicit methods and how they differ from the implicit methods, then you may disregard this section.

Implicit Methods

The majority of finite element programs use implicit methods to carry out a transient solution. Normally, they use Newmark schemes to integrate in time. If the current time step is step n, a good estimate of the acceleration at the end of step n + 1 will satisfy the following equation of motion:

$$Ma'_{n+1} + Cv'_{n+1} + Kd'_{n+1} = F^{ext}_{n+1}$$

where

M	=	mass matrix of the structure
C	=	damping matrix of the structure
K	=	stiffness matrix of the structure
F^{ext}_{n+1}	=	vector of externally applied loads at step n + 1
a'_{n+1}	=	estimate of acceleration at step n + 1
v'_{n+1}	=	estimate of velocity at step n + 1
d'_{n+1}	=	estimate of displacement at step n + 1

and the prime denotes an estimated value.

The estimates of displacement and velocity are given by:

$$d'_{n+1} = d_n + v_n \Delta t + ((1 - 2\beta) a_n \Delta t^2)/2 + \beta a'_{n+1} \Delta t^2$$

or

$$d'_{n+1} = d^*_n + \beta a'_{n+1}\Delta t^2$$

$$v'_{n+1} = v^*_n + \gamma a'_{n+1}\Delta t$$

or

$$v'_{n+1} = v_n + (1-\gamma)a_n\Delta t + \gamma a'_{n+1}\Delta t$$

where Δt is the time step and β and γ are constants.

The terms d^*_n and v^*_n are predictive and are based on values already calculated.

Substituting these values in the equation of motion results in

$$Ma'_{n+1} + C(v^*_n + \gamma a'_{n+1}\Delta t) + K(d^*_n + \beta a'_{n+1}\Delta t^2) = F^{ext}_{n+1}$$

or

$$[M + C\gamma\Delta t + K\beta\Delta t^2]a'_{n+1} = F^{ext}_{n+1} - Cv^*_n - Kd^*_n$$

The equation of motion may then be defined as

$$M^* a'_{n+1} = F^{residual}_{n+1}$$

The accelerations are obtained by inverting the M^* matrix as follows:

$$a'_{n+1} = M^{*-1} F^{residual}_{n+1}$$

This is analogous to decomposing the stiffness matrix in a linear static analysis. However, the dynamics mean that mass and damping terms are also present.

Explicit Methods

The equation of motion

$$Ma_n + Cv_n + Kd_n = F^{ext}_n$$

can be rewritten as

$$Ma_n = F^{ext}_n - F^{int}_n$$

$$a_n = M^{-1} F^{residual}_n$$

where

F^{ext}_n	=	vector of externally applied loads
F^{int}_n	=	vector of internal loads (e.g., forces generated by the elements and hourglass forces)
F^{int}	=	$Cv_n + Kd_n$
M	=	mass matrix

The acceleration can be found by inverting the mass matrix and multiplying it by the residual load vector.

If M is diagonal, its inversion is trivial, and the matrix equation is the set of independent equations for each degree of freedom is as follows:

$$a_{ni} = F_{ni}^{residual} / M_i$$

The central difference scheme is used to advance in time:

$$v_{n+1/2} = v_{n-1/2} + a_n(\Delta t_{n+1/2} + \Delta t_{n-1/2})/2$$

$$d_{n+1} = d_n + v_{n+1/2}\Delta t_{n+1/2}$$

This assumes that the acceleration is constant over the time step.

Explicit methods do not require matrix decompositions or matrix solutions. Instead, the loop is carried out for each time step as shown in the following diagram:

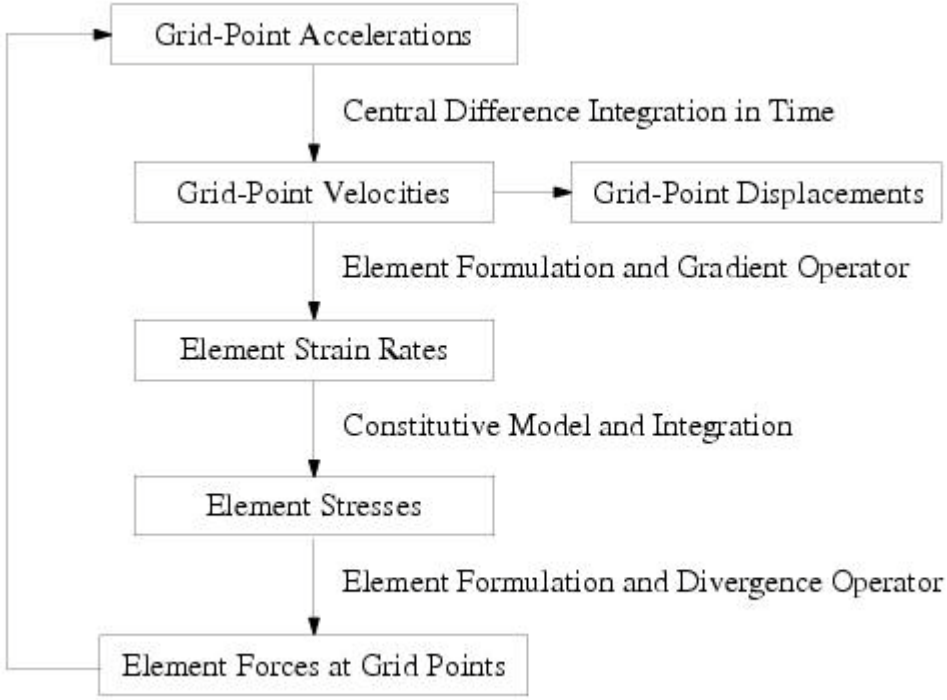

Implicit methods can be made unconditionally stable regardless of the size of the time step. However, for explicit codes to remain stable, the time step must subdivide the shortest natural period in the mesh. This means that the time step must be less than the time taken for a stress wave to cross the smallest element in the mesh. Typically, explicit time steps are 100 to 1000 times smaller than those used with implicit codes.

However, since each iteration does not involve the costly formulation and decomposition of matrices, explicit techniques are very competitive with implicit methods.

2 Principles of the Eulerian and Lagrangian Solvers

Overview

Dytran features two solving techniques, Lagrangian and Eulerian. The code can use either one, or both, and can couple the two types to define an interaction.

The Lagrangian method is the most common finite element solution technique for engineering applications. The Eulerian solver is most frequently used for analyses of fluids or materials that undergo very large deformations.

Lagrangian Solver

When the Lagrangian solver is used, grid points are fixed to locations on the body being analyzed. Elements of material are created by connecting the grid points together, and the collection of elements produces a mesh. As the body deforms, the grid points move with the material and the elements distort (Figure 2-1). The Lagrangian solver is, therefore, calculating the motion of elements of constant mass.

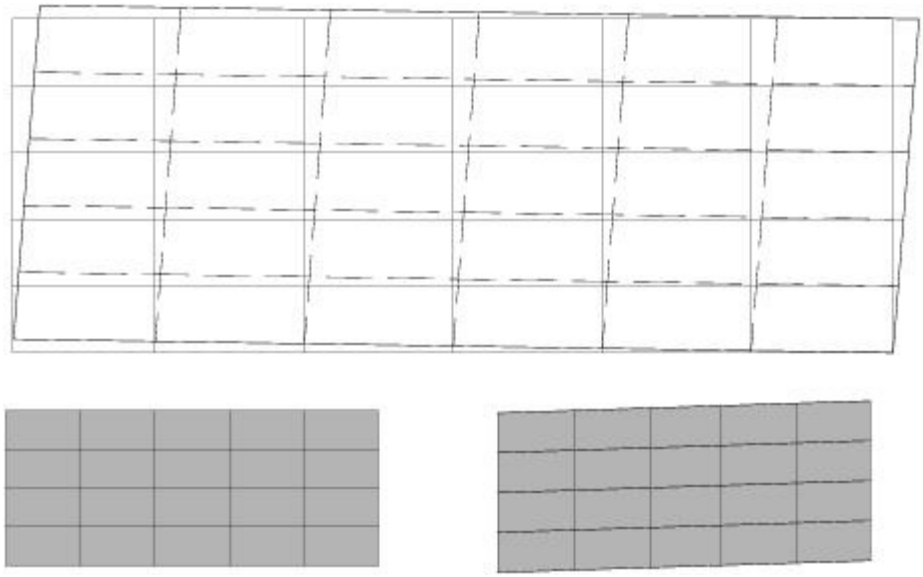

Figure 2-1 Lagrangian Solver

Eulerian Solver

In the Eulerian solver, the grid points are fixed in space and the elements are simply partitions of the space defined by connected grid points. The Eulerian mesh is a “fixed frame of reference.” The material of a body under analysis moves through the Eulerian mesh; the mass, momentum, and energy of the material are transported from element to element. The Eulerian solver, therefore, calculates the motion of material through elements of constant volume (Figure 2-2).

It is important to note that the Eulerian mesh is defined in exactly the same manner as a Lagrangian mesh. General connectivity is used so the Eulerian mesh can be of an arbitrary shape and have an arbitrary

numbering system. This offers considerably more flexibility than the logical rectangular meshes used in other Eulerian codes.

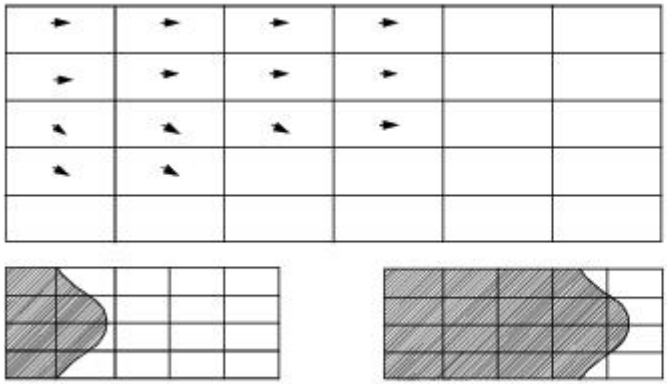

Figure 2-2 Eulerian Solver

However, you should remember that the use of an Eulerian mesh is different from that of the Lagrangian type. The most important aspect of modeling with the Eulerian technique is that the mesh must be large enough to contain the material after deformation. A basic Eulerian mesh acts like a container and, unless specifically defined, the material cannot leave the mesh. Stress wave reflections and pressure buildup can develop from an Eulerian mesh that is too small for the analysis.

Eulerian and Lagrangian meshes can be used in the same calculation and can be coupled using a coupling surface. The surface acts as a boundary to the flow of material in the Eulerian mesh, while the stresses in the Eulerian material exerts forces on the surface causing the Lagrangian mesh to distort.

There are basically two methods to define the interaction between the Lagrangian and Eulerian solvers:

- General Coupling Method
- Arbitrary Lagrange Euler Coupling (ALE Method)

General Coupling

The objective of fluid-structure interaction using the coupling algorithm is to enable the material modeled in Eulerian and Lagrangian meshes to interact. Initially, the two solvers are entirely separate. Lagrangian elements that lie within an Eulerian mesh do not affect the flow of the Eulerian material and no forces are transferred from the Eulerian material back to the Lagrangian structure. The coupling algorithm computes the interaction between the two sets of elements. It thus enables complex fluid-structure interaction problems to be analyzed.

The first task in coupling the Eulerian and Lagrangian sections of a model is to create a surface on the Lagrangian structure. This surface is used to transfer the forces between the two solver domains (Figure 2-3). The surface acts as a boundary to the flow of material in the Eulerian mesh. At the same time, the stresses in the Eulerian elements cause forces to act on the coupling surface, distorting the Lagrangian elements.

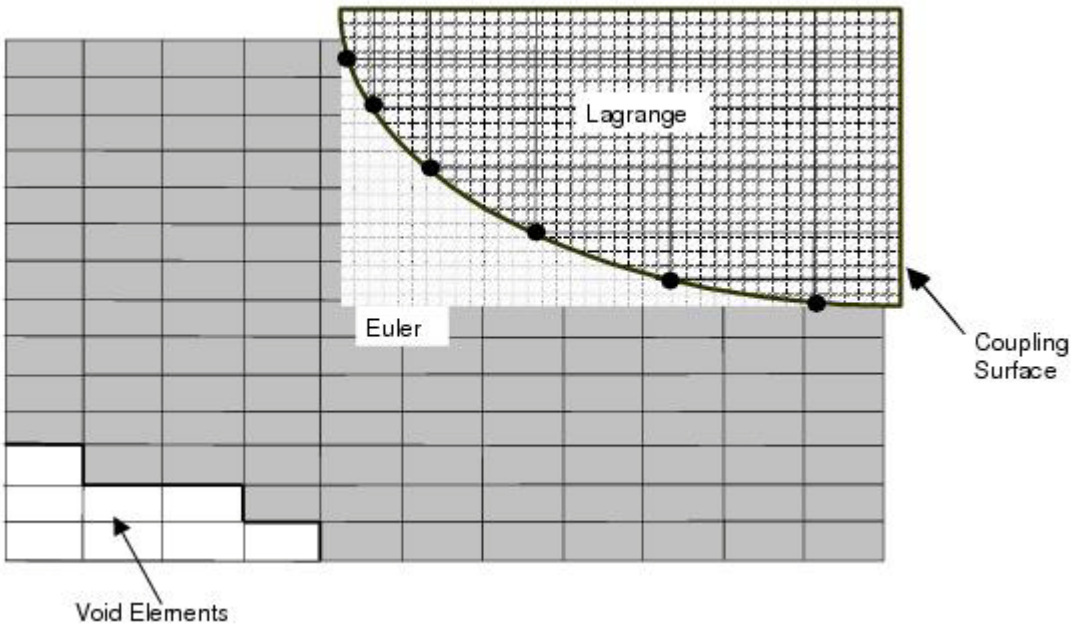

Figure 2-3 General Coupling

By means of a SURFACE entry, you can define a multifaceted surface on the Lagrangian structure. A set of CFACE, CFACE1, CSEGs, element numbers, property numbers, material numbers, or any combination of these identify the element faces in this surface. The method of defining of the surface is, therefore, extremely flexible and can be adapted to individual modeling needs.

The coupling algorithm is activated using the COUPLE entry. It specifies that the surface is used for Euler-Lagrange coupling. You can define whether the inside or the outside domain is covered by the coupling surface by setting the COVER field on the entry. This means that the Euler domain cannot contain material where it is covered by the outside or the inside of the Lagrangian structure. For problems where the Eulerian material is inside a Lagrangian structure (for example, an inflating air bag), COVER should be set to OUTSIDE since the Eulerian elements outside the coupling surface must be covered. For problems where the Eulerian material is outside the Lagrangian structure (for example a projectile penetrating soft material), the inside of the coupling surface must covered, and COVER should be set to INSIDE.

The coupling surface must have a positive volume to meet Dytran's internal requirements. This means that the normals of all the segments of the surface must point outwards. By default, Dytran checks the direction of the normal vectors and automatically reverses them when necessary. However, if you wish to switch off the check to save some computational time in the generation of the problem, you can define this using the REVERSE field on the COUPLE entry.

The coupling algorithm activated using the COUPLE entry is the most general interaction algorithm. It can handle any Euler mesh. There is an option, however, to switch to a faster algorithm by setting the FASTCOUP parameter. This algorithm makes use of knowledge of the geometry of the Euler mesh. As a result, the requirement is that the Euler mesh must be aligned with the basic coordinate system axes.

Closed Volume

The coupling surface must form a closed volume. This requirement is fundamental to the way the coupling works. It means that there can be no holes in the surface and the surface must be closed.

In order to create a closed volume, it may be necessary to artificially extend the coupling surface in some problems. In the following example (Figure 2-4), a plate modeled with shell elements is interacting with an Eulerian mesh. In order to form a closed coupling surface, dummy shell elements are added behind the plate. The shape of these dummy shell elements does not matter. However, it is best to use as few as possible to make the solution more efficient.

The closed volume formed by the coupling surface must intersect at least one Euler element; otherwise, the coupling surface is not recognized by the Eulerian mesh.

Care must be taken when doing so, however. The additional grid points created for the dummy elements do not move, since they are not connected to any structural elements. When the shell elements move so far that they pass beyond these stationary grid points, the coupling surface turns inside out and has a negative volume, causing Dytran to terminate.

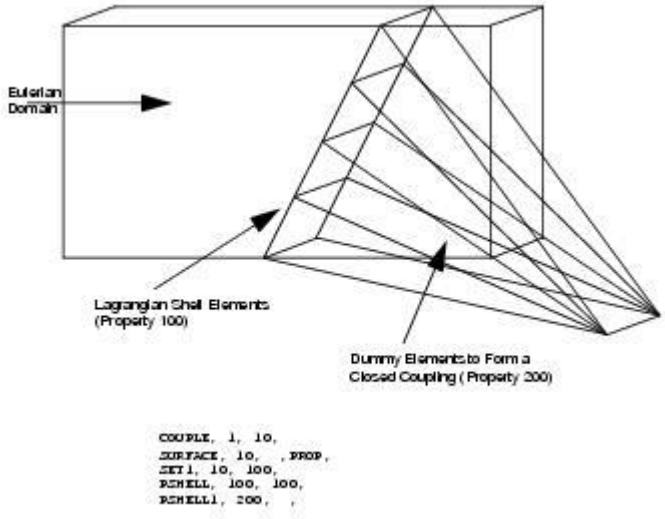

Figure 2-4 Dummy Elements Used to Create a “Closed Volume” in Coupling Surface

A friction force can also be applied tangent to the coupling surface. The friction is computed according to Coulomb's law of friction. The magnitude of the force during sliding equals the magnitude of the normal force multiplied by the friction coefficient. The direction of the friction force is opposite to the relative motion of the surface.

The friction force is defined as:

$$\hat{F}_f = -\mu \cdot \hat{F}_n \cdot \frac{\hat{v}_s}{|\hat{v}_s|}$$

The friction coefficient is defined as follows:

$$\mu = \mu_k + (\mu_s - \mu_k) \cdot e^{-\beta v_s}$$

where

μ_s	is the static friction coefficient.
μ_k	is the kinetic friction coefficient.
β	is the exponential decay coefficient.
v_s	is the relative sliding velocity of Eulerian material and Lagrangian structure.

Please refer to the *Dytran Reference Manual* on the COUPLE entry for more details on the input file definitions.

For use with hydroplaning a cohesive friction model can also be applied. This is enabled by using PARAM, COHESION, which applies to the whole coupling surface. To apply cohesion only for parts/subsurfaces of the coupling surface, use can be made of the entries COUCOHF and COHFRIC.

Arbitrary Lagrange Euler Coupling (ALE Method)

Another method to define fluid-structure interaction, is the Arbitrary Lagrange Euler (ALE) coupling, which allows Eulerian meshes to move. The structure and the Eulerian region are coupled by means of ALE coupling surfaces (Figure 2-5). The structure serves as a boundary condition for the Eulerian region at the interfaces. The Eulerian material exerts a pressure loading on the structure at the interface. The Eulerian region moves according to an ALE motion prescription in order to follow the motion of the structure. The Eulerian material flows through the Eulerian mesh while the mesh grid points can also have an arbitrary velocity.

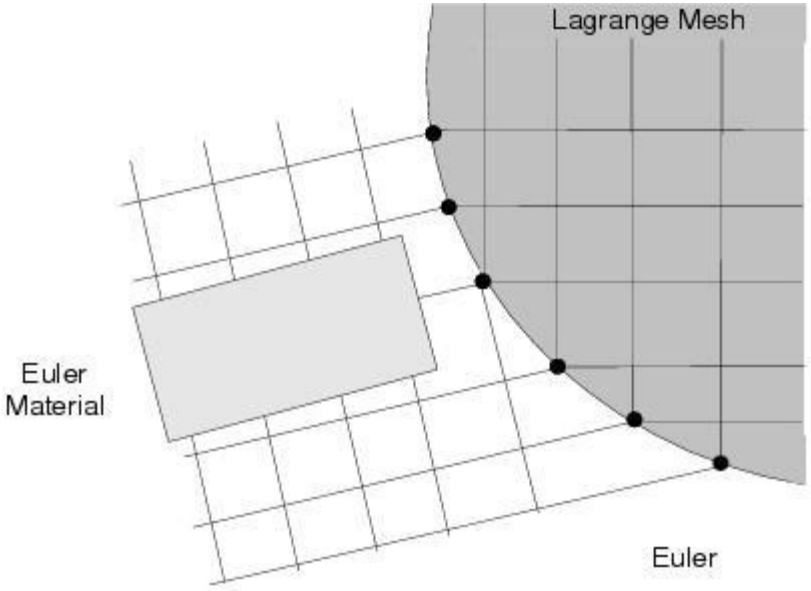

Figure 2-5 ALE Motion

3 Materials

DMAT – General Material

The DMAT material entry is a general material definition and provides a high degree of flexibility in defining material behavior. The basis of the DMAT entry is the reference of a combination of material descriptions: equation of state, yield model, shear model, failure model, and spall model. Each of these functions is defined by its own entry and is described further in Shear Models, Yield Models, Equations of State, Material Viscosity and Material Failure. The only material parameter defined on the DMAT entry is the reference density.

The DMAT entry can be used to define all types of material behavior from materials with very simple linear equations of state to materials with complex yielding and shearing behavior and different failure criteria.

The required input is the reference density, the number of an EOSxxx entry defining the equation of state, and the number of an SHRxxx entry defining the shear properties of the material. The equation of state defines the bulk behavior of the material. It may be a polynomial equation, a gamma law gas equation, or an explosive equation. A single-term polynomial equation produces a linear elastic behavior.

Further material property definitions are optional. A referenced YLDxxx entry selects one of the following: a hydrodynamic response (zero yield stress), a von Mises criterion that gives a bilinear elastoplastic behavior, or a Johnson-Cook yield model where the yield stress is a function of plastic strain, strain rate, and temperature. If no YLDxxx model is referenced, the material is assumed to be fully elastic.

A FAILxxx entry can be referenced to define a failure model for the material. This failure model can be based on a maximum plastic strain limit, a maximum stress limit, or a user-defined failure criterion included in an external subroutine. If no FAILxxx entry is referenced, the material has no failure criterion.

In addition, you may define a global (numerical) failure criterion based on the element time step using PARAM, FAILDT, <value>. Note that this is not a physical failure model, but can help in having the analysis run efficiently by automatically removing elements that are irrelevant for the calculation. This option must be used with care as it may influence the behavior of the analysis when you are too lenient in defining the time-step value at which element failure occurs. The option is available for solid and shell elements.

A PMINxxx entry can be referenced to define the spall characteristics of the material. Currently, only the PMINC entry is available. The entry provides a constant spall limit for the material. When no PMINxxx entry is referenced, the material has no spall limit for Lagrangian elements and a zero spall limit for Eulerian elements.

DMATEL – Elastic Material

The DMATEL entry provides a convenient way of defining the properties of isotropic elastic materials (Figure 3-1). The reference density is defined along with any two of the four elastic material constants: Young's modulus E, Poisson's ratio ν, bulk modulus K, and shear modulus G.

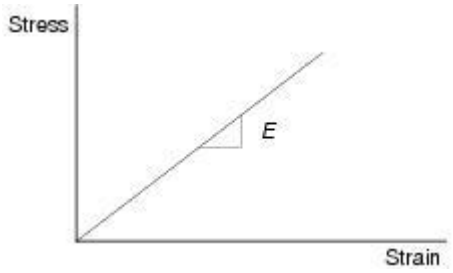

Figure 3-1 Elastic Stress-Strain Curve

The elastic constants are related by the following equations:

$$G = \frac{E}{2(1+v)}, K = \frac{E}{3(1-2v)}$$

DMATEP – Elastoplastic Material

The DMATEP entry defines the properties of an isotropic, elastoplastic material with failure (Figure 3-2).

The reference density is required, together with any two of the four elastic material constants: Young's modulus E, Poisson's ratio v, bulk modulus K, and shear modulus G. When only these elastic properties are defined, the material behavior is linear, isotropic, and elastic. A YLDVM entry can also be referenced, in which case a bilinear or piecewise linear elastoplastic material model is obtained. For CQUADy and CTRIAz elements, a YLDJC entry can be referenced to define a Johnson-Cook yield model. A FAILxxx entry can be referenced to define a failure model for the material. This failure model can be based on a maximum plastic strain limit or a user-defined failure criterion included in an external user subroutine. When no FAILxxx entry is referenced, the material has no failure criterion.

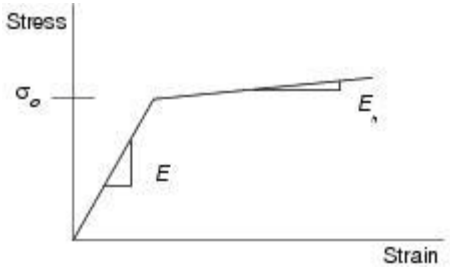

Figure 3-2 Elastic-Plastic, Stress-Strain Curve

DMATOR – Orthotropic Material

The DMATOR entry defines the properties of an orthotropic elastic material. The material model can only be used with Lagrangian solid elements.

The model is for orthotropic linear elastic materials. You must define the material properties in a material coordinate system (a, b, c). The relationship between stress σ and strain ε is:

$$\sigma = [C]\varepsilon$$

where

$[C]$	=	$[T]^t[C_L][T]$
$[T]$	=	the transformation matrix between the material coordinate system (a, b, c) and the basic coordinate system
$[C_L]$	=	the local constitutive matrix defined in the material coordinate system

$$[C_L]^{-1} = \begin{bmatrix} 1/E_a & -v_{ba}/E_b & -v_{ca}/E_c & 0 & 0 & 0 \\ -v_{ab}/E_a & 1/E_b & -v_{cb}/E_c & 0 & 0 & 0 \\ -v_{ac}/E_a & -v_{bc}/E_b & 1/E_c & 0 & 0 & 0 \\ 0 & 0 & 0 & 1/G_{ab} & 0 & 0 \\ 0 & 0 & 0 & 0 & 1/G_{bc} & 0 \\ 0 & 0 & 0 & 0 & 0 & 1/G_{ca} \end{bmatrix}$$

Since $v_{ab}/E_a = v_{ba}/E_b$, $v_{ca}/E_c = v_{ac}/E_a$, and $v_{cb}/E_c = v_{bc}/E_b$, the matrix is symmetrical.

You must define the following properties:

E_a, E_b, E_c Young's moduli in the principal material directions.

v_{ab}, v_{ca}, v_{cb} Poisson ratios between the b- and a-axis, the c- and a-axis, and the c- and b-axis.

G_{ab}, G_{bc}, G_{ca} Shear moduli in the ab, bc, and ca planes.

The material coordinate system is defined by specifying two vectors, V1 and V2 (Figure 3-3).

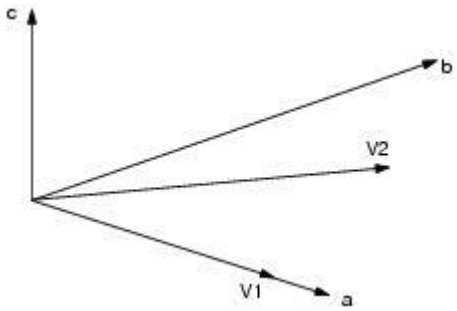

Figure 3-3 Material Coordinate System

The first vector defines the direction of the a-axis. The c-axis is perpendicular to both vectors. The b-axis is perpendicular to the a- and c-axis. The material coordinate system is independent of the element's shape and position. A `FAILxxx` entry can be referenced to define a failure model for the material. The failure model can be based on a maximum stress limit, a maximum pressure limit, or a user-defined criterion included in an external user subroutine.

MAT8 – Fiber-Composite Material with Failure

The orthotropic material model is used in shell elements to build a multilayered composite element. The material describes the elastic behavior of brittle material with failure based on the interactive stress criteria of failure per mode. The elastic stress-strain relation between the fiber and matrix stresses and strains is formulated as

$$\begin{bmatrix}\sigma_{11}\\ \sigma_{22}\end{bmatrix} = \frac{1}{(1-v_{12}v_{21})}\begin{bmatrix}E_{11} & v_{21}E_{11}\\ v_{21}E_{11} & E_{22}\end{bmatrix}\begin{bmatrix}\varepsilon_{11}\\ \varepsilon_{22}\end{bmatrix}$$

evaluated at $t + 1/2\Delta t$.

The shear stress-strain relation is defined as

$$\gamma_{12} = \frac{1}{G_{12}}\sigma_{12} + 3\alpha\bar{\sigma}_{12}^{2}\sigma_{12}$$

where α is an experimentally derived value. Setting α to zero reduces the elastic behavior in relation to orthotropic Hooke's Law.

For the prediction of failure, Dytran has a variety of models available. The first class of models contains the interactive models that predict the onset of failure, but not the failure mode. This class contains the Tsai-Hill and Tsai-Wu failure theories. The second class not only predicts the onset of failure, but provides the fiber compression (fiber buckling), matrix tension (matrix cracking), matrix compression, or in-plane shear failure. Theories that fall in the latter class are the Chang-Chang, maximum stress, modified Tsai-Wu, and Hashin failure theory.

In addition to the closed-form theories mentioned above, Dytran has the option to combine several theories in a combination model to define the failure for each separate mode. If this is not sufficient, it is possible to supply a user model, which can accommodate up to ten user-history variables.

A summary of failure theories is given below.

Tsai-Hill

$$\frac{\sigma_{11}^2}{X^2} - \frac{\sigma_{11}\sigma_{22}}{X^2} + \frac{\sigma_{22}^2}{Y^2} + \frac{\sigma_{12}^2}{S^2} \geq 1$$

Tsai-Wu

$$F_1\sigma_{11} + F_2\sigma_{22} + F_{11}\sigma_{11}^2 + F_{22}\sigma_{22}^2 + 2F_{12}\sigma_{11}\sigma_{22} + F_{66}\sigma_{12}^2 \geq 1$$

$F_1 = \frac{1}{X_T} - \frac{1}{X_C}$,	$F_2 = \frac{1}{Y_T} - \frac{1}{Y_C}$		
$F_{11} = \frac{1}{X_T X_C}$,	$F_{22} = \frac{1}{Y_T Y_C}$,	$F_{66} = \frac{1}{S^2}$,	F_{12} by biaxial test

Modified Tsai-Wu

Matrix failure	$F_2\sigma_{22} + F_{22}\sigma_{22}^2 + F_{66}\sigma_{12}^2 \geq 1$

Maximum Stress

Fiber tension	$\sigma_{11} \geq X_T (\sigma_{11} > 0)$
Fiber compression	$\lvert\sigma_{11}\rvert \geq X_C (\sigma_{11} < 0)$
Matrix tension	$\sigma_{22} \geq Y_T (\sigma_{22} > 0)$
Matrix compression	$\lvert\sigma_{22}\rvert \geq Y_C (\sigma_{22} < 0)$
Matrix shear	$\lvert\sigma_{12}\rvert \geq S$

Hashin

Fiber tension	$\left(\frac{\sigma_{11}}{X_T}\right)^2 + \left(\frac{\sigma_{12}}{S}\right)^2 \geq 1 (\sigma_{11} > 0)$	
Fiber compression	$\lvert\sigma_{11}\rvert \geq X_C (\sigma_{11} < 0)$	
Matrix tension	$\left(\frac{\sigma_{22}}{Y_T}\right)^2 + \left(\frac{\sigma_{12}}{S}\right)^2 \geq 1 (\sigma_{22} > 0)$	
Matrix compression	$\left(\frac{\sigma_{22}}{2S_T}\right)^2 + \left[\left(\frac{Y_C}{2S_T}\right)^2 - 1\right]\frac{\sigma_{22}}{Y_C} + \left(\frac{\sigma_{12}}{S}\right)^2 \geq 1$	$(\sigma_{22} < 0)$

Chang

Fiber breakage	$\left(\frac{\sigma_{11}}{X_T}\right)^2 + T \geq 1$	$(\sigma_{11} > 0)$
Matrix cracking	$\left(\frac{\sigma_{22}}{T_T}\right)^2 + T \geq 1$	$(\sigma_{22} > 0)$
Matrix compression	$\left(\frac{\sigma_{22}}{2S}\right)^2 + \left[\left(\frac{Y_C}{2S}\right)^2 - 1\right]\frac{\sigma_{22}}{Y_C} + T \geq 1$	$(\sigma_{22} < 0)$

$$T = \left(\frac{\sigma_{12}}{S}\right)^2 \frac{1 + \frac{3}{2}\alpha G_{12}\sigma_{12}^2}{1 + \frac{3}{2}\alpha G_{12} S^2}$$

When a failure criterion is satisfied, the next stage is to define how the remaining modes are affected by the failed mode. A standard model is available, which is an average of the various theories provided in the literature. However, the property degradation rules are not fixed and can be easily redefined by the user. The property degradation rules describe how stress increments are related to strain increments in the various directions after failure in a particular mode has occurred.

Material Constant	Failure Mode				
	Fiber Tens	Fiber Comp	Matrix Tens	Matrix Comp	Shear
$E1$	X	X			
$E2$	X	X	X	X	
$v12$	X	X	X	X	
$G12$	X		X		X

For example, in matrix compression failure, the material constants $E2$ (lateral Young's modulus), and $v12$ (Poisson's ratio) are set to zero.

Finally, the model describes how the stresses are relaxed to zero after failure has occurred. The relaxation can start either when a particular mode has failed or when all material properties ($E1$, $E2$, $v12$, $G12$) are degraded to zero according to the property degradation rule. The relaxation always occurs in time, either in problem time units by a propagation velocity, or simply by time steps. This model is referred to as the post-failure degradation rule.

SHEETMAT, BARLT89, and BARLT00 – Anisotropic Plastic Material Models

The SHEETMAT, BARLT89, and BARLT00 models are primarily intended to describe the anisotropic plastic behavior of thin-rolled metal sheets. They can only be used with Lagrangian shell element formulations (`BLT`, `CO-TRIA` and `KEYHOFF`) because these models are based on the plane stress formulation.

The main input parameters of these models can be categorized into three groups: elasticity, criterion of yielding, and rule of hardening. These input parameters (see the following table) reference keywords will be described in the following sections. Furthermore, strain-rate dependency is considered and finally, the use of the Forming Limit Diagram (FLD) is treated in view of postprocessing purposes. BARLT00 only supports isotropic elasticity, anisotropic yielding, and isotropic hardening.

TYPE	SHEETMAT			BARLT89		
	ELASTICITY	YIELDING	HARDENING	ELASTICITY	YIELDING	HARDENING
ISOTROPIC*	ELASTIC=ISO : Exx NUxy (or Gxy)	TYPEYLD=ISO: $R_0 = R_{45} = R_{90} = 1$	TYPEHRD=ISO	ELASTIC=ISO : Exx NUxy (or Gxy)	TYPEYLD=ISO: $R_0 = R_{45} = R_{90} = 1$	TYPEHRD=ISO

TYPE	SHEETMAT			BARLT89		
	ELASTICITY	YIELDING	HARDENING	ELASTICITY	YIELDING	HARDENING
NORMAL ANISOTROPIC	ELASTIC=PLANISO: Exx (or Eyy) Ezz Nuxy (or Gxy) NUxz (or NUyz) Gxz (or Gyz)	TYPEYLD=NORMANI: $R_{00} = R_{45} = R_{90}$	TYPEHRD=NORMANI	not available	TYPEYLD=NORMANI: $R_{00} = R_{45} = R_{90}$	TYPEHRD=NORMANI
PLANAR ANISOTROPIC	not available	TYPEYLD=PLANANI: $R_{00} \neq R_{45} \neq R_{90}$	not available	not available	TYPEYLD=PLANANI: $R_{00} \neq R_{45} \neq R_{90}$	not available
*Default						

Elasticity

SHEETMAT includes two models of elastic behavior: fully isotropic and planar isotropic elasticity. While, BARLT89 and BARLT00 only support fully isotropic elastic behavior. Both forms of elasticity are most easily defined by giving the strain-stress relation expressed in so-called engineering constants for orthotropic materials:

$$\begin{Bmatrix} \varepsilon_{xx} \\ \varepsilon_{yy} \\ \varepsilon_{zz} \\ \gamma_{xy} \\ \gamma_{yz} \\ \gamma_{xz} \end{Bmatrix} = \begin{bmatrix} 1/E_{xx} & -\nu_{xy}/E_{xx} & -\nu_{xz}/E_{xx} & 0 & 0 & 0 \\ -\nu_{xy}/E_{xx} & 1/E_{yy} & -\nu_{yz}/E_{yy} & 0 & 0 & 0 \\ -\nu_{xz}/E_{xx} & -\nu_{yz}/E_{yy} & 1/E_{zz} & 0 & 0 & 0 \\ 0 & 0 & 0 & 1/G_{xy} & 0 & 0 \\ 0 & 0 & 0 & 0 & 1/G_{yz} & 0 \\ 0 & 0 & 0 & 0 & 0 & 1/G_{xz} \end{bmatrix} \begin{Bmatrix} \sigma_{xx} \\ \sigma_{yy} \\ \sigma_{zz} \\ \sigma_{xz} \\ \sigma_{yz} \\ \sigma_{xz} \end{Bmatrix}$$

The isotropic case is the simplest form of linear elasticity for which only the Young's modulus $(E_{xx} = E_{yy} = E_{zz})$ and Poisson's ratio $(\nu_{xy} = \nu_{yz} = \nu_{xz})$ or shear modulus $(G_{xy} = G_{yz} = G_{xz})$ must be defined. Planar isotropic material behavior is equivalent to transversely isotropic material behavior, which means that the through-the-thickness (elastic) properties may differ from the in-plane isotropic (elastic) properties. The values of E_{xx} (or E_{yy}), E_{zz}, ν_{xy} (or G_{xy}), ν_{xz} (or ν_{yz}) and G_{xz} (or G_{yz}) are required to define a planar isotropic material.

The engineering constants must be specified with respect to the rolling direction of the material which is defined by a local material coordinate system. This coordinate system may differ from the local element coordinate system and may be defined via XMAT, YMAT, and ZMAT on the SHEETMAT, BARLT89, and BARLT00 entries (or by specifying THETA on the CQUAD4/CTRIA3 entry).

As a result of the rolling process, the plastic properties normal to the sheet are likely to be different from the in-plane properties which is referred as normal anisotropy. In addition, the properties may depend on the in-plane orientation with respect to the rolling direction, which is known as planar anisotropy. SHEETMAT and BARLT89 material models can represent normal anisotropy in both yielding and hardening. However, planar anisotropy is confined to yielding. BARLT00 material model only represents planar anisotropy in yielding and isotropic hardening.

Yielding Criteria

Three possibilities are provided for yielding behavior: isotropic, normal anisotropic, and planar anisotropic yielding. Yielding anisotropy can be defined by Lankford parameters, R_{00}, R_{45}, and R_{90}.

R_{00} represents the width-to-thickness plastic strain ratio measured from a uniaxial test in rolling direction. R_{90} represents the ratio measured from a uniaxial test in transverse rolling direction. R_{45} represents the ratio measured from a test at 45° to the rolling direction (see Figure 3-4).

For fully isotropic material, the in-plane and out-of-plane (i.e., normal) material properties are the same which means that the width plastic strain must be equal to the through-the-thickness plastic strain, implying $R_{00} = R_{45} = R_{90} = 1$. These values are the defaults on the SHEETMAT, BARLT89, and BARLT00 entries.

A material is called normal anisotropic when the material is in-plane isotropic, but has different out-of-plane properties compared to the in-plane properties. The R value ($R_{00} = R_{45} = R_{90}$) is not equal to one.

Consequently, only the R_{00} value is required.

The SHEETMAT , BARLT89, and BARLT00 definition material models also allow (planar) anisotropic yielding behavior to be modeled. This implies that the R value depends on the in-plane orientation with respect to the rolling direction. Therefore, you must specify all of the values for R_{00}, R_{45}, and R_{90}, individually.

Since BARLT00 only represents planar anisotropy in yielding, one of the following two options must be defined.

- Direct input of 8 BARLT00 parameters such as ALPHA1 ~ ALPHA8.
- Nominal yield stresses in 0°, 45° and 90° to rolling direction and biaxial nominal yield stress and R_{00}, R_{45}, and R_{90}. Rb which is Lankford parameter in biaxial test is optional.

SHEETMAT

SHEETMAT entry defines the Krieg constitutive material model. The plasticity model of Krieg uses the standard Hill yield criterion, which is also known as the Hill-48 yield criterion (Krieg, 1996). The yielding directionality is controlled via the yield matrix Q_{ij} in the yield function ϕ:

$$\phi = \sigma_m Q_{mn} \sigma_n - \sigma_y^2$$

where σ_n is Cauchy stress in Voigt notation.

The coefficients of the yield matrix, Q_{ij} are governed by the Lankford coefficients. The non-zero coefficients are given as

$$Q_{11} = 1$$

$$Q_{12} = Q_{21} = -\frac{R_{00}}{R_{00}+1}$$

$$Q_{22} = \frac{R_{00}}{R_{00}+1} \times \frac{1+R_{90}}{R_{90}}$$

$$Q_{44} = Q_{55} = Q_{66} = \frac{(R_{00}+R_{90})(1+2\times R_{45})}{R_{90}(1+R_{00})}$$

Isotropic yielding condition, $R_{00} = R_{45} = R_{90} = 1$, is equivalent to von Mises yielding criterion. The effect of the R value on the yield surface is schematically shown in Figure 3-4.

BARLT89

BARLT89 uses Barlat-89 yield function introduced by Barlat and Lian (Barlat & Lian, 1989). Barlat-89 yield criterion is developed for planar anisotropy under plane stress assumption and given by

$$\phi = a|K_1 + K_2|^M + a|K_1 - K_2|^M + c|2K_2|^M - 2\sigma_y^M$$

$$K_1 = \frac{\sigma_{xx} + h\sigma_{yy}}{2}$$

$$K_2 = \sqrt{\left(\frac{\sigma_{xx} - h\sigma_{yy}}{2}\right)^2 + p^2\sigma_{xy}^2}$$

where

x, y, and z	=	orthotropic axes in rolling, transverse, and normal directions, respectively
σ_{xx}, σ_{yy}, and σ_{xy}	=	plane stress components in orthotropic axes
σ_y	=	uniaxial yield stress (effective stress) in the rolling direction
M, a, c, h, and p	=	material constants

When $M = 2$, Barlat-89 yield criterion reduces to Hill-48 criterion.

The yielding directionality is controlled via the yield parameters a, c, h, and p. There are two approaches to obtain them:

1. Using uniaxial, biaxial, and shear tests yield stress result:

$$a = 2 - c = \frac{2\left(\frac{\sigma_y}{\tau_{s2}}\right)^M - 2\left(1 + \frac{\sigma_y}{\sigma_{90}}\right)^M}{1 + \left(\frac{\sigma_y}{\sigma_{90}}\right)^M - \left(1 + \frac{\sigma_y}{\sigma_{90}}\right)^M}$$

$$h = \frac{\bar{\sigma}}{\sigma_{90}}$$

$$p = \frac{\sigma_y}{\tau_{s1}}\left(\frac{2}{2a + 2^M c}\right)^{\frac{1}{M}}$$

where

σ_{90}	=	Yield stress for uniaxial tension in the transverse to the rolling direction, when $\sigma_{yy} = \sigma_{90}$ and $\sigma_{xx} = \sigma_{xy} = 0$
τ_{s2}	=	Yield stress for biaxial test, when $\sigma_{yy} = -\sigma_{xx} = \tau_{s2}$ and $\sigma_{xy} = 0$
τ_{s1}	=	Yield stress for shear test, when $\sigma_{yy} = \sigma_{xx} = 0$ and $\sigma_{xy} = \tau_{s1}$

2. Using R values obtained from uniaxial tension tests at 0, 45, 90 degrees inclination with respect to the rolling direction:

$$a = 2 - c = 2 - 2\sqrt{\frac{R_0}{1 + R_0} \times \frac{R_{90}}{1 + R_{90}}}$$

$$h = \sqrt{\frac{R_0}{1 + R_0} \times \frac{1 + R_{90}}{R_{90}}}$$

while p cannot be calculated analytically, it can be obtained numerically from solving the following equation for any angle φ (typically $\varphi = 45°$):

$$R_\varphi = \frac{2M\sigma_y^M}{\left(\frac{\partial f}{\partial \sigma_{xx}} + \frac{\partial f}{\partial \sigma_{yy}}\right)\sigma_\varphi} - 1$$

where

R_φ	=	width to thickness strain rate ratio in uniaxial tension in a direction making an angle φ with the rolling direction
σ_φ	=	uniaxial yield stress in a direction making an angle φ with the rolling direction

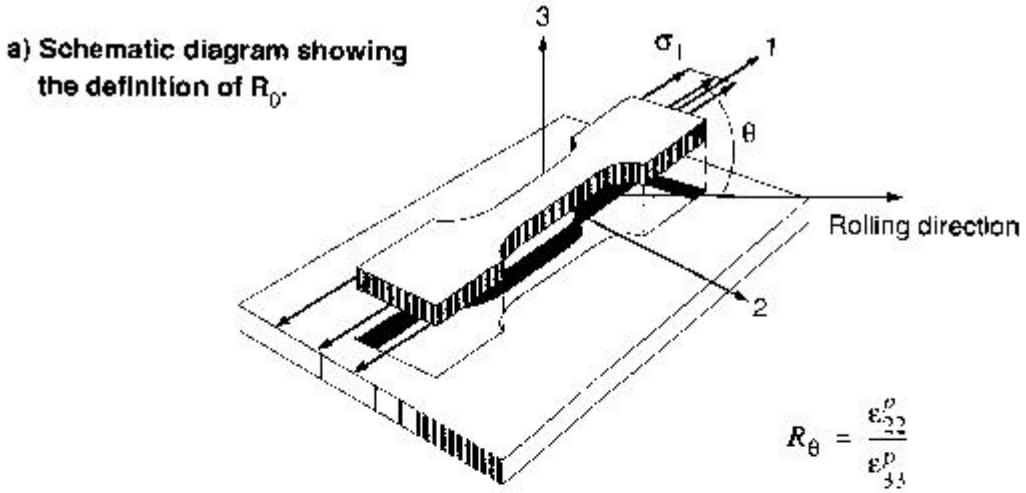

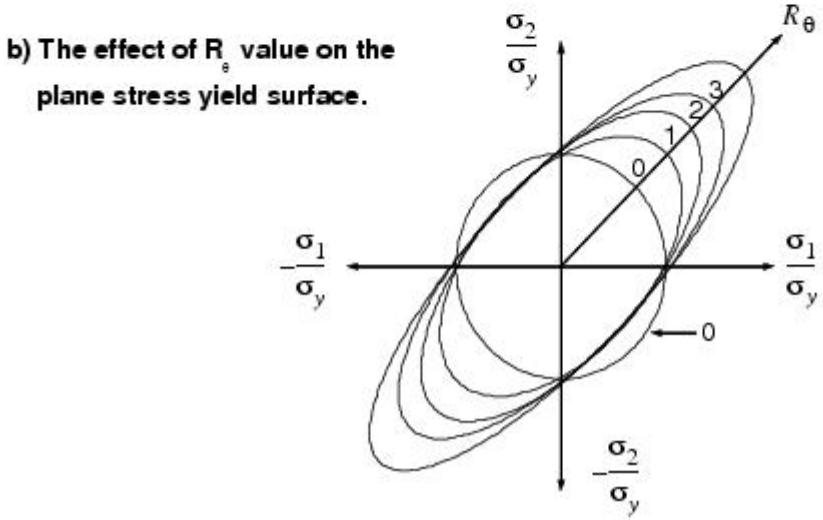

Figure 3-4 Anisotropic Plasticity

BARLT00

BARLT00 uses the yield function which is introduced in Barlat et al (2003) and Yoon et al (2004). The yield function is developed for planar anisotropy under plane stress condition.

$$f = \phi' + \phi'' = 2\bar{\sigma}^a$$

where

$$\phi' = \left|X'_1 + X'_2\right|^a$$

$$\phi'' = \left|2X''_1 + X''_2\right|^a + \left|X''_1 + 2X''_2\right|^a$$

Each variable is set to

$$X_1 = \frac{1}{2}\left(X_{xx} + X_{yy} + \sqrt{(X_{xx} - X_{yy})^2 + 4X_{xy}^2}\right)$$

$$X_2 = \frac{1}{2}\left(X_{xx} + X_{yy} + \sqrt{(X_{xx} - X_{yy})^2 + 4X_{xy}^2}\right)$$

$X_{\alpha\beta}$ is defined as

$$X' = L'\sigma$$

$$X'' = L''\sigma$$

$$\begin{bmatrix} X_{xx} \\ X_{yy} \\ X_{xy} \end{bmatrix} = \begin{bmatrix} L_{11} & L_{12} & 0 \\ L_{21} & L_{22} & 0 \\ 0 & 0 & L_{33} \end{bmatrix} \begin{bmatrix} \sigma_{xx} \\ \sigma_{yy} \\ \sigma_{xy} \end{bmatrix}$$

Each component of matrix L' and L'' is

$$\begin{bmatrix} L'_{11} \\ L'_{12} \\ L'_{21} \\ L'_{22} \\ L'_{33} \end{bmatrix} = \begin{bmatrix} 2/3 & 0 & 0 \\ -1/3 & 0 & 0 \\ 0 & -1/3 & 0 \\ 0 & 2/3 & 0 \\ 0 & 0 & 1 \end{bmatrix} \begin{bmatrix} \alpha_1 \\ \alpha_2 \\ \alpha_7 \end{bmatrix}$$

$$\begin{bmatrix} L''_{11} \\ L''_{12} \\ L''_{21} \\ L''_{22} \\ L''_{33} \end{bmatrix} = \frac{1}{9}\begin{bmatrix} -2 & 2 & 8 & -2 & 0 \\ 1 & -4 & -4 & 4 & 0 \\ 0 & -4 & -4 & 1 & 0 \\ -2 & 8 & 2 & -2 & 0 \\ 0 & 0 & 1 & 0 & 9 \end{bmatrix} \begin{bmatrix} \alpha_3 \\ \alpha_4 \\ \alpha_5 \\ \alpha_6 \\ \alpha_9 \end{bmatrix}$$

The material requires 8 alpha parameters to define flow rule.

The effective stress is defined from the flow rule.

$$\bar{\sigma}(\sigma) = \left(\frac{1}{2}\right)^{\frac{1}{a}} (\phi' + \phi'')^{\frac{1}{a}}$$

The alpha parameters can be obtained from the test results, 3 uniaxial stresses, σ_0, σ_{45}, and σ_{90} and biaxial stress, σ_b and 3 uniaxial Lankford parameters, r_0, r_{45}, and r_{90} and biaxial Lankford parameter, r_b.

$$\sigma_{xx} = \sigma_\varphi cos^2\varphi$$

$$\sigma_{yy} = \sigma_\varphi sin^2\varphi$$

$$\sigma_{xy} = \sigma_\varphi cos\varphi sin\varphi$$

For biaxial case,

$$\sigma_{xx} = \sigma_b$$

$$\sigma_{yy} = \sigma_b$$

$$\sigma_{xy} = 0$$

Using σ_0, σ_{45}, σ_{90} and σ_b, 4 effective stress equations can be made.

The strain rate can be defined from the flow rule and the assumption of incompressibility.

$$\dot{\varepsilon}_{xx} = \dot{\lambda}\frac{\partial f}{\partial \sigma_{xx}}$$

$$\dot{\varepsilon}_{yy} = \dot{\lambda}\frac{\partial f}{\partial \sigma_{yy}}$$

$$\dot{\varepsilon}_{xy} = \frac{\dot{\lambda}}{2}\frac{\partial f}{\partial \sigma_{xy}}$$

$$\dot{\varepsilon}_{11} + \dot{\varepsilon}_{22} + \dot{\varepsilon}_{33} = 0$$

The definition of Lankford parameters is

$$r_\varphi = \frac{\dot{\varepsilon}_{22}}{\dot{\varepsilon}_{33}} = \frac{\dot{\varepsilon}_{22}}{\dot{\varepsilon}_{11} + \dot{\varepsilon}_{22}} \tag{3-1}$$

$$\dot{\varepsilon}_{11} = \dot{\varepsilon}_{xx} cos^2\varphi + \dot{\varepsilon}_{yy} sin^2\varphi + 2 cos\varphi sin\varphi \dot{\varepsilon}_{xy}$$

$$\dot{\varepsilon}_{22} = \dot{\varepsilon}_{xx} sin^2\varphi + \dot{\varepsilon}_{yy} cos^2\varphi - 2 cos\varphi sin\varphi \dot{\varepsilon}_{xy}$$

Using the Equation (3-1),

$$\dot{\varepsilon}_{11} + \dot{\varepsilon}_{22} = \dot{\varepsilon}_{xx} + \dot{\varepsilon}_{yy}$$

Using the Euler's theorem and flow rule,

$$\dot{\varepsilon}_{11} = \dot{\varepsilon}_{xx} cos^2\varphi + \dot{\varepsilon}_{yy} sin^2\varphi + 2 cos\varphi sin\varphi \dot{\varepsilon}_{xy}$$

$$= \frac{\dot{\lambda}}{\sigma_\varphi}\left(\sigma_\varphi cos^2\varphi \frac{\partial f}{\partial \sigma_{xx}} + \sigma_\varphi sin^2\varphi \frac{\partial f}{\partial \sigma_{yy}} + \sigma_\varphi sin\varphi cos\varphi \frac{\partial f}{\partial \sigma_{xy}}\right)$$

$$= \frac{\dot{\lambda}}{\sigma_\varphi}\left(\sigma_{xx}\frac{\partial f}{\partial \sigma_{xx}} + \sigma_{yy}\frac{\partial f}{\partial \sigma_{yy}} + \sigma_{xy}\frac{\partial f}{\partial \sigma_{xy}}\right)$$

$$= \frac{\dot{\lambda}}{\sigma_\varphi} 2a\bar{\sigma}^a$$

The Equation (3-1) can be written as

$$r_\varphi = \frac{\dot{\varepsilon}_{22}}{\dot{\varepsilon}_{11} + \dot{\varepsilon}_{22}} = \frac{\dot{\varepsilon}_{11}}{\dot{\varepsilon}_{xx} + \dot{\varepsilon}_{yy}} - 1 = \frac{2a\bar{\sigma}^a}{\left(\frac{\partial f}{\partial \sigma_{xx}} + \frac{\partial f}{\partial \sigma_{yy}}\right)\sigma_\varphi} - 1$$

From the definition, biaxial Lanford parameter is

$$r_b = \left.\frac{\frac{\partial f}{\partial \sigma_{yy}}}{\frac{\partial f}{\partial \sigma_{xx}}}\right|_{\sigma_b}$$

Then additional 4 equations can be made.

Using 8 equations, the alpha parameters can be obtained.

The g matrix can be made using 4 equations from flow rule and 4 equations from r value calculation.

Under uniaxial tension in 0 degree from rolling direction, stress is σ_a. $\sigma_{xx} - \sigma_0$ and $\sigma_{yy} = \sigma_{xy} = 0$.

$$g_1(\alpha) = g_1(\alpha_1, \alpha_2, \ldots, \alpha_8) = f\big|_{\sigma_0} - 2\bar{\sigma}^a = 0$$

In 45 degrees, stress is $\sigma_{45} \cdot \sigma_{xx} = \sigma_{yy} = \sigma_{xy} = \frac{1}{2}\sigma_{45}$ and in 90 degrees, stress is $\sigma_{90} \cdot \sigma_{yy} = \sigma_{90}$ and $\sigma_{xx} = \sigma_{yy} = 0$.

$$g_2(\alpha) = f\big|_{\sigma_{45}} - 2\bar{\sigma}^a = 0$$

$$g_2(\alpha) = f\big|_{\sigma_{45}} - 2\bar{\sigma}^a = 0$$

$$g_3(\alpha) = f\big|_{\sigma_{90}} - 2\bar{\sigma}^a = 0$$

Under biaxial tensional stress, $\sigma_b \cdot \sigma_{xx} = \sigma_{yy} = \sigma_b$ and $\sigma_{xy} = 0$

$$g_4(\alpha) = f\big|_{\sigma_b} - 2\bar{\sigma}^a = 0$$

Using r value, r_φ,

$$g_{4\sim7}(\alpha) = \frac{\dot{\varepsilon}_{22}}{\dot{\varepsilon}_{11} + \dot{\varepsilon}_{22}} - r_\varphi = \frac{\frac{\partial f}{\partial \sigma_{xx}} sin^2\varphi + \frac{\partial f}{\partial \sigma_{yy}} cos^2\varphi + \frac{\partial f}{\partial \sigma_{xy}} sin\varphi cos\varphi}{\frac{\partial f}{\partial \sigma_{xx}} + \frac{\partial f}{\partial \sigma_{yy}}} - r_\varphi = 0$$

Using r value in 0 degree, r_0, $\sigma_{xx} = \sigma_{0x}$ and $\sigma_{yy} = \sigma_{xy} = 0$,

$$g_5(\alpha) = \frac{\left.\frac{\partial f}{\partial \sigma_{yy}}\right|_{\sigma_0}}{\left.\frac{\partial f}{\partial \sigma_{xx}}\right|_{\sigma_0} + \left.\frac{\partial f}{\partial \sigma_{yy}}\right|_{\sigma_0}} - r_0 = 0$$

Using r value in 45 degree, r_{45} and $\sigma_{xx} = \sigma_{yy} = \sigma_{xy} = \frac{1}{2}\sigma_{45}$,

$$g_6(\alpha) = \frac{\frac{1}{2}\left(\left.\frac{\partial f}{\partial \sigma_{xx}}\right|_{\sigma_{45}} + \left.\frac{\partial f}{\partial \sigma_{yy}}\right|_{\sigma_{45}} - \left.\frac{\partial f}{\partial \sigma_{xy}}\right|_{\sigma_{45}}\right)}{\left.\frac{\partial f}{\partial \sigma_{xx}}\right|_{\sigma_0} + \left.\frac{\partial f}{\partial \sigma_{yy}}\right|_{\sigma_0}} - r_{45} = 0$$

Using r value in 90 degree, r_{90}, $\sigma_{yy} = \sigma_{90}$, and $\sigma_{xx} = \sigma_{xy} = 0$,

$$g_7(\alpha) = \frac{\left.\frac{\partial f}{\partial \sigma_{xx}}\right|_{\sigma_{90}}}{\left.\frac{\partial f}{\partial \sigma_{xx}}\right|_{\sigma_{90}} + \left.\frac{\partial f}{\partial \sigma_{yy}}\right|_{\sigma_{90}}} - r_{90} = 0$$

Using r value in biaxial test, r_b, $\sigma_{xx} = \sigma_{yy} = \sigma_{by}$, and $\sigma_{xy} = 0$,

$$g_8(\alpha) = \frac{\left.\frac{\partial f}{\partial \sigma_{yy}}\right|_{\sigma_b}}{\left.\frac{\partial f}{\partial \sigma_{xx}}\right|_{\sigma_b}} - r_b = 0$$

From the above equations,

$$g(\alpha) = \begin{bmatrix} g_1(\alpha) \\ g_2(\alpha) \\ \cdots \\ g_8(\alpha) \end{bmatrix}$$

$$Vg(\alpha) = \begin{bmatrix} \frac{\partial g_1}{\partial \alpha_1} & \frac{\partial g_1}{\partial \alpha_2} & \cdots & \frac{\partial g_1}{\partial \alpha_8} \\ \frac{\partial g_2}{\partial \alpha_1} & \frac{\partial g_2}{\partial \alpha_2} & \cdots & \frac{\partial g_2}{\partial \alpha_8} \\ \cdots & \cdots & \cdots & \cdots \\ \frac{\partial g_8}{\partial \alpha_1} & \frac{\partial g_8}{\partial \alpha_2} & \cdots & \frac{\partial g_8}{\partial \alpha_8} \end{bmatrix}$$

Jacobian of $g(\alpha)$ is

The values can be obtained by multi-dimensional Newton-Raphson method.

$$X_{i+1} = X_i - \nabla g^{-1}(X_i) g(X_i)$$

However, this approach is not practical since it is not easy to calculate Jacobian matrix of g equations.

In another way, using the least square approach,

$$E = \sum_{j=1}^{4} \left(\frac{\sigma_{pre}}{\sigma_{exp}} - 1 \right) + \sum_{j=1}^{4} \left(\frac{r_{pre}}{r_{exp}} - 1 \right)$$

Minimizing E value can be used to get the optimal alpha values. The equation is useful when there are more or less test results than 8.

However, E value can have many solutions when the number of constraints is less than the number of unknown alpha parameters, 8. To get one solution, additional constraint (Yoon et al, 2004) is added when r_b is not set.

$$L''_{12} = L''_{21}$$

And E value will be evaluated using

$$E = \sum_{j=1}^{4} \left(\frac{\sigma_{pre}}{\sigma_{exp}} - 1 \right) + \sum_{j=1}^{4} \left(\frac{r_{pre}}{r_{exp}} - 1 \right) + \left(\frac{L''_{12}}{L''_{21}} - 1 \right)$$

Reference

- Barlat et al. “Plane stress yield function for aluminum alloy sheets—part 1: theory”, *International Journal of Plasticity,* 19, pp.1297-1319 (2003).
- Yoon et al, “Plane stress yield function for aluminum alloy sheets—part II: FE formulation and its implementation”, *International Journal of Plasticity*, 20, 495-522 (2004).

Hardening Rules

The work-hardening rule defines the way the yield surface changes with plastic straining. Besides perfect plasticity where yield stress does not change with plastic strain, two possibilities are provided with SHEETMAT and BARLT89: isotropic hardening and normal anisotropic hardening and BARLT00: isotropic hardening only. SHEETMAT, BARLT89, and BARLT00 material models supports only Scalar hardening where the magnification of the size of the yield surface can change without change in shape or movement of the center of the yield surface.

Isotropic hardening (default) means that the yield surface changes uniformly in all directions so that the yield stress increases in all stress directions as plastic straining occurs.

Normal anisotropic hardening means the growth of the yield surface may require more plastic strain in thickness direction than in other directions. This distinct hardening in thickness direction can be controlled by a hardening matrix in which the coefficients are also given by the Lankford coefficients.

The uniaxial yield stress is given as a function of uniaxial [effective] plastic strain [and effective plastic strain rate].

$$\sigma_y = f(\bar{\varepsilon}^p) \times g(\dot{\bar{\varepsilon}}^p)$$

where

$\bar{\varepsilon}^p$	=	effective plastic strain
$\dot{\bar{\varepsilon}}^p$	=	effective plastic strain rate

The hardening function can be expressed as a table giving the variation of yield stress with effective plastic strain or by means of the following power-law function:

$$f(\bar{\varepsilon}^p) = a + b(\bar{\varepsilon}^p + c)^n$$

where:

a	=	stress constant
b	=	hardening parameter
c	=	strain offset
n	=	strain-hardening exponent

Also, the strain-rate dependency is expressed by

$$g(\bar{d}^p) = 1 + k(\bar{d}^p)^m$$

where:

k	=	strain-rate sensitivity constant
m	=	strain-rate exponent

The power-law coefficients (a, b, c, and n) and rate dependency coefficients(k and m) are usually determined by a least squares fit of experimental true stress-strain data, obtained from uniaxial tensile tests.

For anisotropic materials the coefficients can be different for the (uniaxial) out-of-plane direction, the rolling, and transverse rolling direction, as well as at 45° to the rolling direction.

The representation of normal or planar anisotropy is achieved by defining a single power-law yield function. The different stress-plastic strain curves are recovered from the power-law yield function by means of multiplication by constants.

Strain-Rate Dependence

In some metals, the rate of stretching affects the mechanical properties; the material yields at a higher effective stress state for higher imposed strain rates. The yield stress for a plastic process is also higher. This effect can be accounted for in the power-law yield function by defining the strain-rate sensitivity constant k, and the strain-rate exponent m. By default, strain-rate dependence is not taken into account.

Forming Limit Diagram

A forming limit diagram (FLD) can be input on the SHEETMAT, BARLT89, and BARLT00entries to evaluate actual and potential problems in sheet-metal forming processes. The diagram forms the lower bound of experimental strains corresponding to regions affected by necking. This implies strains below the limit curve are acceptable.

The forming limit diagram is composed of two polynomial functions (see Figure 3-5.). You can supply the coefficients representing these functions for the material under consideration.

Two different ways of postprocessing are possible. First, a contour plot of the Forming Limit Parameter (FLP) can be made. The FLP denotes the ratio of predicted strain and allowable strain. In equation form:

$$FLP = \frac{e_1}{FLD(e_2)}$$

where e_1 and e_2 are respectively major and minor principal engineering strain at the integration point.

The parameter is accessible via the output variable FLP# (where # equals the integration layer number). The FLP contour plot shows an overall view of regions where necking (followed by failure) possibly occurs. Failure is indicated when FLP is greater than or equal to one.

The second method of visualization is to use the minor and major principal strains (output variables EPSMN# and EPSMX#) and plotting these strains for any particular element versus the experimental forming limit diagram. By convention, these strains are output as true strain. The forming limit diagram is usually plotted against engineering strains. As a result, the output variables EPSMN# and EPSMX# must be converted to engineering strains.

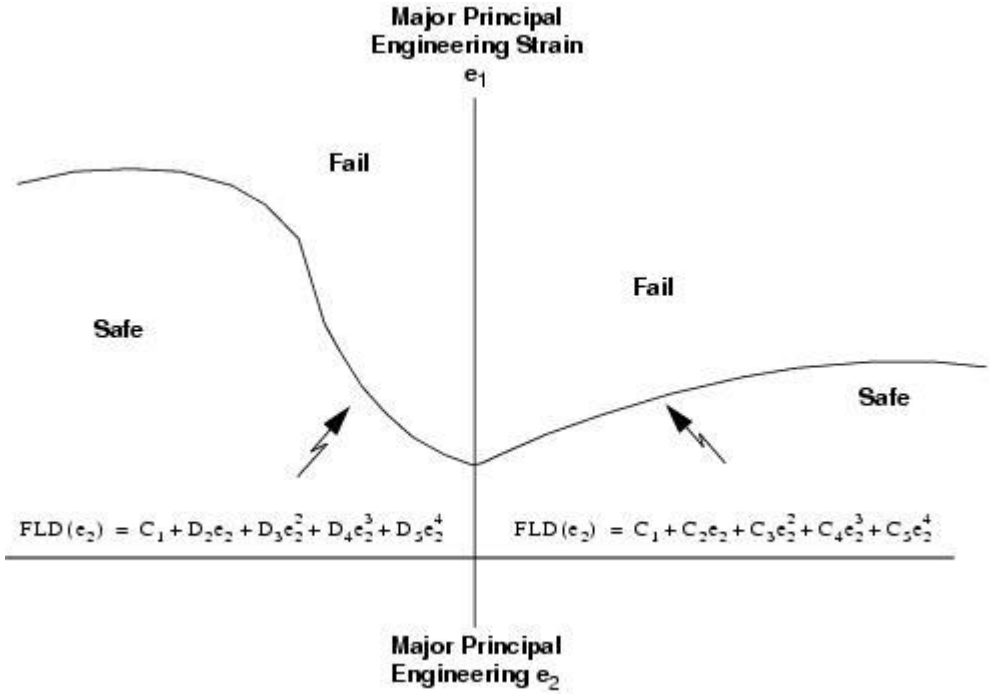

Figure 3-5 Forming Limit Diagram Represented by Two Polynomials

DYMAT14 – Soil and Crushable Foam

This model is for materials exhibiting compressible plasticity; that is, their behavior is pressure dependent. It can be used to model aspects of the behavior of a wide range of materials that contain voids and crush or compact under pressure. Examples include soils, foams, concrete, metallic honeycombs, and wood.

The material model is based on that developed by Krieg and Key. It uses isotropic plasticity theory and the response of the material to deviatoric (shear) loading and hydrostatic (pressure) loading is completely uncoupled.

Deviatoric Behavior

When the YSURF option is used on the DYMAT14 entry, the yield surface in principal stress space is a surface of revolution centered about the hydrostatic pressure line. It is defined by $\Phi_S(J_2, p) = 0$, where

$$\Phi_S = (J_2, p) = J_2 - (B_0 + B_1 p + B_2 p^2)$$

where p is the pressure, J_2 is the second invariant of the stress deviation tensor:

$$J_2 = \frac{1}{2} S_{ij} S_{ij}$$

where: S_{ij} are the deviatoric stresses. J_2 can also be defined in terms of the principal stresses σ_{ij}:

$$J_2 = \frac{1}{6}[(\sigma_{11} - \sigma_{22})^2 + (\sigma_{22} - \sigma_{33})^2 + (\sigma_{33} - \sigma_{11})^2] + \sigma_{12}^2 + \sigma_{22}^2 + \sigma_{31}^2$$

The coefficients B_0, B_1 and B_2 can be related to the user-defined constants A_0, A_1, and A_2. This relation depends on the YSTYP field on the DYMAT14 entry. If the YSTYP field is DYTRAN, then

$$B_0 = A_0$$

$$B_1 = A_1$$

$$B_2 = A_2$$

Thus, if A_1 and A_2 are zero, the yield surface is cylindrical. If only A_2 is zero, the surface is conical; otherwise, the surface has a shape as shown in Figure 3-6.

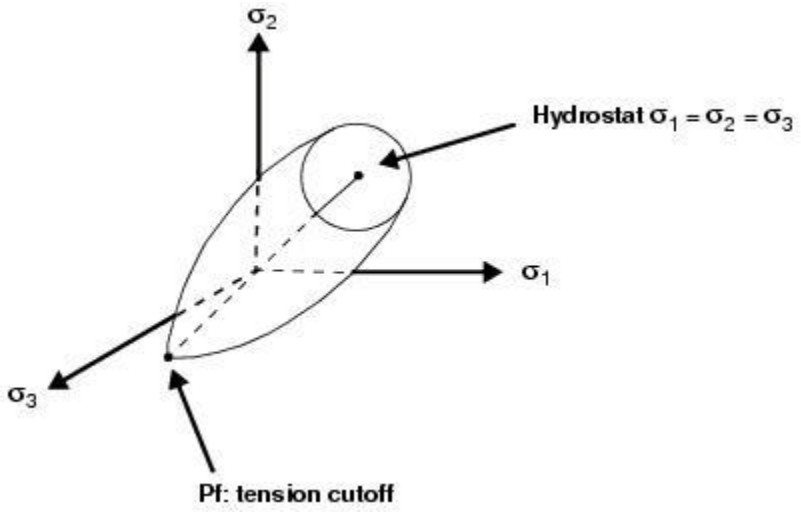

Figure 3-6 Yield Surface with Hydrostat

If the YSTYP field is DYNA, then

$$B_0 = \frac{1}{3}A_0^2$$

$$B_1 = \frac{2}{3}A_0A_1$$

$$B_2 = \frac{1}{3}A_1^2$$

and A_2 is ignored.

In this case, the yield surface is cylindrical when A_1 is zero and it has a shape as shown inFigure 3-6 when A_1 is nonzero.

For both options of YSTYP the yield stress σ_y can be expressed in terms of the coefficients A_0, A_1, and A_2. The yield stress is defined as:

$$\sigma_y = \sqrt{3}J_2, \text{ where } J_2 = \{J_2 | \Phi_S(J_2,p) = 0\}$$

Thus,

$$\sigma_y = \sqrt{3(B_0 + B_1p + B_2p^2)}$$

$$= \begin{cases} \sqrt{3(A_0 + A_1 p + A_2 p^2)} & \text{if YSTYP = DYTRAN} \\ A_0 + A_1 p & \text{if YSTYP = DYNA} \end{cases}$$

The cut-off pressure can be supplied by the user but should not have a positive value. When the cut-off pressure is left blank, Dytran calculates this value as the intersection point of the yield surface with the hydrostat. When only B_0 is nonzero (and therefore only A_0 is nonzero), the cut-off pressure is calculated as –100 times the bulk modulus defined on the DYMAT14 entry.

The open end of the cylinder, cone, or paraboloid points into compression and is capped by a plane that is normal to the hydrostat. There is no strain hardening on the yield surface, so the relationship between deviatoric stress σ' and deviatoric strain ε' is elastic perfectly plastic as shown in Figure 3-7.

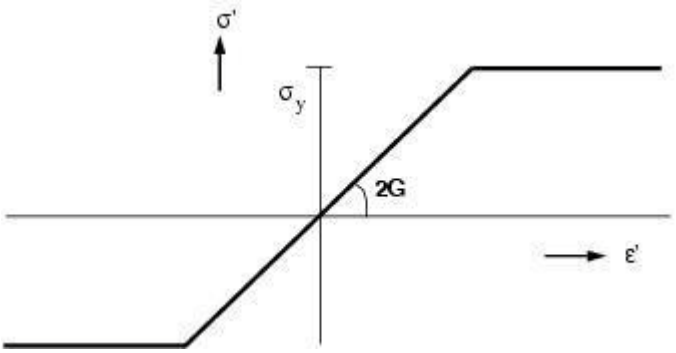

Figure 3-7 Stress-Strain Curve

In other words, in case of yielding, the yield surface remains stationary as yielding occurs. The elastic behavior is governed by the shear modulus G.

Hydrostatic Behavior

The hydrostatic component of the loading causes volumetric yielding. This means that the cap on the open end of the yield surface moves along the hydrostat as volumetric yielding occurs. The relationship between hydrostatic pressure and volumetric strain is defined using a TABLED1 entry and can be of any shape (Figure 3-8).

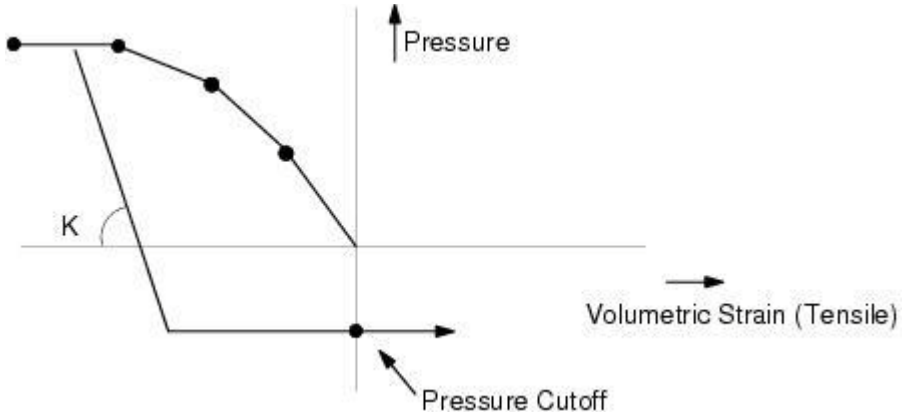

Figure 3-8 Volumetric Yielding

The curve can be defined in terms of the crush factor or volumetric strain. The crush factor is defined as $1 - V/V0$ where V is the current volume and $V0$ the initial volume. It is a number between 0 and 1 where 0 indicates no crush and 1 indicates that the material is completely crushed and has zero volume. The crush factor, in fact, is minus the engineering strain. The volumetric strain is defined as

$$\int_{to}^{t} \frac{dV}{V} \text{ or } ln(V/V0)$$

The volumetric strain must always be negative.

The material unloads elastically from any point on the curve with a user-defined bulk modulus K. You can also specify a minimum pressure (*PMIN*) cutoff (Figure 3-9a) or a failure pressure (*PFRAC*) cutoff (Figure 3-9b). In the first case, since pressure is positive in compression, this corresponds to a tensile cutoff for the material. The pressure cannot fall below the minimum value. If the initial loading is tensile, the material will behave elastically with a bulk modulus K until the minimum pressure is reached. Further tensile straining produces no increase in pressure. In the second case, you specify a failure pressure rather than a minimum pressure. If the pressure falls below the failure pressure, the element fails and cannot carry tensile loading for the remainder of the analysis. It can still carry compressive loading.

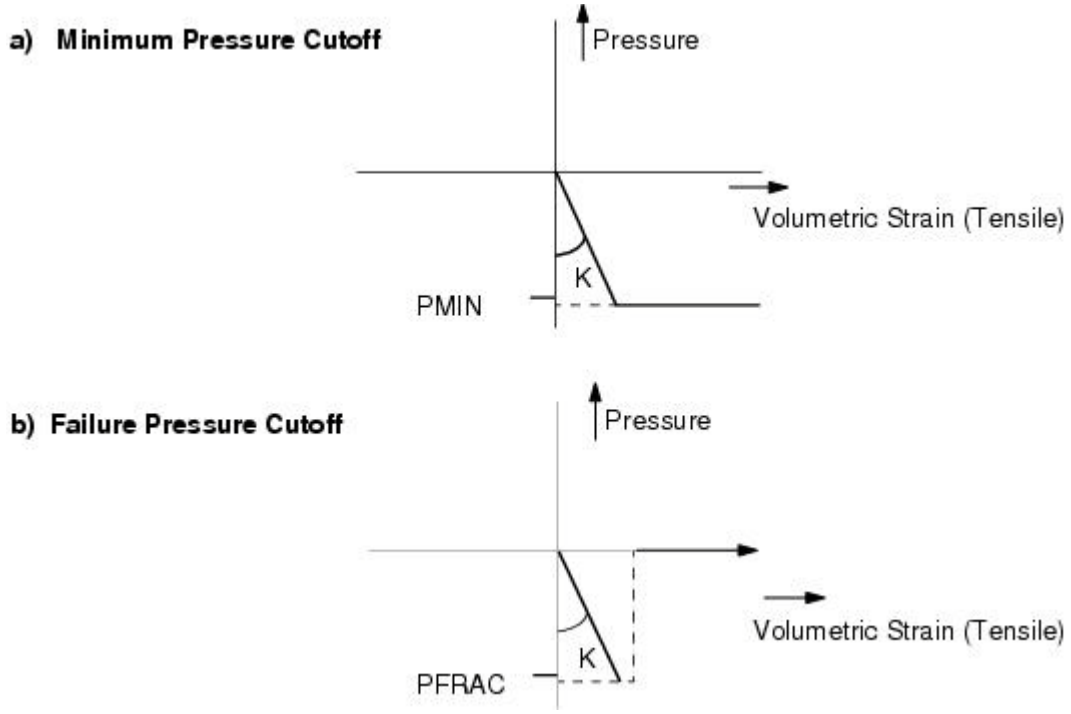

Figure 3-9 Pressure as Function of Volumetric Strain

Under compressive loading, the material follows the strain-pressure curve (Figure 3-10).

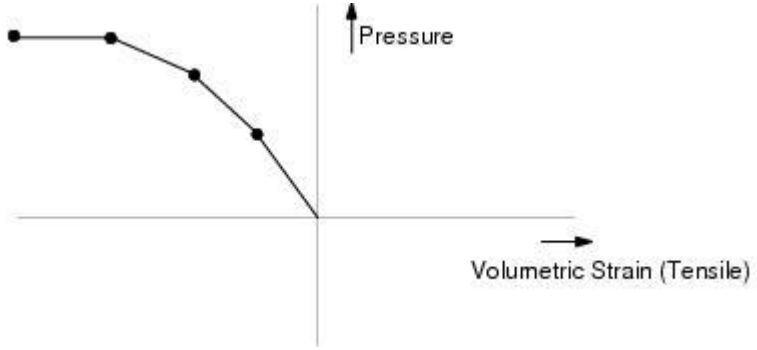

Figure 3-10 Pressure as Function of Volumetric Strain in Compression

If the material then unloads, it does so elastically until the minimum (or failure) pressure is reached, after which further tensile straining does not produce any increase in pressure (Figure 3-11).

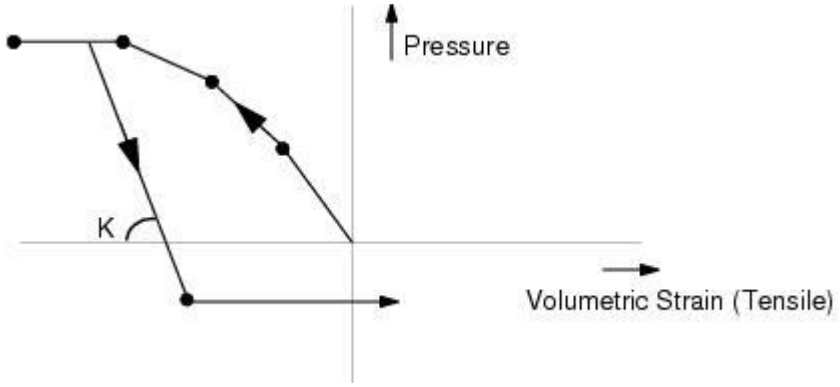

Figure 3-11 Pressure as Function of Volumetric Strain in Compression and Expansion

Determination of Yield Curve

The remainder of this section describes the experiments that can be performed to obtain the pressure-strain curve and values for A_0, A_1, and A_2 for the `YSURF` option.

The most accurate way is to perform a volumetric test and a uniaxial compression test. If a volumetric test is not available, a uniaxial compression test can give a good approximation.

1. Volumetric test

   All sides are equally compressed.

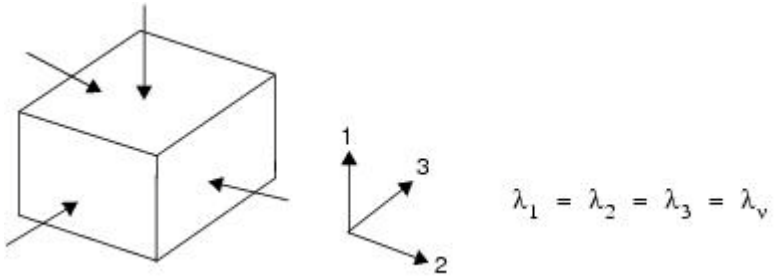

   The volumetric test can be performed by exerting pressure on the foam via a fluid.

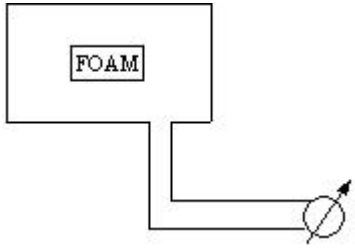

The volumetric change is equal to additional fluid entering the chamber.

The test results directly in a pressure-crush curve:

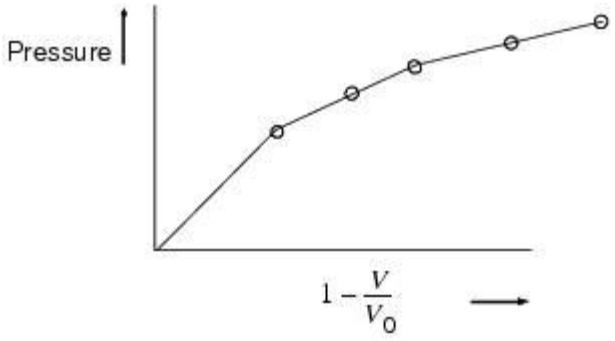

2. Uniaxial compression test

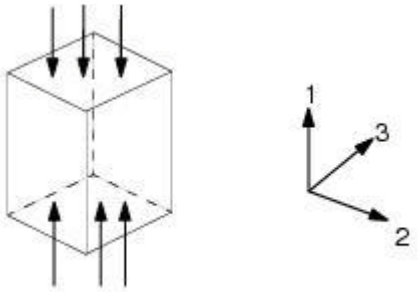

The stress in the 1-direction t_{11} can be measured as a function of $\frac{V}{V_0}$. Note that the engineering stress is equivalent to the true stress since Poisson effects are typically small for crushable foams. As for the strains holds:

$$e_{11} = ln\frac{V}{V_0},\ e_{22} \approx 0,\ e_{33} \approx 0$$

During crushing, the stresses are computed by the following equations:

Dyna Method

$$t_{11} = -\frac{2}{3}A_0 + p\left(-\frac{2}{3}A_1 - 1\right)$$

$$t_{22} = \frac{1}{3}A_0 + p\left(\frac{1}{3}A_1 - 1\right)$$

$$t_{33} = \frac{1}{3}A_0 + p\left(\frac{1}{3}A_1 - 1\right)$$

Dytran Method

$$t_{11} = -\frac{2}{3}\sqrt{3(A_0 + A_1 p + A_2 p^2)} - p$$

$$t_{22} = \frac{1}{3}\sqrt{3(A_0 + A_1 p + A_2 p^2)} - p$$

$$t_{33} = \frac{1}{3}\sqrt{3(A_0 + A_1 p + A_2 p^2)} - p$$

Therefore, when the volumetric test can be carried out, you obtain the $p\left(\frac{V}{V_0}\right)$ relation. From the uniaxial test, we find $t_{11}\left(\frac{V}{V_0}\right)$. For the DYNA option, the constants A_0 and A_1 can then be fitted from the $p\left(\frac{V}{V_0}\right) - t_{11}\left(\frac{V}{V_0}\right)$ curve:

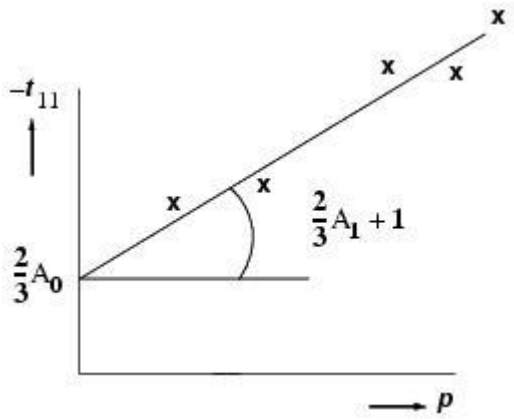

For the DYTRAN option, the constants A_0, A_1, and A_2 must be fitted from a $p\left(\frac{V}{V_0}\right) - t_{11}\left(\frac{V}{V_0}\right)$ curve, which is not a straight line.

When the volumetric test is not available, the following approximation can be made:

$$t_{22} = t_{33} = 0$$

So that the pressure becomes:

$$p = -\frac{1}{3}(t_{11} + t_{22} + t_{33}) = -\frac{1}{3}t_{11}$$

When t_{11} can be measured from a uniaxial test, the pressure curve is determined. The constants A_0, A_1, and A_2 are determined such that the above equations hold.

Dyna:

$$A_0 = 0.0$$
$$A_1 = 3.0$$

Dytran:

$$A_0 = 0.0$$
$$A_1 = 0.0$$
$$A_2 = 3.0$$

DYMAT24 – Piecewise Linear Plasticity

This model can be used for isotropic, elastoplastic materials where the stress-strain characteristic is too complex to be modeled by a bilinear representation. You can specify a table containing a piecewise linear approximation of the stress-strain curve (Figure 3-12) for the material.

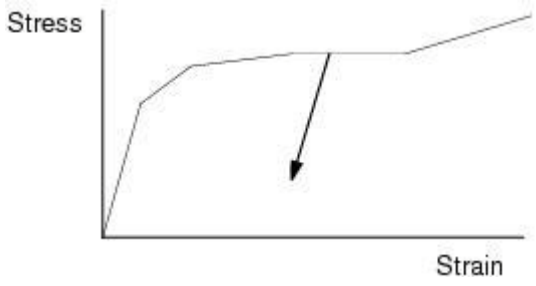

Figure 3-12 Stress-Strain Curve

Every iteration the stress σ is determined from the current equivalent strain ε by interpolating from the stress-strain table:

$$\sigma = [(\sigma_i - \sigma_{i-1})(\varepsilon - \varepsilon_{i-1})/(\varepsilon_i - \varepsilon_{i-1})] + \sigma_{i-1}$$

where σ_i and ε_i are the points in the table.

The stress-strain characteristic used internally in Dytran is defined in terms of true stress and equivalent plastic strain. However, for convenience, the stress-strain characteristic can be input in any of the following ways:

- True stress/true strain.
- Engineering stress/engineering strain.

- True stress/plastic strain.
- Plastic modulus/plastic strain.

Alternatively, you can specify the hardening modulus and yield stress, in which case a bilinear representation is used:

$$\sigma = \sigma_y + E_l \bar{\varepsilon}_p$$

where $\bar{\varepsilon}_p$ is the equivalent plastic strain. Hardening is assumed to be isotropic; the yield surface expands as the material yields.

This material can be used with all solid, shell (except for membranes), and Hughes-Liu beam elements. Strain-rate sensitivity and failure can be included for all of these elements. Strain-rate sensitivity can be defined in two ways:

1. You can specify a table giving the variation of a scale factor S with strain-rate $\dot{\varepsilon}$. The scale factor is multiplied by the stress found from the stress-strain characteristic to give the actual stress. The failure criterion is based on plastic strain. When the plastic strain exceeds the specified value, the element fails. All stresses are set to zero, and the element can carry no load.
2. You can specify the constants `D` and `P` in Cowper-Symonds rate enhancement formula:

   $$\frac{\sigma_d}{\sigma_y} = 1 + \left(\frac{\dot{\varepsilon}}{D}\right)^{1/P}$$

   where σ_d is the dynamic stress, σ_y is the static yield stress, and ε is the equivalent strain rate.

DYMAT25 - Cap Material Model

The cap material model can be used for geomechanical problems with materials like soil, concrete and rock. This section gives a brief description of the model and references to literature where more details on the material model can be found.

The cap model is characterized by the following constitutive equations:

$$\varepsilon = \varepsilon^e + \varepsilon^p, \text{ and } \sigma = C(\varepsilon - \varepsilon^p)$$

where ε, ε^e, and ε^p are the total, elastic and plastic strain tensor, C the elasticity matrix and σ the stress tensor. The flow rule is given by:

$$\dot{\varepsilon}_p = \sum_{k=1}^{e} \dot{\lambda}_k \frac{\partial f_k}{\partial \sigma}$$

where the sum is over the active yield surfaces f_k, i.e., the failure envelope $(k = 1)$, the hardening cap surface $(k = 2)$, and the fixed tension cutoff surface $(k = 3)$. The yield conditions are defined by:

$f_1(\sigma) \le 0\,,\ f_2(\sigma, \kappa) \le 0\,,\ f_3(\sigma) \le 0$

The hardening parameter κ for the cap model is related to the plastic volume change by a hardening law.

The cap model is a plasticity model described by a yield surface that is defined by means of a failure envelope, a hardening cap and a tension cut off. Figure 3-13 shows the typical yield surfaces in a cap model.

The failure envelope surface is denoted by

$$f_1 = \sqrt{J_{2D}} - \min(F_e(J_1), T_{mises})$$

and the cap by

$$f_2 = \sqrt{J_{2D}} - F_c(J_1, \kappa) \text{ for } L(\kappa) \ge J_1 \ge X(\kappa)$$

where J_1 is the first invariant (trace) of the stress tensor, J_{2D} is the second invariant of the stress deviator, κ is an internal state variable that measures hardening as a functional of the history of plastic volumetric strain and $L(\kappa)$, $X(\kappa)$ define the J_1 range of the cap. Note that J_1 is chosen as negative in tension.

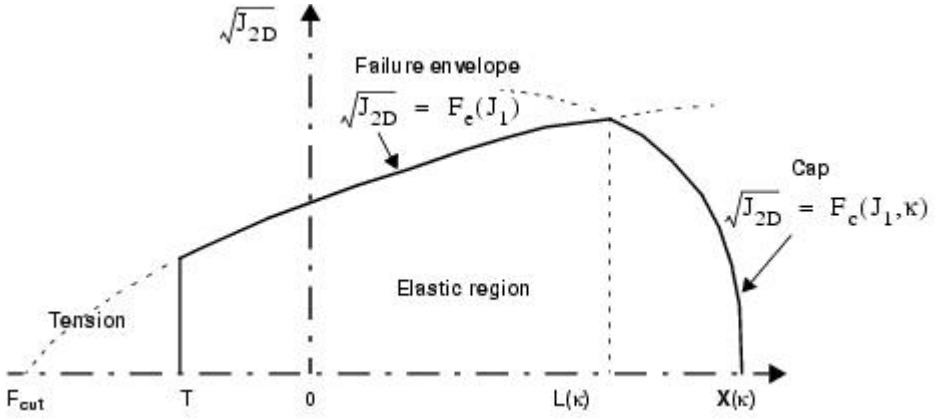

Figure 3-13 Typical Yield Surfaces in a Cap Model

The functions F_e and F_c are given by (see Appendix A. References 1. and 2.):

$$F_e(J_1) = \alpha - \gamma\exp(-\beta J_1) + \theta J_1$$

$$F_c(J_1,\kappa) = \frac{1}{R}\sqrt{[X(\kappa) - L(\kappa)]^2 - [J_1 - L(\kappa)]^2}$$

$$T_{mises} = \frac{1}{R}|X(\kappa) - L(\kappa)|\,.$$

The von Mises type transition failure surface is defined by the following:

The intersection of the cap with the (hydrostatic) J_1 axis is given by:

$$X(\kappa) = \kappa + RF_e(\kappa)$$

and $L(\kappa)$ is defined by:

$$(\kappa) = \kappa = \begin{cases} \kappa & \text{if} \quad \kappa > (\\ 0 & \text{if} \quad \kappa \le (\end{cases}$$

The hardening parameter κ is related to the actual plastic volume change:

$$\varepsilon_v^p(X) = W\{1 - \exp[-D(X(\kappa) - X_0)]\}$$

The tension cut off surface is given by the function:

$$f_3 = T - J_1$$

where T is the maximum hydrostatic tension sustainable by the material.

Kinematic work hardening for the failure envelope surface is based on the approach of Isenberg et. Al. [1978]. It is switched on by specifying N. The failure envelope surface is replaced by a family of envelope surfaces that are bounded by an initial yield surface and by a limiting failure envelope surface. Which member of the family is taken, is implemented by replacing in all yield relations the stress tensor σ by $\sigma - \varsigma$ where ς is a deviatoric tensor that accumulates in time. This tensor ς is called the "back stress tensor" and is defined by

$$\frac{d\varsigma}{dt} = \bar{c}\bar{F}(\sigma,\varsigma)\frac{d\varepsilon^p}{dt}$$

$$\bar{F} = max\left(0,1 - \frac{(\sigma-\varsigma)\bullet\varsigma}{2NF_e(J_1)}\right.$$

Here ε^p is the deviatoric plastic strain tensor, N denotes the size of the yield surface and represents the radial distance between the outside of the initial yield surface and the inside of the limit surface. After each increment of ς, it is checked whether its second invariant exceeds N. In that case, ς is scaled by a scalar such that its second invariant equals N. For consistency between the limit surface of the kinematic hardening cap model and the failure envelope of the standard cap model, the parameter α is placed by $\alpha - N$.

DYMAT26 – Crushable Orthotropic Material

The DYMAT26 entry defines the properties of an orthotropic, crushable material model. It can only be used with Lagrangian solid elements.

The input required for the material consists of two parts: data for the fully compacted state and data for the crushing behavior. For the fully compacted material, the input consists of the density, the elastic modulus for the fully compacted material, Poisson's ratio for the fully compacted material, the yield stress for the fully compacted material, and the relative volume at which the material is fully compacted.

The behavior during crushing is orthotropic and is characterized by uncoupled strain behavior when the initial Poisson's ratios are not supplied. During crushing, the elastic moduli (and the Poisson's ratios only if they are supplied) vary from their initial values to the fully compacted values. This variation is linear with relative volume.

When the material is fully compacted, the behavior is elastic perfectly plastic with isotropic plasticity.

The load tables define the magnitude of the average stress in a given direction as the material's relative volume changes. At defining the curves, care should be taken that the extrapolated values do not lead to negative yield stresses.

RUBBER1 – Mooney-Rivlin Rubber Model

The RUBBER1 entry defines the properties of a Mooney-Rivlin rubber model. It can only be used with Lagrangian solid elements.

The constitutive behavior of this material is defined as a total stress-total strain relationship. Rather than by Hooke's law, the nonlinear elastic material response is formulated by a strain energy density function

accounting for large strain components. The strain energy density function is defined according to the Mooney-Rivlin model:

$$W(I_1, I_2, I_3) = A(I_1 - 3) + B(I_2 - 3) + C\left(\frac{1}{I_3^2} - 1\right) + D(I_3 - 1)^2$$

The constants A and B, and Poisson's ratio v are the input parameters for the model. The constants C and D are related to the input parameters as:

$$C = \frac{1}{2}A + B$$

$$D = \frac{A(5v - 2) + B(11v - 5)}{2(1 - 2v)}$$

I_1, I_2, and I_3 are strain invariants in terms of stretches. Stretches are defined as:

$$\frac{\delta x_i}{\delta X_j} = \lambda_{ij}$$

where x_i and X_j are, respectively, the coordinates of the deformed and the original geometry.

For rubber-like materials, the shear modulus G is much less than the bulk modulus K. In this case, $G = 2(A + B)$.

The stresses are computed as:

$$\tau = (detF)^{-1} \cdot F \cdot \sigma \cdot F^T$$

where σ is the second Piola-Kirchhoff stress tensor:

$$\sigma = 2\frac{\partial W}{\partial C}$$

The Cauchy-Green stretch tensor C is defined as:

$$C = F^T F$$

where F is the deformation gradient tensor

$$F = \frac{\delta x}{\delta X}$$

In terms of principal stretches λ_1,λ_2, λ_3 (for example, the stretches in the coordinate system where all shear strains and shear stresses vanish) the expressions for the deformation gradient tensor F, and the Cauchy-Green stretch tensor C simplify to

$$F = \begin{bmatrix} \lambda_1 & 0 & 0 \\ 0 & \lambda_2 & 0 \\ 0 & 0 & \lambda_3 \end{bmatrix}, C = \begin{bmatrix} \lambda_1^2 & 0 & 0 \\ 0 & \lambda_2^2 & 0 \\ 0 & 0 & \lambda_3^2 \end{bmatrix}$$

The strain invariants I_1, I_2, and I_3 read

$$I_1 = \lambda_1^2 + \lambda_2^2 + \lambda_3^2$$

$$I_2 = \lambda_1^2\lambda_2^2 + \lambda_2^2\lambda_3^2 + \lambda_3^2\lambda_1^2$$

$$I_3 = \lambda_1^2\lambda_2^2\lambda_3^2$$

The stresses can be written as

$$J\tau_{ii} = \lambda_i \frac{\partial W}{\partial \lambda_i}$$

where $J = \lambda_1\lambda_2\lambda_3 = \frac{dV}{dV_0}$

Determination of Rubber Material Parameters

The remainder of this section describes the experiments that can be performed to obtain the material parameters as they appear in the strain-energy density function. The most commonly performed tests are uniaxial, planar (shear), and volumetric tests.

A planar or shear test can be used to determine the shear modulus $G(= 2(A + B))$. Tensile or compression tests provide the same information. Since rubber is a nearly incompressible material, the volume is assumed to be constant. Therefore, the principal stretches λ_1, λ_2, and λ_3 can be written as

$$\lambda_1 = \lambda_s, \lambda_2 = 1, \lambda_3 = \frac{1}{\lambda_s}$$

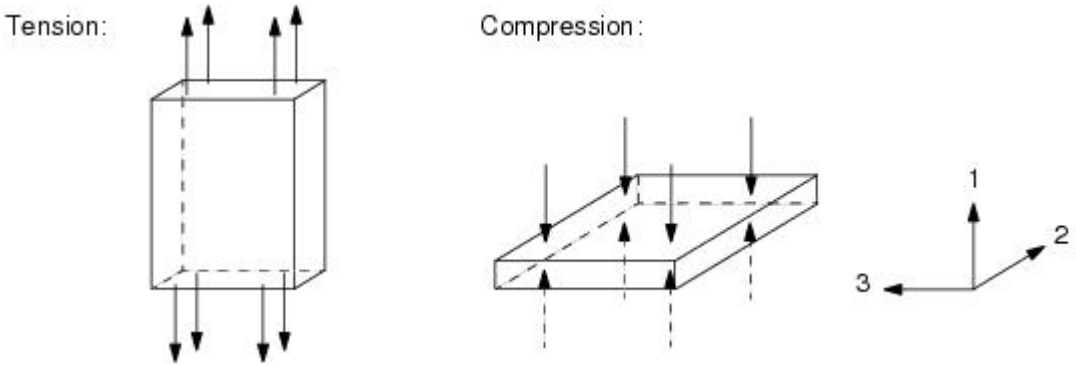

The stresses in the 1- and 3-direction are given by

$$\tau_{11} = \lambda_1 \frac{\partial W}{\partial \lambda_1} = \lambda_1 \left[\frac{\partial W}{\partial I_1} \frac{\partial I_1}{\partial \lambda_1} + \frac{\partial W}{\partial I_2} \frac{\partial I_2}{\partial \lambda_1} + \frac{\partial W}{\partial I_3} \frac{\partial I_3}{\partial \lambda_1} \right] = 2(A+B)\left(\frac{1}{\lambda_s^2} - 1 \right)$$

$$\tau_{33} = \lambda_3 \frac{\partial W}{\partial \lambda_3} = \lambda_3 \left[\frac{\partial W}{\partial I_1} \frac{\partial I_1}{\partial \lambda_3} + \frac{\partial W}{\partial I_2} \frac{\partial I_2}{\partial \lambda_3} + \frac{\partial W}{\partial I_3} \frac{\partial I_3}{\partial \lambda_3} \right] = 2(A+B)\left(\frac{1}{\lambda_s^2} - 1 \right)$$

The corresponding forces per unit cross-sectional area then become

$$F_1 = \tau_{11} \frac{A_1}{A_{0_1}} = \frac{\tau_{11}}{\lambda_s} = 2(A+B)\left(\lambda_s - \frac{1}{\lambda_s} \right) = G\left(\lambda_s - \frac{1}{\lambda_s} \right)$$

$$F_3 = \tau_{33} \frac{A_3}{A_{0_3}} = \tau_{33} \lambda_s = 2(A+B)\left(\lambda_s - \frac{1}{\lambda_s} \right) = G\left(\lambda_s - \frac{1}{\lambda_s} \right)$$

where A_{0_1} and A_{0_3} are the original areas. A_1 and A_3 are given as

$$A_1 = \frac{1}{\lambda_s A_{0_1}}, \; A_3 = \lambda_s A_{0_3}$$

Fitting the measured force versus stretch curve with curve from the model, $F = G\left(\lambda_s - \frac{1}{\lambda_s} \right)$, the shear modulus can be estimated.

The experiment is usually performed with a thin, short, and wide rectangular strip of material fixed at its wide edges to rigid loading clamps that are moved apart (Figure 3-14).

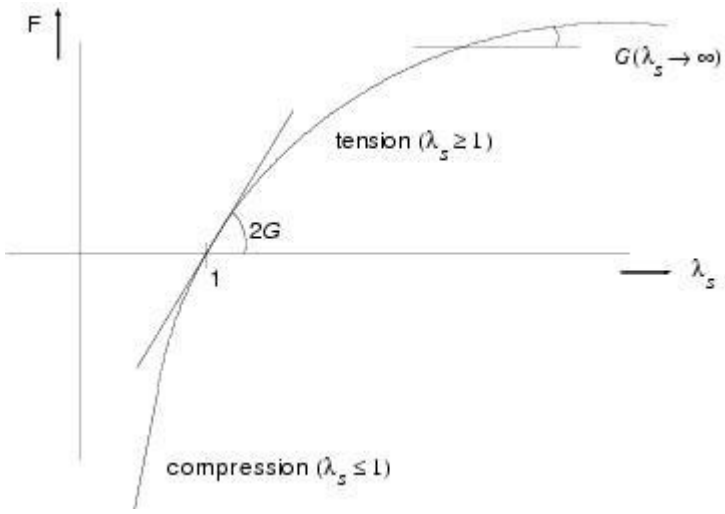

Figure 3-14 Force Versus Stretch Diagram

The above test does not show how the constants A and B can be determined. For this purpose, a uniaxial test (elongation or compression) is recommended. No sides are clamped and one side (the 1-direction, see figure below) is either elongated or compressed. Since the material is nearly incompressible, the principal stretches are then given by

$$\lambda_1 = \lambda_\mu, \lambda_2 = \lambda_3 = \frac{1}{\sqrt{\lambda_\mu}}$$

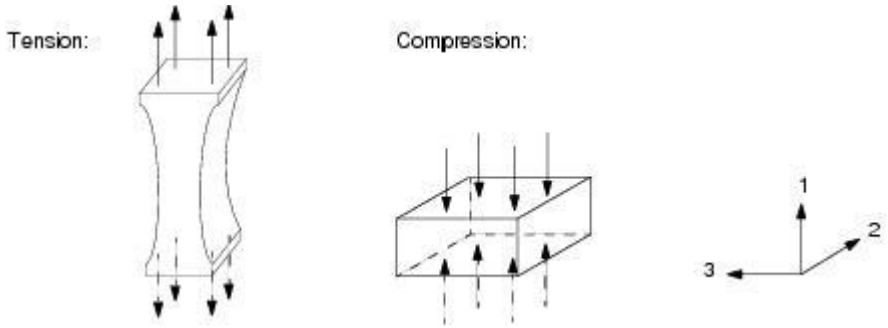

The stress per unit deformed cross-sectional area in uniaxial direction is given by

$$\tau_{11} = \lambda_1 \frac{\partial W}{\partial \lambda_1} = 2A(\lambda_\mu^2 - 1) + 4B(\lambda_\mu - 1)$$

The corresponding force applied to a unit original cross-sectional area F then becomes

$$F = \tau_{11}\frac{A_1}{A_{0_1}} = \frac{\tau_{11}}{\lambda_\mu} = 2A\left(\lambda_\mu - \frac{1}{\lambda_\mu}\right) + 4B\left(1 - \frac{1}{\lambda_\mu}\right)$$

where A_{0_1} is the original area at time zero, and A_1 is given as

$$A_1 = \frac{1}{\lambda_\mu}A_{0_1}$$

Furthermore, since

$$\frac{dF}{s\lambda_\mu} = 2A + \frac{2A + 4B}{\lambda_u^2}, \frac{d^2F}{d\lambda_\mu^2} = -\frac{4A + 8B}{\lambda_\mu^3}$$

it follows that F is an increasing convex function due to the only relevant physical conditions

$A > 0$

$A + 2B > 0$

The analytical function is schematically shown in Figure 3-15.

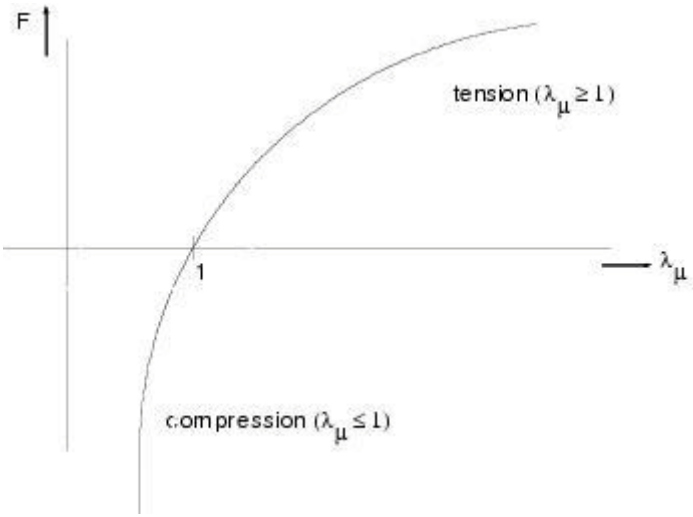

Figure 3-15 Force Versus Stretch Diagram

Linear fitting can easily be achieved by applying the transformation

$$\tilde{F} = \frac{\lambda_\mu}{\lambda_\mu - 1}F$$

For the Mooney-Rivlin approach, the force $\tilde{F}$ then becomes

$$\tilde{F} = 2A\lambda_\mu + 2(A + 2B)$$

which is a straight line with slope $2A$ and the intersection point with $\lambda_\mu = 0$ axis equal to $2(A + 2B)$. It must be noted, however, that the transformation can only be applied to the measured force for intervals of λ_μ, where the measured force is an increasing convex function of the principal stretch λ_μ. A reasonable estimation interval for compression (λ_1, λ_2), and for tension (λ_3, λ_4) is indicated in Figure 3-16.

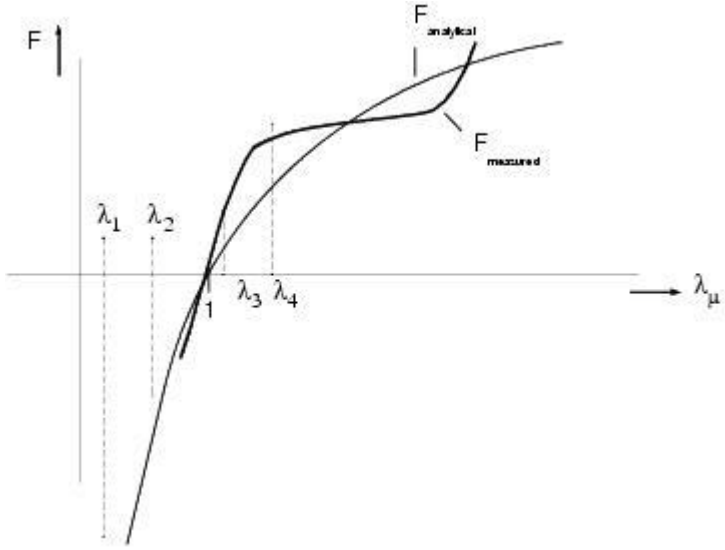

Figure 3-16 Force Versus Stretch Diagram

The final test to be discussed is a volumetric compression test. It can be used to determine the bulk modulus K. The test can be performed in two ways.

1. Two sides clamped (the 2- and 3-directions), one side compressed (the 1-direction):

$$\lambda_1 = \lambda_v, \lambda_2 = \lambda_3 = 1.$$

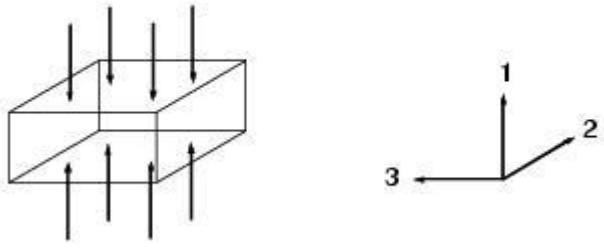

Since the area A_1 does not change shape, the force applied to a unit cross-sectional area is equal to the stress

$$F = \tau_{11} = 2(A + 2B)\left(\lambda_v^2 - \frac{1}{\lambda_v^4}\right) + 4D(\lambda_v^4 - \lambda_v^2)$$

The constant D was defined as

$$D = \frac{A(5v - 2) + B(11v - 5)}{2(1 - 2v)}$$

and

$$v = \frac{3K - 2G}{6K + 2G}$$

the force can be written as

$$F = \frac{1}{2}K\lambda_v^2(\lambda_v^2 - 1) - \left(\frac{14}{3}A + \frac{32}{3}B\right)\lambda_v^4 + \left(\frac{20}{3}A + \frac{44}{3}B\right) + \lambda_v^2 - \frac{2(A + 2B)}{\lambda_v^4}$$

The material is assumed to be nearly incompressible; therefore, $\lambda_v = 1 - \varepsilon$ with $\varepsilon \ll 1$. Applying this assumption to the above equation and neglecting higher-order terms yields

$$F \approx -\left(K + \frac{4}{3}G\right)\varepsilon$$

As a result, the slope of the measured force curve around $\lambda_v = 1$ gives an estimate for $K + \frac{4}{3}G$.

When G is known, using the expression for Poisson's ratio v results in a value for the input parameter v.

2. All sides equally compressed:

$$\lambda_1 = \lambda_2 = \lambda_3 = \lambda_v$$

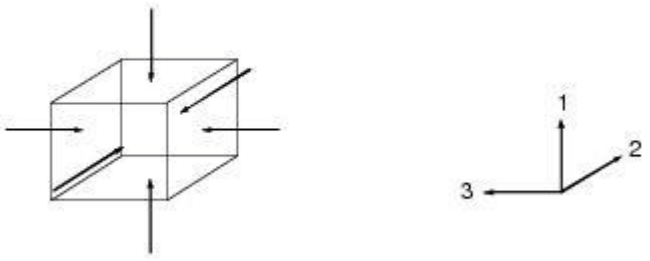

For this test, the pressure P can be measured. An analytical expression for the pressure according to the Mooney-Rivlin approach is

$$P = -\frac{1}{3}(\tau_{11}+\tau_{22}+\tau_{33}) = 2A\left(\frac{1}{\lambda_v^{15}}-\frac{1}{\lambda_v}\right)+4B\left(\frac{1}{\lambda_v^{15}}-\lambda_v\right)-4D\lambda_v^3(\lambda_v^6-1)$$

Again, substitution of $\lambda_v = 1-\varepsilon$ and neglecting higher-order terms of ε yields

$$P = 2(14A+32B+12D)\varepsilon = 3K\varepsilon$$

Therefore, the slope of the pressure curve at $\lambda_v = 1$ determines the bulk modulus K and Poisson's ratio v.

RUBBER2 – Ogden Rubber Model

The RUBBER2 entry defines the properties of an Ogden rubber model. It can only be used with Lagrangian solid elements.

The constitutive behavior of this material is defined as a total stress-total strain relationship. Rather than by Hooke's law, the nonlinear elastic material response is formulated by a strain energy density function accounting for large strain components. The strain energy density function is defined according to the Ogden model:

$$W = \sum_{i=1}^{}\sum_{i-1}\frac{\mu_j}{\alpha_j}(\bar{\lambda}_i^{\alpha_j}-1)+\frac{1}{2}K(J-1)^2$$

where μ_j and α_j, are the material constants, $\bar{\lambda} = \lambda/(\sqrt[3]{J}$ and $J = \lambda_1\lambda_2\lambda_3$.

For rubber-like materials, the shear modulus is much less than the bulk modulus. The shear modulus,

$$G = \frac{1}{2}\sum_{j=1}^{n}\mu_j\alpha_j$$

And the bulk modulus,

$$K = \frac{2G(1+\nu)}{3(1-2\nu)}$$

where, ν is the Poisson's ratio which is close to 0.5.

Stretches (deformation gradient tensor) are defined as:

$$\frac{\partial x_i}{\partial X_i} = F_{ij}$$

where x_i and X_i are, respectively, the coordinates of the deformed and the original geometry.

The right Cauchy-Green tensor are computed as:

$$C_{ij} = F_{ki}F_{kj}$$

The principal Kirchoff stress components are given by:

$$\tau_{ii}^{E} = \lambda_i \frac{W}{\partial \lambda_i} \text{ (this is not sum)}$$

where λ_i is the principal stretch.

The standard basis is extracted using standard formula:

$$\tau_{ij} = q_{ik}q_{jl}\tau_{kl}^{E}$$

where q_{ij} is the component of the orthogonal tensor containing the eigenvectors of the principal basis.

The Cauchy stress tensor is calculated using:

$$\sigma_{ij} = J^{-1}\tau_{ij}$$

FOAM1 – Foam Material (Polypropylene)

This model is used for an isotropic, crushable material model where Poisson's ratio is effectively zero.

The yield behavior is assumed to be completely determined by one stress-strain curve. In effect, this means that a uniaxial compression or tension test, a shear test, or a volumetric compression test all yield the same curves when stress (or pressure) is plotted versus strain (or relative volume $\frac{V}{V_0}$). The yield surface in three-dimensional space is a sphere in principal stresses

$$\tau_{11}^2 + \tau_{22}^2 + \tau_{33}^2 = R_s^2$$

where the radius of the sphere R_s depends on the strains as follows

$$R_s = f(R_e)$$

with

$$\varepsilon_{11}^2 + \varepsilon_{22}^2 + \varepsilon_{33}^2 = R_e^2$$

and f is the function supplied in the stress-strain table.

FOAM2 – Foam Material with Hysteresis

This model is used for an isotropic, crushable material model where Poisson's ratio is effectively zero and the unloading curve is a user-specified nonlinear hysteresis response stress-strain curve. The yield stress can also be made strain rate dependent.

The yield behavior is assumed to be completely determined by one stress-strain curve and a scale factor depending on the strain rate. In effect, this means that a uniaxial compression or tension test, a shear test, or a volumetric compression test all yield the same curves when stress (or pressure) is plotted versus strain (or relative volume $\frac{V}{V_0}$). The yield surface in three-dimensional space is a sphere in principal stresses

$$\tau_{11}^2 + \tau_{22}^2 + \tau_{33}^2 = R_s^2$$

where the radius of the sphere R_s depends on the strains and strain rates as follows

$$R_s = f_1(R_e) f_2(R_r)$$

with

$$\varepsilon_{11}^2 + \varepsilon_{22}^2 + \varepsilon_{33}^2 = R_e^2$$

and

$$\dot{\varepsilon}_{11}^2 + \dot{\varepsilon}_{22}^2 + \dot{\varepsilon}_{33}^2 = R_r^2$$

and f_1 is the function supplied in the stress-strain table and f_2 (if defined) is the function supplied in the factor-strain rate table.

The unloading curve is a nonlinear hysteresis response curve which is constructed such that the ratio of the dissipated energy (area between compressive loading and unloading curve) to total energy (area under the loading curve) is equal to the energy dissipation factor alpha.

In the case of linear unloading, Dytran automatically constructs a piecewise linear unloading curve, whose segments are parallel to the corresponding segments of the loading curve, except for the first and last segment which pass through the origin and point P (the point on the compression curve where the unloading starts), respectively. In the case of quadratic and exponential unloading, the curves are respectively constructed from a parabolic function $a_0\varepsilon^2 + a_1\varepsilon$ and an exponential function $a_0(e^{-a_1\varepsilon} - 1)$. The coefficients are computed such that the unloading curve starts in point P, and the area between the loading and unloading curves satisfies the energy dissipation condition.

When the unloading reaches the origin, further unloading follows a straight line with a slope equal to the Young's modulus until the tensile stress is reached. Either a minimum or a failure cut-off stress can be specified. In the first case the stress cannot fall below the minimum value, in the second case the stress is set to zero when the minimum is reached.

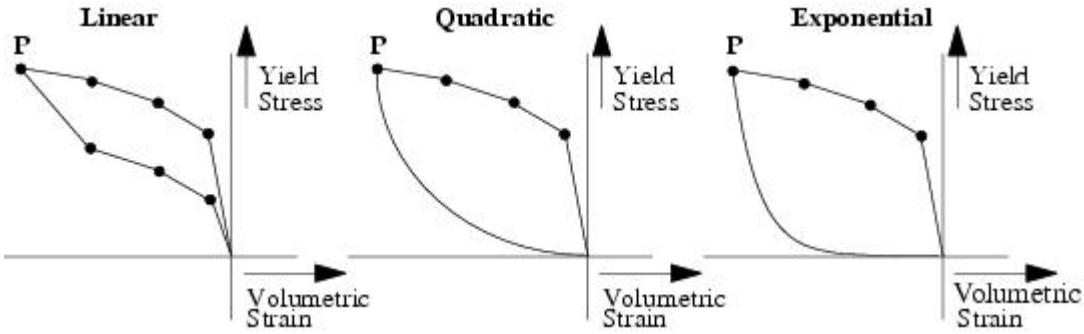

Figure 3-17 FOAM2 Unloading Curves

Mechanical Properties of Snow (Multisurface Plasticity)

Snow is a very specific material between water and ice. In micro term, the structure of snow looks like a general porous material where the degree of compaction can vary largely. Therefore, from the constitutive equation point of view, snow belongs to the family of soils. One of the plasticity models that applies to snow is a multisurface one.

The multisurface plasticity model for snow, see [Ref. 3.] and [Ref. 4.] *(warning: there are misprinting in the papers)* is characterized by two independent hardening (softening) mechanisms and a set of yield functions as shown in the following form:

$$f_c(I_1,J_2,q_c(\alpha_c)) = \sqrt{J_2 + \frac{c_c}{q_c}(\bar{I}_1 + q_c)^4} - \kappa_c \bar{I}_1 - \sqrt{c_c q_c^3} = 0$$

$$f_t(I_1,q_t(a_t)) = I_{1/3} - q_t = 0$$

I_1 and J_2 are the first and second invariant of the stress tensor and $\bar{I}_1 = T - I_1$. The material parameter T is related to the cohesion of snow. $q_c(q_t)$ is the hardening (softening) parameter associated with the yield surface $f_c(f_t)$. c_c determines the shape of f_c. Hence, it is a model parameter that may be set independently from the specific type of snow. κ_c is a material parameter related to the angle of friction. Figure 3-18 contains a plot of the yield functions f_c and f_t in the meridian plane at different stages of the hardening process of f_c and the softening process of f_t, respectively.

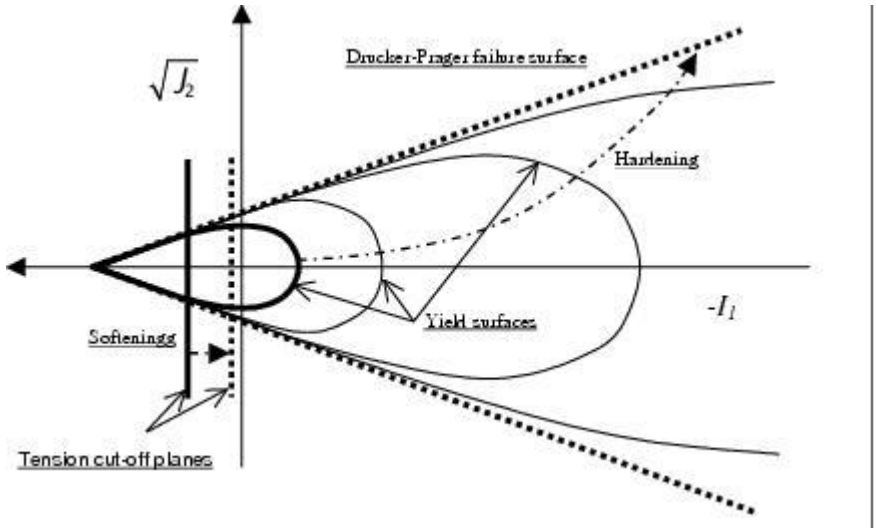

Figure 3-18 Snow Model: Plots of Loading Functions in the Meridian Plane

f_t defines a so-called "tension-cut-off"-plane perpendicular to the hydrostatic axis. For simplicity, a linear softening law is adopted:

$$q_t = f_{tu} - D_s \alpha_t$$

where f_{tu} is the hydrostatic tensile strength of snow, D_s is the softening modulus and α_t represents the accumulated plastic volumetric tensile strain.

For the implementation in Dytran, the accumulated plastic strain is updated if the tensile-pressure is bigger than the current q_t. The incremental strain is calculated using the difference of the pressure divided by the bulk modulus. Then the new q_t is updated to be used in the next cycle. Furthermore, the deviatoric stresses are brought to zero.

f_c constitutes a smooth yield function closed along the compressive and the tensile branch of the hydrostatic axis. Its shape in the stress space changes continuously in the course of hardening, see Figure 3-18. A specific hardening law, similar to the one used in the Cap Model [Ref. 6.] was adopted for snow on the basis of results from hydrostatic compression tests:

$$q_c = \frac{1}{2a_c} ln\left(1 - \frac{\alpha_c}{b_c}\right) \text{ if } \alpha_c \le f_c b_c$$

$$q_c = \frac{\alpha_c - f_c b_c}{2(a_c b_c (1 - f_c))} - \frac{ln(1 - f_c)}{2a_c} \text{ if } \alpha_c > f_c b_c$$

a_c and b_c are parameters determined from hydrostatic compression tests. f_c is a parameter that avoids singularity in above equations at $\alpha_c = b_c$. It is set to 0.99. As α_c grows, the model obtains a shape similar to the Drucker-Prager failure criterion; see Figure 3-18. The following relation obtains the correlation between the proposed model for snow and the Drucker-Prager model.

$$\kappa_c = \alpha_{DP}$$

The plasticity evolution is done using an additive plasticity model and associative flow rule (with isotropic hardening law) as follows:

$$\varepsilon = \varepsilon^e + \varepsilon^p$$

$$\sigma = C : (\varepsilon - \varepsilon^p)$$

$$\dot{\varepsilon} = \dot{\lambda}\frac{\partial f_c}{\partial \sigma}$$

The incremental plastic strains can be derived as follows:

$$\begin{aligned}\Delta\varepsilon^p &= \Delta t\dot{\lambda}\left.\frac{\partial f_c}{\partial\sigma}\right|_{n+1}\\ &= \Delta\lambda\left[\frac{\partial f_c}{\partial J_{2D}}\frac{\partial J_{2D}}{\partial\sigma}+\frac{\partial f_c}{\partial I_1}\frac{\partial I_1}{\partial\sigma}\right]_{n+1}\\ &= \Delta\lambda\left[\frac{S}{2\sqrt{J_2+\frac{c_c}{q_c}(\bar{I}_1+q_c)^4}}+\kappa_c-\frac{4\frac{c_c}{q_c}(\bar{I}_1+q_c)^3}{2\sqrt{J_2+\frac{c_c}{q_c}(\bar{I}_1+q_c)^4}}\right]\end{aligned}$$

They consist of deviatoric and volumetric plastic strains as follows:

$$\begin{aligned}\Delta e^p &= \Delta\lambda\frac{S}{2\sqrt{J_2+\frac{c_c}{q_c}(\bar{I}_1+q_c)^4}}\\ \Delta\varepsilon_v^p &= 3\Delta\lambda\left[\kappa_c-\frac{4\frac{c_c}{q_c}(\bar{I}_1+q_c)^3}{2\sqrt{J_2+\frac{c_c}{q_c}(\bar{I}_1+q_c)^4}}\right]\end{aligned}$$

$\Delta\lambda$ is calculated according to the following procedure. First the trial stresses are updated using elastic assumption.

$$\begin{aligned}\sigma_{n+1} &= K\ trace\ \varepsilon^e_{n+1}+2Ge^e_{n+1}\\ &= \sigma^E-K\ trace\ \Delta\varepsilon^p_{n+1}-2Ge^p_{n+1}\end{aligned}$$

From the above formulation we can derive the following relation.

$$\sigma_{n+1}-\sigma^E = \Delta\lambda\left[-3K\left\{\kappa_c-\frac{4\frac{c_c}{q_c}(\bar{I}_1+q_c)^3}{2\sqrt{J_2+\frac{c_c}{q_c}(\bar{I}_1+q_c)^4}}\right\}1-2G\frac{S}{2\sqrt{J_2+\frac{c_c}{q_c}(\bar{I}_1+q_c)^4}}\right]$$

Using the Newton iteration scheme as follows:

$$f_c(\sigma_{n+1})\approx f_c(\sigma^E)+\left.\frac{\partial f_c}{\partial\sigma}\right|_{J_1^E}:(\sigma_{n+1}-\sigma^E)$$

The following relation is obtained.

$$f_c(\sigma^E) + \left(\frac{S}{2\sqrt{J_2 + \frac{c_c}{q_c}(\bar{I}_1 + q_c)^4}} \right) : \Delta\lambda(\sigma_{n+1} - \sigma_E) = 0$$

Therefore, $\Delta\lambda$ can be calculated as follows:

$$\Delta\lambda = \frac{f_c(\sigma^E)}{G\frac{J_{2D}}{\sqrt{J_2 + \frac{c_c}{q_c}(\bar{I}_1 + q_c)^4}}}$$

$$= \frac{f_c(\sigma^E)}{9K\left(\kappa_c - \frac{4\frac{c_c}{q_c}(\bar{I}_1 + q_c)^3}{2\sqrt{J_2 + \frac{c_c}{q_c}(\bar{I}_1 + q_c)^4}} \right)^2 + G\frac{J_{2D}}{J_2 + \frac{c_c}{q_c}(\bar{I}_1 + q_c)^4}}$$

In this way the volumetric equivalent plastic strain can be updated with the consequence that the yield surface is growing. Therefore a few iterations are needed to bring the trial stresses, σ_{n+1}, back to the updated yield surface with a chosen accuracy.

Using this model an excellent agreement between simulation and the experiment results has been achieved as mentioned in [Ref. 3.] and [Ref. 6.]

4 Models

Shear Models

The shear model is referenced from a DMAT entry. It defines the shear behavior of the material. At present, an elastic shear model is available with a constant or polynomial shear modulus. For Lagrangian solids, a linear viscoelastic shear model is also available.

SHREL – Constant Modulus Shear Model

The SHREL entry defines a shear model with a constant shear modulus G (Figure 4-1). The model is referenced from a DMAT entry that defines the general material properties.

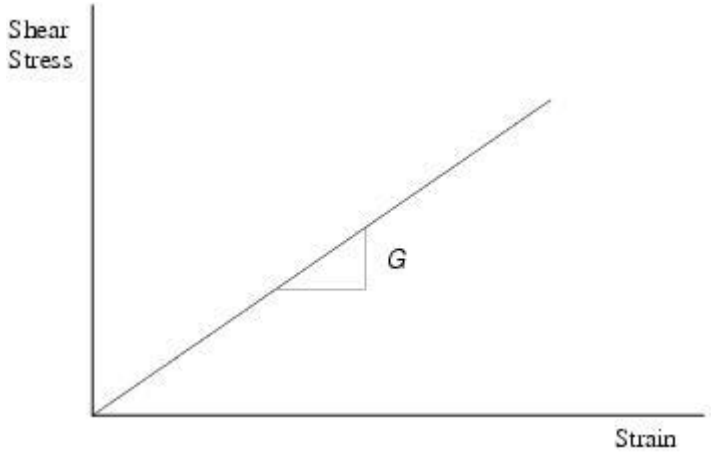

Figure 4-1 Elastic Shear as Function of Strain.

SHRLVE – Linear Viscoelastic Shear Model

The deviatoric stress components are given by

$$\sigma'_{ij}(t) = 2\int_0^t G(t-\tau)\frac{\partial \varepsilon'_{ij}(\tau)}{\partial \tau}d\tau + 2G_\infty \varepsilon'_{ij}(t) + 2\eta_0 \frac{\partial \varepsilon'_{ij}(t)}{\partial t} \qquad (4\text{-}1)$$

where $G(t-\tau) = (G_0 - G_\infty)e^{-\beta(t-\tau)}$.

The variables in the above equations are as follows:

$\sigma'_{ij}(t)$	=	deviatoric stress component
$\varepsilon'_{ij}(\tau)$	=	deviatoric strain component
$G(t-\tau)$	=	shear relaxation modulus
G_∞	=	long term shear modulus
G_0	=	short term shear modulus
η_0	=	shear viscosity constant
β	=	decay coefficient

To understand the behavior of this material, it is instructive to look at a mechanical spring-damper model (Figure 4-2) with a force/deflection behavior that is identical to the linear viscoelastic stress-strain behavior.

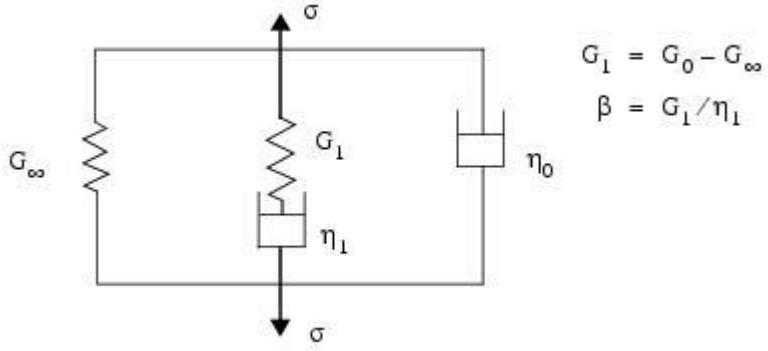

Figure 4-2 Generalized Maxwell Model

The mechanical model is a Maxwell element in parallel with a single spring and a single damper. The stress-strain relation for this mechanical model is derived first. The strain $\varepsilon(t)$ is equal for all elementary parts in the generalized Maxwell model.

The stress in each of the elementary bodies is given by

Spring: $$\sigma_\infty(t) = 2G_\infty\varepsilon(t) \quad \text{(a)}$$

Dashpot $$\sigma_0(t) = 2\eta_0\frac{d\varepsilon(t)}{dt} \quad \text{(b)}$$

Maxwell Element $$\frac{d\sigma_1(t)}{dt} + \frac{G_1}{\eta_1}\sigma_1(t) = 2G_1\frac{d\varepsilon(t)}{dt} \quad \text{(c)}$$

(4-2)

(4-2)c is easily derived by noting that for a Maxwell element the strain rate is the sum of the strain rates of the spring and the damper

$$\begin{aligned}\left(\frac{d\varepsilon(t)}{dt}\right)_{Maxwell} &= \left(\frac{d\varepsilon(t)}{dt}\right)_{spring} + \left(\frac{d\varepsilon(t)}{dt}\right)_{damper} \\ &= \frac{1}{2G_1}\left(\frac{d\sigma(t)}{dt}\right)_{spring} + \frac{1}{2\eta_1}(\sigma(t))_{damper}\end{aligned} \tag{4-3}$$

Since the stresses in the spring and the damper are equal, (4-2)c can be found by reordering (4-3)

$$\text{Maxwell element: } \sigma_1(t) = 2\int_0^t G_1 e - \beta_1(t-\tau)\frac{d\varepsilon(\tau)}{d(\tau)}d\tau \tag{4-4}$$

where $\beta_1 = G_1/\eta_1$

Since the elementary parts are linked in parallel, the stress in the generalized Maxwell model can be found by adding the stresses as given by Equations (4-2), (4-2)b, and (4-2)c

$$\sigma(t) = 2\int_0^t G_1 e^{-\beta(t-\tau)}\frac{d\varepsilon^{(\tau)}}{d\tau}d\tau + G_\infty\varepsilon(t) + 2\eta_0\frac{d\varepsilon(\tau)}{d(t)} \tag{4-5}$$

(4-5) is completely analogous to (4-1).

Based on (4-2), two types of behavior can immediately be distinguished

I = Solid behavior: $G_\infty > 0$

II = Liquid behavior: $G_\infty = 0$

Fluid behavior occurs when the additional spring G_∞ is removed from the generalized Maxwell model.

By means of some examples, the material response is demonstrated. The examples show the stress response to enforced strain.

Example 1: Constant Strain Rate

$$\frac{d\varepsilon(t)}{dt} = \dot{\varepsilon}_0, \varepsilon(t) = \dot{\varepsilon}_0 t \tag{4-6}$$

Substituting (4-6) into (4-5) and solving for the integral gives

$$\sigma(t) = 2\left\{(\mu_1(1-e^{-\beta t})) + G_\infty + \mu_0\right\}\dot{\varepsilon}_0 \tag{4-7}$$

and

$$\frac{d\sigma(t)}{dt} = 2\left\{(G_1 e^{-\beta t}) + G_\infty\right\}\dot{\varepsilon}_0 \tag{4-8}$$

The above relations are sketched in Figure 4-3.

Due to the additional dashpot μ_0, an instantaneous response occurs for both the solid and the fluid.

The stress in the solid rises more strongly towards a constant stress rate. The fluid reaches a maximum value for its stress.

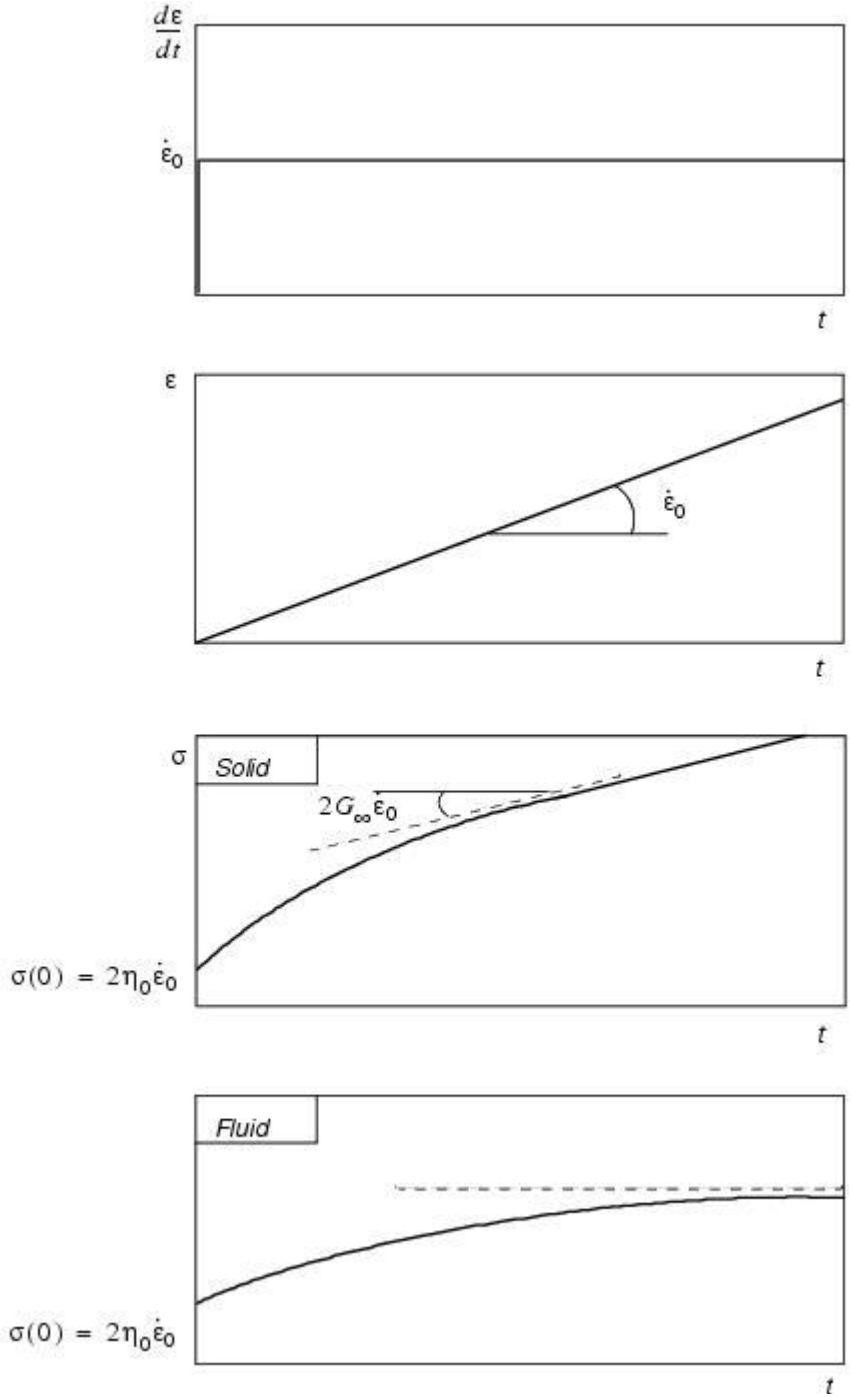

Figure 4-3 Response of Solid and Fluid to Constant Strain (Example 1)

Example 2:

Constant strain rate for $0 \geq t < t_0$.

Zero strain rate for $t \geq t_0$.

This example demonstrates the stress relaxation behavior of a linear viscoelastic material. It shows that although the strain is not increasing, the stress relaxes until it reaches a constant value. For a fluid, the stress relaxes completely to zero.

$$\begin{cases} 0 \leq t \leq t_0 & \dfrac{d\varepsilon(t)}{dt} = \dot{\varepsilon}_0 t \quad ; \quad \varepsilon(t) = \dot{\varepsilon}_0 t \\ t \geq t_0 & d\varepsilon(tdt) = 0 \quad ; \quad \varepsilon(t) = \dot{\varepsilon}_0 t_0 \end{cases} \tag{4-9}$$

Substituting (4-9) into (4-5) and solving the integral gives

$0 \leq t \leq t_0$: $\sigma(t)$ and $\dfrac{d\sigma(t)}{dt}$ as given by Equations (4-7) and (4-8)

$$t \geq t_0: \sigma(t) = 2\left\{(\mu_1(e^{-\beta(t-t_0)} - e^{-\beta t})) + G_\infty t_0\right\}\dot{\varepsilon}_0 \tag{4-10}$$

$$\frac{d\sigma(t)}{dt} = -2G_1(e^{-\beta(t-t_0)} - e^{-\beta t}) \tag{4-11}$$

The response is sketched in Figure 4-4. Until $t = t_0$, the response is equal to that shown in Figure 4-3.

The instantaneous relaxation at $t = t_0$ is again due to the additional dashpot η_0.

A solid relaxes to a finite value, equal to the stress in the G_∞ spring of the generalized Maxwell model. A fluid relaxes completely to zero.

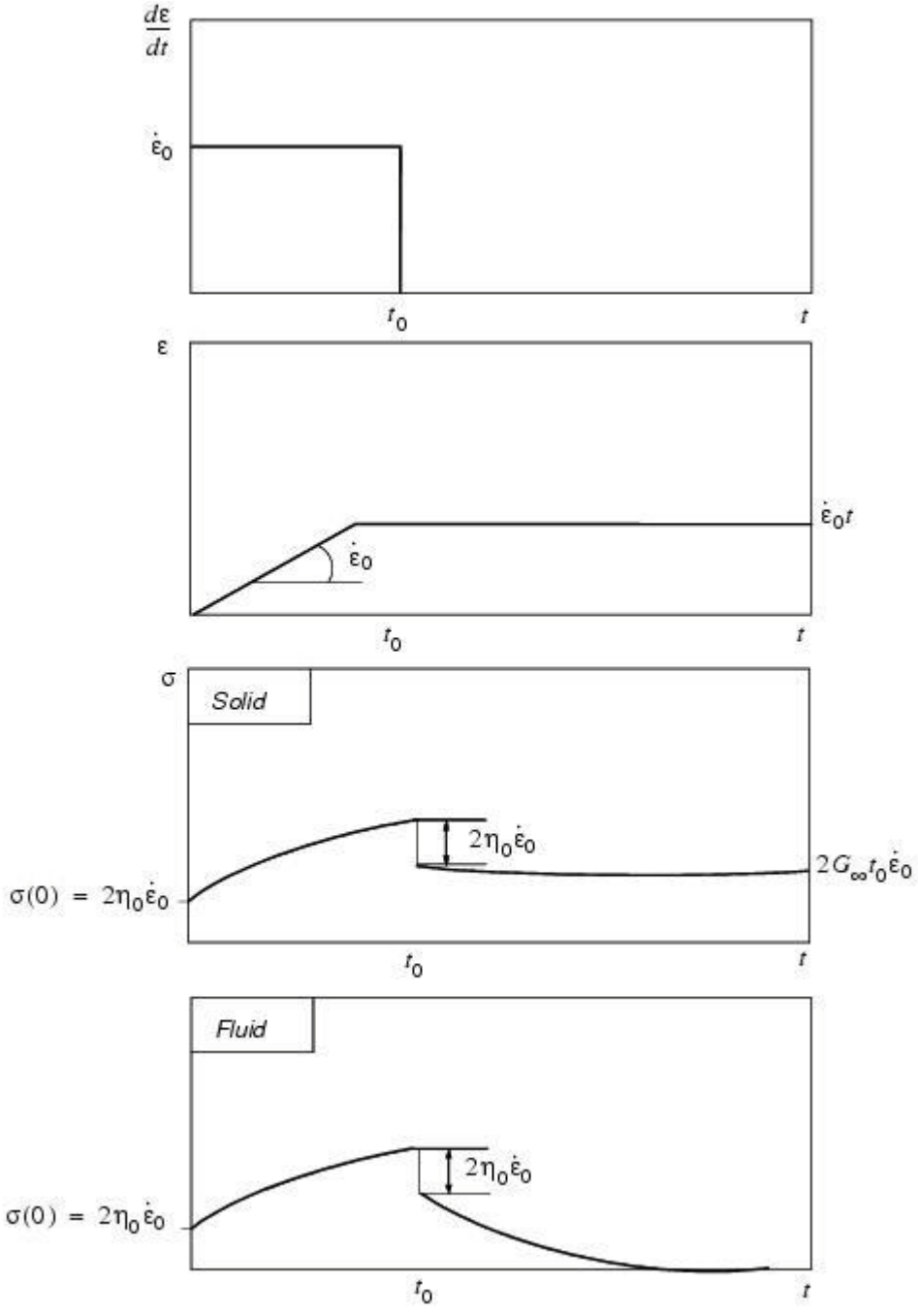

Figure 4-4 Stress Relaxation of Linear Viscoelastic Material After a Period of Constant Strain Rate (Example 2).

SHRPOL – Polynomial Shear Model

The SHRPOL model defines a polynomial shear model where the shear modulus is related to the effective plastic shear strain by a cubic equation.

$$G = G_0 + G_1\gamma + G_2\gamma^2 + G_3\gamma^3$$

where γ = effective plastic shear strain and G_0, G_1, G_2, and G_3 are constants.

Yield Models

Yield models may be referenced by DMAT, DMATEP, or DYMAT24 entries. The yield models can be used to model elastic perfectly plastic behavior, bilinear elastoplastic behavior, piecewise linear behavior, or hydrodynamic behavior (zero yield stress).

YLDHY – Hydrodynamic Yield Model

The YLDHY entry defines a yield model with constant zero yield stress. This model should be used for fluids that have no shear strength and are, therefore, hydrodynamic.

YLDMC – Mohr-Coulomb Yield Model

The YLDMC entry defines a Mohr-Coulomb yield model. The yield stresses are defined by giving bilinear curve as shown in the Figure 4-5.

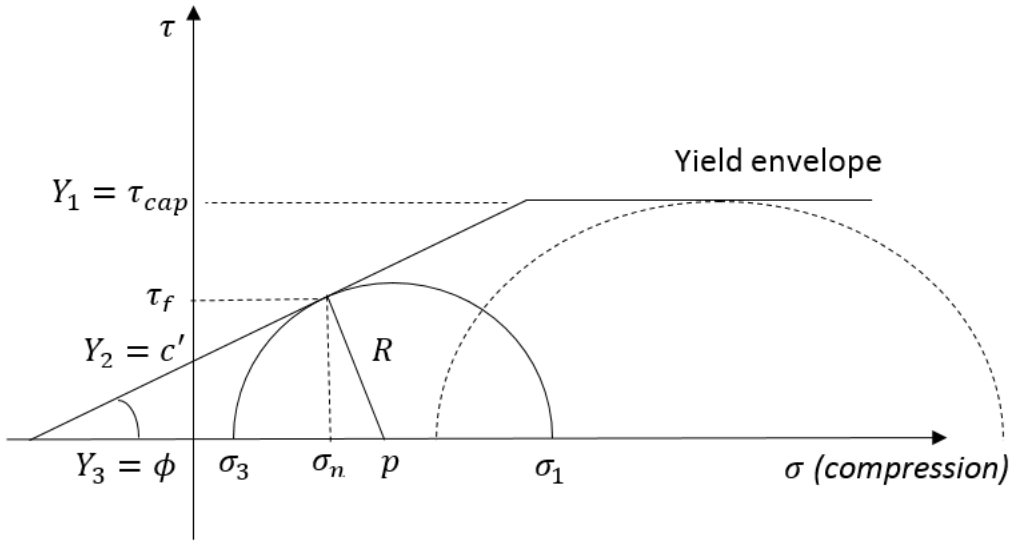

Figure 4-5 Relationship of stress under yield envelope

The stresses can be calculated by the geometry shown in Figure 4-5.

$$R = (c'\cot\phi + p)\sin\phi = c'\cos\phi + p\sin\phi$$

where $\sigma_n = R\cos\phi$

$$\tau_f = c' + \sigma_n \tan\phi$$

c'	=	cohesion
σ_n	=	normal stress on yield plane
τ_f	=	shear stress on yield plane
ϕ	=	internal friction angle
p	=	current pressure on element

The principal stress relationship can be described as equations below.

$$\sigma_1 = p + R$$

$$\sigma_3 = p - R$$

$$\sin\phi = \frac{R}{c'\cot\phi + p} = \frac{\frac{\sigma_1 - \sigma_3}{2}}{c'\cot\phi + \frac{\sigma_1 + \sigma_3}{2}}$$

$$\sigma_1 = \sigma_3\left(\frac{1+\sin\phi}{1-\sin\phi}\right) + 2c'\sqrt{\frac{1+\sin\phi}{1-\sin\phi}}$$

where

σ_1	=	maximum principal stress
σ_3	=	minimum principal stress
$\frac{1+\sin\phi}{1-\sin\phi}$	=	$\tan^2\left(\frac{\pi}{4} + \frac{\phi}{2}\right)$

The yield plane is given in the Figure 4-6 when maximum principal stresses and minimum principal stresses.

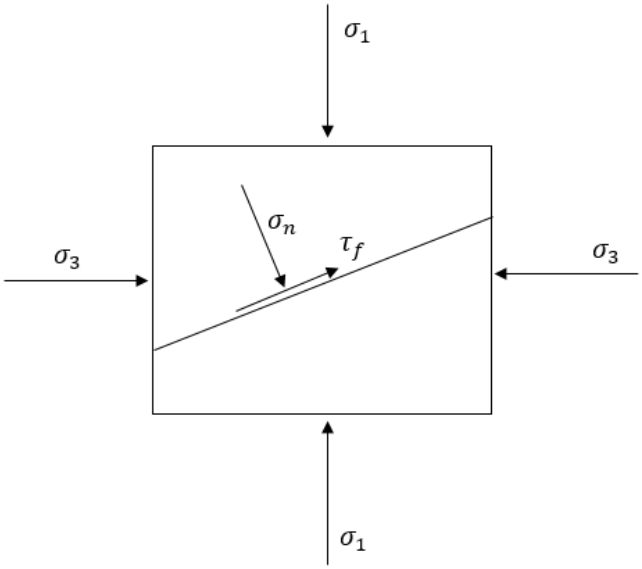

Figure 4-6 2D-yield plane when principal stresses are applied

YLDVM – von Mises Yield Model

The YLDVM entry defines a von Mises yield model. The yield stress and hardening modulus are defined by giving either a bilinear or piecewise linear stress-strain curve. With Lagrangian and Eulerian solid elements, only an elastic perfectly plastic yield model can be used. The hardening modulus is not used.

Bilinear Representation

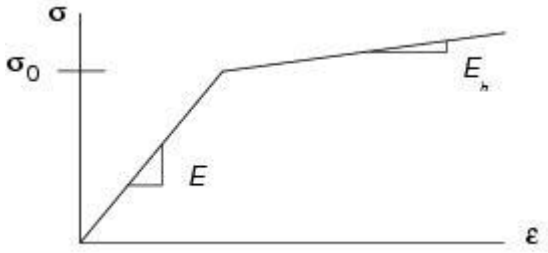

where the yield stress σ_y is given by

$$\sigma_y = \sigma_0 + \frac{EE_h}{E - E_h}\varepsilon_p$$

where

σ_0	=	yield stress
E	=	Young's modulus
E_h	=	hardening modulus
ε_p	=	equivalent plastic strain

Piecewise Linear Representation

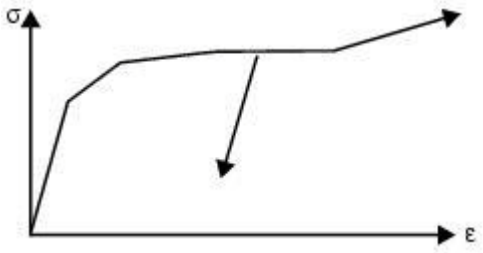

During every iteration, the stress *s* is determined from the current equivalent strain ε by interpolating from the stress-strain table

$$\sigma = [(\sigma_i - \sigma_{i-1})(\varepsilon - \varepsilon_{i-1})/(\varepsilon_i - \varepsilon_{i-1})] + \sigma_{i-1}$$

where σ_i and ε_i are the points in the table. The stress-strain characteristic used internally in Dytran is in terms of true stress and equivalent plastic strain. However, for convenience, the stress-strain characteristic can be input in any of the following ways:

- True stress/true strain.
- Engineering stress/engineering strain.
- True stress/plastic strain.
- True stress/plastic modulus.

True stress is defined as

$$\sigma_{true} = \frac{F}{A}$$

where F = current force, A = current area.

Plastic strain ε_{pl} is

$$\varepsilon_{pl} = \varepsilon_{true} - \varepsilon_{el}$$

where ε_{true} = true strain, ε_{el} = elastic strain.

True strain is defined as

$$\varepsilon_{true} = \int \frac{dl}{l}$$

where dl = incremental change in length, l = current length.

By comparison, engineering stress σ_{eng} and strain ε_{eng} are given by $\sigma_{eng} = \frac{F}{A_0}$ where A_0 = original area and

$\varepsilon_{eng} = \frac{(I - I_0)}{I_0}$ where I_0 = original length.

True stress/true strain and engineering strain are related by the following formulas:

$$\sigma_{true} = \sigma_{eng}(1 + \varepsilon_{eng})$$

$$\varepsilon_{true} = ln(1 + \varepsilon_{eng})$$

At small strains, there is little difference between true stress-strain and engineering stress-strain. However, at moderate and large strains there can be very large differences, and it is important that the correct stress-strain characteristic is input.

When defining the material properties using Young's modulus, yield stress, and hardening modulus, the hardening modulus must be estimated from a plot of true stress versus true strain. This estimate may well require a measured material characteristic to be replotted.

Some simple examples follow:

True Stress Versus True Strain

The slope of the first segment of the curve gives the Young's modulus for the material (when it is not defined explicitly) and the first nonzero stress point gives the yield stress σ_y (Figure 4-7). The point corresponding to the origin can be omitted.

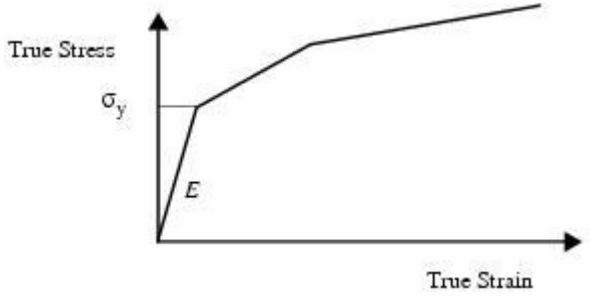

Figure 4-7 True Stress Versus True Strain Curve

Engineering Stress Versus Engineering Strain

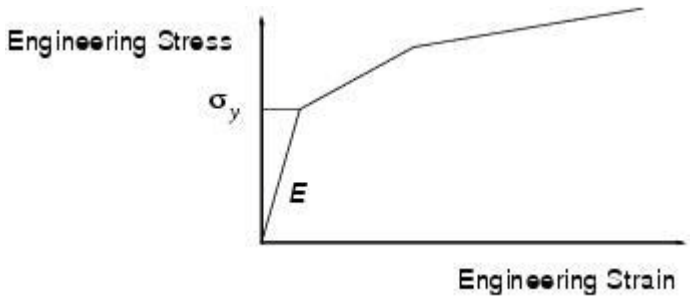

Figure 4-8 Engineering Stress Versus Engineering Strain Curve

True Stress Versus Plastic Strain

Since the curve is defined in terms of the equivalent plastic strain, there is no elastic part in the curve (Figure 4-9). The first point must be the yield stress of the material at zero plastic strain. Young's modulus is defined separately.

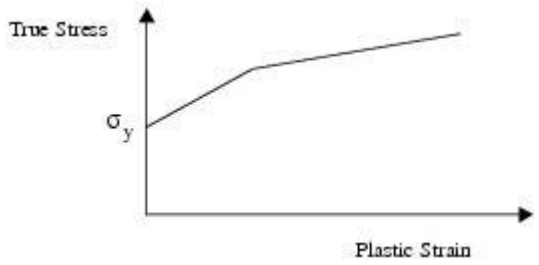

Figure 4-9 True Stress Versus Plastic Strain Curve

True Stress Versus Plastic Modulus

This option is slightly different since the curve is specified as a series of pairs of stress and hardening moduli, rather than as a series of pairs of stress and strain. Young's modulus and yield stress are defined explicitly so that the table consists of pairs of values with the hardening modulus (x-axis) and the true stress (y-axis) at the end of the segment (Figure 4-10).

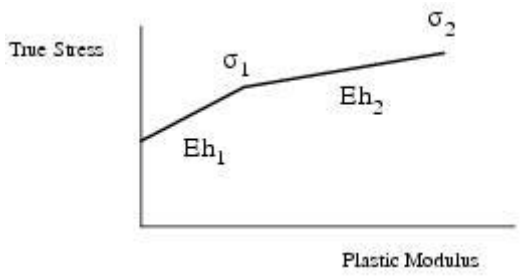

Figure 4-10 True Stress Versus Plastic Modulus Curve

Yielding occurs when the von Mises stress

$$\sigma_{vm} = \sqrt{[(\sigma_1 - \sigma_2)^2 + (\sigma_2 - \sigma_3)^2 + (\sigma_3 - \sigma_1)^2]/2}$$

exceeds the yield stress σ_y. The principal stresses are σ_1, σ_2, and σ_3.

Isotropic hardening is assumed, which means that the yield surface increases in diameter as yielding occurs, but its center does not move.

This yield model can be used with beam, shell, and solid elements. When used with shell or solid elements, strain-rate sensitivity and failure can be included. Strain-rate sensitivity can be defined in two ways:

1. You can specify a table giving the variation of a scale factor S with strain-rate $d\varepsilon/(dt)$. The scale factor is multiplied by the stress found from the stress-strain characteristic to give the actual stress. The failure criterion is based on plastic strain. When the plastic strain exceeds the specified value, the element fails. All the stresses are set to zero, and the element can carry no load. (This failure criterion is referred to from the DMATEP or the DYMAT24 entry.)

2. You can specify the constants D and P in Cowper-Symonds rate enhancement

   formula $\frac{\sigma_d}{\sigma_y} = 1 + \left\{\frac{\dot{\varepsilon}}{D}\right\} 1/P$

   where σ_d is the dynamic yield stress, σ_y is the static yield stress, and is $\dot{\varepsilon}$ the equivalent strain rate.

YLDJC – Johnson-Cook Yield Model

The YLDJC entry defines a Johnson-Cook yield model in which the yield stress is a function of the plastic strain, strain rate, and temperature

$$\sigma_y = (A + B\varepsilon_p^n)(1 + C ln(\dot{\varepsilon}/\dot{\varepsilon}_0))(1 - T^{*m})$$

where

T^*	=	$\frac{(T - T_r)}{(T_m - T_r)}$
ε_p	=	effective plastic strain
$\dot{\varepsilon}$	=	effective strain rate
$\dot{\varepsilon}_0$	=	reference strain rate
T	=	temperature
T_r	=	room temperature
T_m	=	melt temperature
A, B, n, C, and m are constants.		

YLDTM – Tanimura-Mimura Yield Model

The YLDTM entry defines a Tanimura-Mimura yield model in which the yield stress is a function of the plastic strain, strain rate, and temperature

$$\sigma_y = \left[A + B\varepsilon_p + (C + D\varepsilon_p)\left(1 - \frac{A + B\varepsilon_p}{\sigma_{cr}}\right) ln\left(\frac{\dot{\varepsilon}}{\dot{\varepsilon}_s}\right)\right](1 - T^{*m}) + E\left(\frac{\dot{\varepsilon}}{\dot{\varepsilon}_0}\right)^k$$

where

T^*	=	$\frac{T - T_r}{T_m - T_r}$
T	=	temperature
T_r	=	room temperature
T_m	=	melt temperature
ε_p	=	effective plastic strain
$\dot{\varepsilon}$	=	effective strain rate
$\dot{\varepsilon}_s$	=	quasi-static strain rate
$\dot{\varepsilon}_0$	=	reference strain rate
σ_{cr}	=	critical yield stress
A, B, C, D, m, E, and k are constants.		

This yield model is suitable for a wide range of strain rates, strains and temperatures.

YLDZA – Zerilli-Armstrong Yield Model

The YLDZA entry defines a Zerilli-Armstrong yield model in which the yield stress is a function of the plastic strain, strain rate, and temperature

$$\sigma_y = (A + B\varepsilon_p^n)e^{\left[-mT + Ctln\left(\frac{\dot{\varepsilon}}{\dot{\varepsilon}_0}\right)\right]} \quad \text{for Fcc metals}$$

$$\sigma_y = (A + B\varepsilon_p^n) + De^{\left(-mT + Ctln\left(\frac{\dot{\varepsilon}}{\dot{\varepsilon}_0}\right)\right)} \quad \text{for Bcc metals}$$

where

ε_p	=	effective plastic strain
$\dot{\varepsilon}$	=	effective strain rate
$\dot{\varepsilon}_0$	=	reference strain rate
T	=	temperature
A, B, n, C, m, and D are constants.		

This yield model can be used for both Fcc type of metals, like iron and steels, as well as Bcc type of metals, like aluminum and alloys.

YLDRPL – Rate Power Law Yield Model

The YLDRPL entry defines a rate power law yield model in which the yield stress is a function of the plastic strain and strain rate.

$$\sigma_y = MAX(C, A + B\varepsilon_p^n \dot{\varepsilon}^m)$$

where

ε_p	=	effective plastic strain
$\dot{\varepsilon}$	=	effective strain rate
A, B, n, m, and C are constants.		

YLDPOL – Polynomial Yield Model

The YLDPOL entry defines a polynomial yield model in which the yield stress is a function of the plastic strain

$$\sigma_y = MIN(\sigma_{max}, A + B\varepsilon_p + C\varepsilon_p^2 + D\varepsilon_p^3 + E\varepsilon_p^4 + F\varepsilon_p^5)$$

where

ε_p = effective plastic strain

σ_{max} = maximum yield stress

A, B, C, D, E, and F are constants.

YLDSG – Steinberg-Guinan Yield Model

The YLDSG entry defines a Steinberg-Guinan yield model in which the yield stress is a function of the plastic strain, strain rate, and temperature:

$$A_T = A_1(1 + A_3\varepsilon_p)^{A_4}$$

$$\sigma_y = min(A_2, A_T)\left[1 - H(T - T_r) + Bp\left(\frac{\rho}{p_{ref}}\right)^{1/3}\right], T < T_m$$

$$\sigma_y = 0, T \geq T_m$$

where

ε_p	=	effective plastic strain
T	=	temperature
T_r	=	room temperature
T_m	=	melt temperature
p	=	pressure
ρ	=	density

$A_1, \ldots, A_4$, H and B are constants.

Equations of State

Equations of state are referenced from the DMAT entry. The equation of state for a material is of the basic form

Pressure = f (density, specific internal energy)

The simplest equation of state is the gamma law equation of state, defined by the EOSGAM entry. The only input required is the ratio of specific heats for an ideal gas.

The EOSIG entry defines the properties of the Ignition and Growth equation of state and the reaction rate equation used to model high explosives.

The EOSJWL entry defines an equation of state based on the JWL explosive model. It is used to calculate the pressure of the detonation products of high explosives. The JWL model is empirically based and requires the input of five constants.

The EOSDEF entry defines the properties of the deflagration equation of state and the reaction rate to model the burning of solid propellants.

The EOSNA entry defines an equation of state based on the Noble-Abel gas law. This is an adjustment of the ideal gas law that takes into account the volume of gas molecules.

The EOSPOL entry defines a polynomial equation of state.

The EOSTAIT entry defines an equation of state based on the Tait model in combination with a cavitation model.

EOSDEF-Deflagration

The pressure in the reaction products (in "gas" state) is defined by the Noble-Abel equation of state as follows:

$p = (\gamma - 1)\frac{\rho}{1 - b\rho}e$ for reacted product.

$T = \frac{(\gamma - 1)e}{R}$ where γ, b are constants and R is the gas constant.

The ability of the material to quickly produce gases when burnt is characterized by the burn rate coefficient and by the ratio of initial surface area divided by initial volume. This ratio is denoted by SAVR, and their product is called the vivacity. Propellants burn faster and have larger vivacity as their fragmentation degree increases.

The chemical reaction rate for conversion of un-reacted explosive to reaction products is described by the following reaction rate equations:

$\xi = wSAVR$	vivacity
$\phi = (1 - F)^X + YF$	form function
$\frac{dF}{dt} = \xi\phi p^\beta$	time derivative of burn fraction

Where:	
w =	burning rate coefficient

β =	burning rate exponent
SAVR =	initial surface area divided by volume
Y=	parameter form function
S=	parameter form function

As the solid propellant burns at its exposed burning surface, the burning surface moves inward in the direction perpendicular to itself. This movement of the burning surface in parallel layers is known as Robert's law.

Since the mechanism of the burning involves several chemical reactions it is difficult to predict the burning rate from the chemical and physical properties of the propellants. Instead an empirical law is available that shows good agreement with experiment. This law is called the Saint-Robert law and also Vieille's law. This law states that the linear burning rate of any propellant can be expressed by the simple expression: $\gamma = wp^{\beta}$

Here γ is the burning rate coefficient and β the burning rate exponent. Here β ranges from 0.2 to 0.8.

Vivacity $\xi = wSAVR$, where w is the burning rate coefficient and usually comes from burn rate vs pressure tests from closed bomb, cinephotomicroscopy or combination thereof, (for details refer to Appendix A, Reference 35.). The initial surface area to volume ratio *SAVR* can be calculated based on the grain geometry, (for details refer to Appendix A, Reference 36.). Examples of the common propellant geometries are shown in the figure below, which each provide unique *SAVR* value.

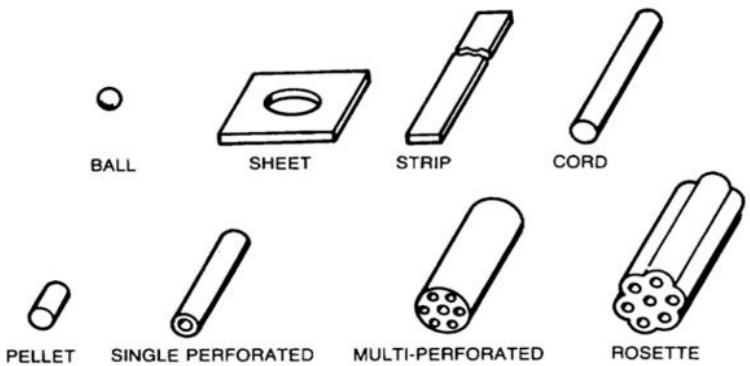

Figure 4-11 Common propellant geometries

Form function $\phi = \frac{S}{S_0}$ is the ratio of the current surface area over the initial surface area during the burning of the propellant (for details refer to Appendix A, Reference 37.). It provides the propellant grain geometry to influence the burning rate over the burn fraction.

To simplify the input as current grain surface area is unknown during analysis, a two parameter input is used to approximate typical grain geometry surface burning profiles. Using x and s input to

$\phi = [(1-F)^X + SF]$ different form functions can be approximated as shown below. Typically spherical ball and cylindrical pellet grains are regressive while single perforated cylindrical grains are neutral and multi-perforated cylindrical grains are progressive. Adding material variability and thin region material loss in burning can be approximated with combinations of parameters.

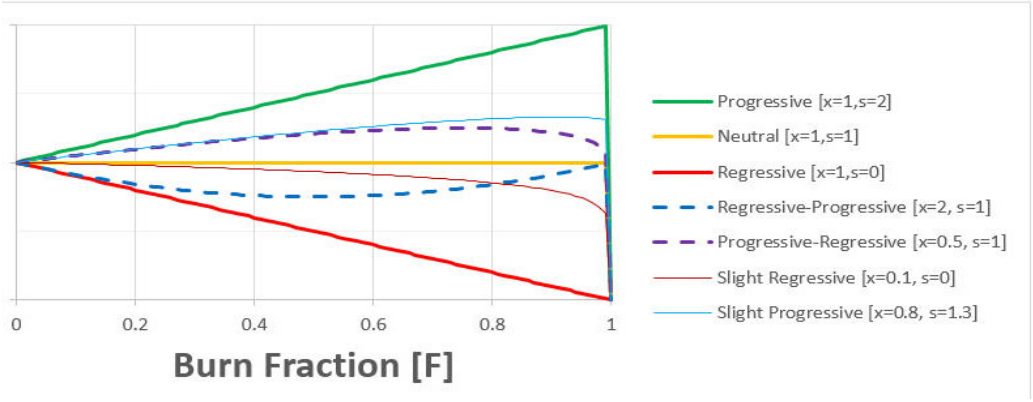

Figure 4-12 Different combination of parameters

Chemical Energy E can also be calculated by the Adiabatic Flame Temperature (K) T_f multiplied by the gas constant R (J/kg.K) as it is solved as adiabatic combustion. This also shows that the chemical energy is a specific energy value (J/kg).

Initialization of deflagration is achieved by setting region of ignition with SIE at the Chemical Energy value.

EOSGAM – Gamma Law Equation of State

The EOSGAM model defines a gamma law equation of state for gases where the pressure is a function of the density, the specific internal energy, and the ideal gas ratio of specific heats γ of an ideal gas

$$p = (\gamma - 1)\rho e$$

where

e	=	specific internal energy unit mass
ρ	=	overall material density
γ	=	ratio of specific heats (C_p/C_v)

The EOSGAM equation of state can also be used to model viscous gases.

EOSIG - Ignition and Growth Explosive Material Model

The IG model governs the simulation of the reaction zone of explosive material where the transition from the fully un-reacted to the fully reacted state occurs. Prior to the start of the reaction, its "un-reacted" EOS (described by (4-12)) models the explosive. After the reaction has completed, the explosive is modeled by the JWL equation of state for the detonation product (described by (4-13)). The reaction rate relation controls the fraction of explosive reacting per cycle during the transition from the un-reacted to the reacted state.

$$X^i = X(t)$$

Note:	$X^{i+1} = X(t+\Delta t)$ where t denotes time.

IG Model

The Jones-Wilkins-Lee equation of state is used in the ignition and growth calculations for both the un-reacted and the reaction products. The JWL equation of state defines the pressure in the un-reacted explosives as:

$$p_e^{i+1} = A_e\left(1-\frac{\omega_e\eta_e^{i+1}}{R_{1e}}\right)e^{-R_{1e}/\eta_e^{i+1}} + B_e\left(1-\frac{\omega_e\eta_e^{i+1}}{R_{2e}}\right)e^{-R_{2e}/\eta_e^{i+1}} + \omega_e\eta_e^{i+1}\rho_0 E_e^{i+1} \qquad (4\text{-}12)$$

where:

$\eta_e = \frac{\rho_e}{\rho_0}$	=	The relative density of the unreacted explosive.
E_e	=	The specific internal energy per unit mass of unreacted explosive.
ρ_0	=	The initial density of the explosive.
A_e, B_e, ω_e, R_{1e}, R_{2e}	=	The input constants of the unreacted explosive.

Similarly, a JWL form defines the pressure in the reaction products as follows:

$$p_p^{i+1} = A_p\left(1-\frac{\omega_p\eta_p^{i+1}}{R_{1p}}\right)e^{-R_{1p}/\eta_p^{i+1}} + B_p\left(1-\frac{\omega_p\eta_p^{i+1}}{R_{2p}}\right)e^{-R_{2p}/\eta_p^{i+1}} + \omega_p\eta_p^{i+1}\rho_0 E_p^{i+1} \qquad (4\text{-}13)$$

where

$\eta_p = \frac{\rho_p}{\rho_0}$	=	The relative density of the reaction product.
E_p	=	The specified internal energy per unit mass of the reacted product.
A_p, B_p, ω_p, R_{1p}, R_{2p}	=	The input constants of the reaction product.

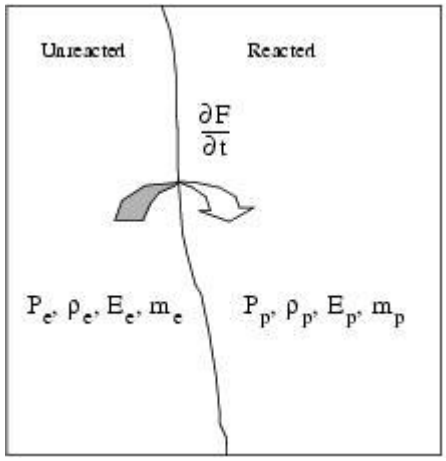

Figure 4-13 A Mixture Zone in the IG Explosive Element

The mixture of un-reacted explosive and reaction products is defined by the reacted fraction F, where:

F = 0 ⟶ no reaction

F = 1 ⟶ complete conversion from explosion to products

For equilibrium of the mixture equation of states as described above is defined as pressure equilibrium. The pressure in the mixture elements is assumed to be in equilibrium, thus:

$$p_e^{i+1} = p_p^{i+1} = p^{i+1} \tag{4-14}$$

The mass of the un-reacted and reacted material change during the conversion of explosive as follows:

$$m_e^{i+1} = m_e^i - \frac{\partial F}{\partial t} M \Delta t \tag{4-15}$$

$$m_p^{i+1} = m_p^i - \frac{\partial F}{\partial t} M \Delta t \tag{4-16}$$

where M denotes the element's mass, and $\frac{\partial F}{\partial t}$ denotes the chemical reaction rate for conversion of unreacted explosive to reaction products. The rate of reaction takes the following form:

$$\frac{\partial F}{\partial t} = I(1-F)^x(\eta_e - 1 - a)^r + G(1-F)^x F^y (P)^z \tag{4-17}$$

where F is the fraction of reacted explosive and t is time. In the above equation, there are seven user defined constants (I, a, G, r, x, y, and z).

The specific internal energies of the un-reacted and reaction material are not assumed to be in equilibrium and change according to:

$$E_e^{i+1} = E_e^i - \frac{(p^{i+1}+p^i)}{2} \frac{(V^{i+1}-V^i)}{\eta_e^{i+1}\rho_0(V^{i+1}+V^i)} \tag{4-18}$$

and

$$E_p^{i+1} = E_p^i + \frac{\partial F}{\partial t}E_{chem}\Delta t - \frac{(p^{i+1}+p^i)}{2} \frac{(V^{i+1}-V^i)}{\eta_p^{i+1}\rho_0(V^{i+1}+V^i)}$$

In the above equations, E_{chem} denotes the chemical energy of explosive per unit mass. The total volume V is known from the deformed shape of the element.

The behavior of the ignition and growth detonation model in the mixed phase is described by the above eight equations. The following variables in a mixture element are solved for at the end of each time step:

$$(p_e^{i+1}, p_p^{i+1}, \eta_e^{i+1}, \eta_p^{i+1}, E_e^{i+1}, E_p^{i+1}, m_e^{i+1}, m_p^{i+1})$$

For a known fraction of reacted explosive F in a time step, these variables are solved by iteration on volumetric changes until a pressure equilibrium ($p_e \cong p_p$) in the element is reached.

During the iteration process, the pressure difference is used as a convergence parameter to check for a converged solution. Each iteration adjusts the volume of un-reacted and reaction products in the mixed element. When a converged solution is obtained, a final check is performed to verify the assumption that the volumes of the mixture elements be additive:

$$V^{i+1} = (1-F)V_e^{i+1} + FV_p^{i+1} \tag{4-19}$$

where

$$V_e^{i+1} = \frac{M}{\eta_e^{i+1}\rho_0} \tag{4-20}$$

$$V_p^{i+1} = \frac{M}{\eta_p^{i+1}\rho_0} \tag{4-21}$$

Finally, the speed of sound of the material is computed as the derivative of pressure with respect to density. For a mixture IG element, the speed of sound is computed as the average of the un-reacted and reacted state speed of sound based on volume fractions:

$$c^2 = \frac{\left(V_e \frac{\partial p_e}{\partial \rho_e} + V_p \frac{\partial p_p}{\partial \rho_p} \right)}{M}$$

where $p_e \cong p_p$, as it follows from the pressure equilibrium assumption in the model.

The scheme of IG material model solution is given the following flow-chart.

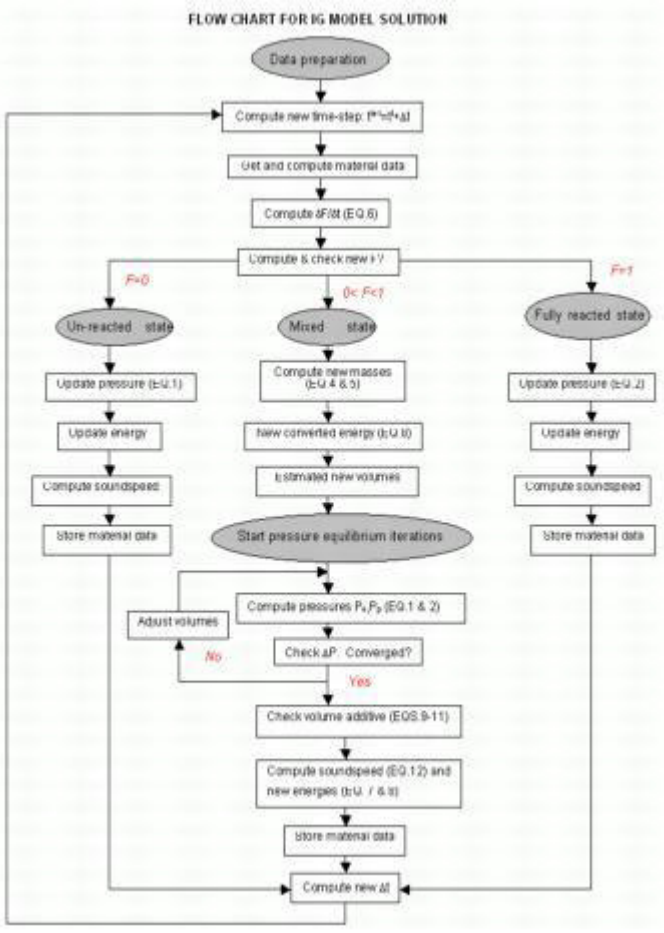

EOSJWL – JWL Equation of State

The equation of state

$$P = p_0 + A\left(1 - \frac{\omega\eta}{R_1}\right)e^{\frac{-R_1}{\eta}} + B\left(1 - \frac{\omega\eta}{R_2}\right)e^{\frac{-R_2}{\eta}} + \omega\eta\rho_0 e + \frac{\omega\rho\lambda Q}{\rho_0}$$

$$\frac{d\lambda}{dt} = a(1-\lambda)^m p^n$$

can only be used with Eulerian elements where:

e	=	specific internal energy per unit mass
ρ_0	=	reference density
ρ	=	overall material density
η	=	$\frac{\rho}{\rho_0}$
A, B, p_0, R_1, R_2, a, m, n and Q are constants		

These parameters are defined in Appendix A, Reference 10.

$$\lambda$$

33. A DETSPH entry must be used to specify the detonation time, the location of the detonation point, and the velocity of a spherical detonation wave. When no DETSPH entry is present, all the material detonates immediately and completely.

EOSMG - Mie-Gruneisen Equation of State

The Mie-gruneisen equation is useful in high-strain rate processes. The pressure is split in a part that only depends on density and a part that only depends on temperature.

$$p = p_c + p_T$$

The cold pressure is computed from the Rankine-Hugoniot equations and is given by

$$p_c = \frac{\rho_0 c_0^2 \eta}{(1-s\eta)^2}\left(1 - \frac{\Gamma_0\eta}{2}\right)$$

Here, ρ_0 is the reference density, c_0 is the speed of sound, $\eta = 1 - \frac{\rho_0}{\rho}$ is the volumetric compressive strain. The defining equation for the parameter s is the linearization of the relationship between linear shock speed U_s and particle velocity U_p:

$$U_s = c_0 + sU_p$$

The thermal part of the pressure follows from thermodynamic considerations and reads

$$p_T = \Gamma_0 \rho_0 e$$

where e is the specific internal energy and the parameter Γ_0 is given by

$$\Gamma_0 \rho_0 = \frac{\beta K_T}{C_V}$$

where K_T is the isothermal bulk modulus, C_V is the specific heat at constant volume and β is the volumetric thermal expansion coefficient. Γ_0 is the Gruneisen parameter at reference density. The Gruneisen parameter at other densities is given by $\Gamma = \Gamma_0 \frac{\rho_0}{\rho}$.

EOSNA – Noble-Abel equation of state

The Noble-Abel equation of state is a first approximation to the van der Waals equation of gases. For details refer to Appendix A, Reference 34.

First assume a non-interacting gas. Then the pressures is given by the ideal gas laws as $P = (\gamma - 1)\rho e$.

Introducing the specific volume defined by $v = \frac{1}{\rho}$, is rewritten as $p = (\gamma - 1)\frac{e}{v}$.

Taking interactions into account, it is assumed that particles are hard spheres. Their effect is to reduce the volume so that the molecules can move in freely. This effect is modeled by replacing *v* by *v-b:*

$p = (\gamma - 1)\frac{e}{(v - b)}$ or in terms of density as: $p = (\gamma - 1)\frac{\rho e}{(1 - \rho b)}$

For deriving the equations $\gamma = \frac{C_P}{C_V}$ $R = C_{P - C_V}$. For details refer to Appendix A, Reference 38.

EOSPOL – Polynomial Equation of State

The EOSPOL model defines a polynomial equation of state where the pressure is related to the relative volume and specific internal energy by a cubic equation.

In compression $(\mu > 0)$

$$p = a_1\mu + a_2\mu^2 + a_3\mu^3 + (b_0 + b_1\mu + b_2\mu^2 + b_3\mu^3)\rho_0 e$$

In tension $(\mu \le 0)$

$$p = a_1\mu + (b_0 + b_1\mu)\rho_0 e$$

where

μ	=	$\eta - 1$
η	=	ρ / ρ_0
ρ	=	overall material density
ρ_0	=	reference density
e	=	specific internal energy per unit mass

The EOSPOL equation of state can also be used to model viscous fluids; see also Material Viscosity in this chapter.

EOSTAIT – Tait Equation of State

The EOSTAIT model defines a equation of state based on the Tait model in combination with a cavitation model where the pressure p is defined as follows:

No cavitation $\rho > \rho_c$,

$$p = a_0 + a_1(\eta^\gamma - 1)$$

Cavitation $\rho \le \rho_c$,

$$p = p_c$$

where

η	=	ρ/ρ_0
ρ	=	overall material density
ρ_0	=	reference density
ρ_c	=	critical density which produces the cavitation pressure p_c

The pressure can not fall below the cavitation pressure $p_c = a_0 + a_1(((\rho_c)/(\rho_0))^{\gamma} - 1)$, although the density can continue to decrease below its critical value ρ_c.

The EOSTAIT equation of state can also be used to model viscous fluids, see Material Viscosity in this chapter.

Material Viscosity

Viscous fluid material models are available for the single material Euler solver, the Roe fluid solver, and the multi-material Euler solver. The viscous behavior is referenced from the entry to define the equation of state (EOSGAM, EOSPOL, or EOSTAIT. For these viscous materials, the stress tensor t_{ij} is defined as:

$$t_{ij} = -p \cdot \delta_{ij} + s_{ij}$$

$$\frac{dp}{dt} = \frac{K}{\rho}\frac{d\rho}{dt}$$

and

$$s_{ij} = 2\mu \cdot \frac{de_{ij}^{d}}{dt}$$

where K denotes the bulk modulus, ρ the density, s_{ij} the deviatoric stress tensor, p the pressure, e_{ij}^{d} the deviatoric strain tensor, and μ the coefficient of viscosity. The Euler solvers compute the stresses directly from the velocity gradients.

Material Failure

One of the nonlinear features of a material's behavior is failure. When a certain criterion (failure criterion) is met, the material fails and no longer sustains its loading and breaks. In a finite-element method, this means

that the element, where the material reaches the failure limit, cannot carry any stresses anymore. The stress tensor is effectively zero. The element is flagged for failure, and, essentially, is no longer part of the structure.

Failure criteria can be defined for a range of materials and element types. The failure models are referenced from the material definition entries.

There are several different failure models available in Dytran:

FAILMPS	Constant, maximum plastic strain
FAILEX	User-specified failure
FAILEX1	User-specified (extended) failure
FAILEST	Constant, maximum equivalent stress and minimum time step
FAILMES	Constant, maximum equivalent stress
FAILPRS	Constant, maximum pressure
FAILSDT	Constant, maximum plastic strain and minimum time step
FAILJC	The Johnson-Cook failure model

In addition, for all material definitions defined for Lagrangian solid and shell (CQUAD4) elements, a failure criterion based on minimum time step can be defined using the following PARAM entry:

FAILSDT	Constant, minimum time step

FAILMPS – Maximum Plastic Strain Failure Model

The most commonly used failure model is the one that is based on a maximum equivalent plastic strain. The material fails completely when the plastic strain reaches beyond the defined limit. The element no longer carries any load and is removed from the calculation.

The failure model can be used with Eulerian and Lagrangian solid elements, shell elements, and Hughes-Liu beam elements.

FAILEX – User Failure Subroutine

You can define the failure mechanism in the user-written subroutine `exfail.f`. The subroutine must ultimately return the failure flag for the elements that it processes. The mechanism by which failure is described must programmed in the subroutine. The failure flag indicates either failure or no failure. Dytran processes the resulting failure flags and sets the element stresses to zero if the failure flag indicates material failure.

FAILEX1 – User Failure Subroutine

The FAILEX1 user-defined failure model uses essentially the same concept as the FAILEX failure model. In addition to ultimate failure, you can define a so-called property degradation prior to complete material failure. Property degradation means that the material properties that describe the material's elastic behavior

are allowed to degrade to zero before the material completely fails. Effectively, property degradation influences the element's capability to carry loading as it gets weaker during this process.

Depending on the model that you program in the subroutine, you can have all properties degrade completely before material failure occurs, or you can define that when a certain property reaches a limit, material failure occurs. The routine should return the material properties and the failure flag for all elements that are input to the routine. Dytran processes the returned data accordingly in the stress and force calculations.

This model can only be used in combination with an orthotropic material model (DMATOR) for Lagrangian solid elements.

FAILEST – Maximum Equivalent Stress and Minimum Time Step Failure Model

This failure model uses the equivalent stress as the criterion for failure. When the equivalent stress (the first invariant of the stress tensor) reaches the defined limit the material loses its ability to carry deviatoric stresses. The hydrodynamic strength (the ability to sustain a pressure) is retained until the time-step criterion is reached. Usually after the first failure mode occurs, the element deforms heavily under its loading. To avoid element becoming so distorted that it controls the time step, you can define the time-step at which you wish to have the element removed from the calculation.

This failure model is available for Lagrangian solid elements only.

FAILJC – Johnson-Cook Failure Model

Failure is determined from a damage model. Damage is an element variable and increments are given by the plastic strain increment divided by a fracture strain. In addition the damage variable is transported along with material as it move from one Euler element to the other.

It is only available for the Multi-material Euler solver with strength. The use of coupling surfaces is not supported.

FAILMES – Maximum Equivalent Stress Failure Model

This failure model uses the equivalent stress (the first invariant of the stress tensor) as the failure criterion. When the element's equivalent stress reaches beyond the defined stress criterion the element fails completely and is no longer a part of the structure.

This failure model is available for Lagrangian solid elements only.

FAILPRS – Maximum Pressure Failure Model

The maximum pressure failure model defines that the material fails completely when the pressure in the element reaches the defined pressure. This model may be used to model a compressive failure mode in an easy way. The material will not fail on tensile loading.

This failure model is applicable to the orthotropic material (DMATOR) for Lagrangian solid elements only.

FAILSDT – Maximum Plastic Strain and Minimum Time Step Failure Model

This failure model uses the equivalent plastic strain as the failure criterion at which the deviatoric strength of the material is lost. When the plastic strain as defined for the failure model is reached, the material retains its hydrodynamic strength. After the first failure mode has occurred, the elements may deform heavily and start controlling the time step. To avoid this behavior, you can define the time step at which the element must be removed from the calculation or fails completely.

This failure model is available for Lagrangian solid elements only.

FAILDT – Minimum Time Step Failure Model

This (numerical) failure model defines the minimum time step that an element can reach before it is effectively removed from the analysis. Please note that this failure model is not based on physics, but is meant to maintain analysis effectivity. There are occasions where elements determine the time step although they are actually irrelevant to the analysis. For example, in cases where part of the structure breaks off due to physical material failure, the elements in the debris may control the time step. When these elements are no longer relevant but control the time step, your analysis may undesirably slow down. Using the time step based failure criterion then helps you in maintaining an effective analysis as the undesired elements are removed from the computation.

This failure model is available for all material definitions for Lagrangian solid and shell (CQUAD4) elements.

Spallation Models

A spallation model defines the minimum pressure prior to spallation. At present there is only one spallation model, PMINC, that defines a constant spallation pressure.

PMINC – Constant Minimum Pressure

A constant minimum pressure must be defined that must be less than or equal to zero. Note that the pressure is positive in compression. If the pressure in an element falls below the minimum pressure, the element spall and the pressure and yield stress are set to zero. The material then behaves like a fluid. When the pressure subsequently becomes positive, the material is no longer in a spalled state. The pressure can then decrease again to the specified minimum (the spall limit) before spallation occurs again.

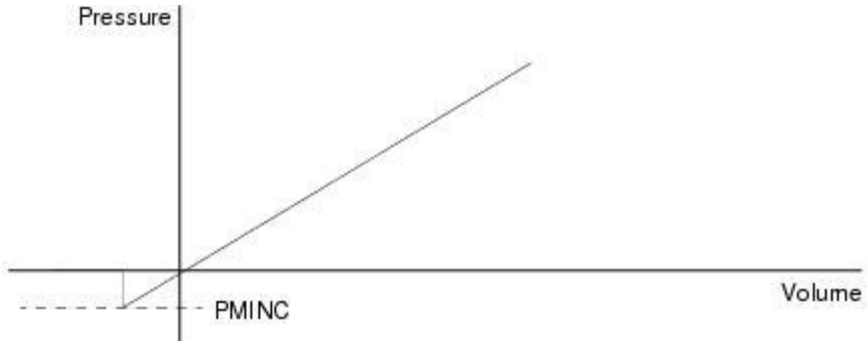

Figure 4-14 Minimum Pressure Cutoff

Artificial Viscosities

The types of artificial viscosity used in Dytran are bulk viscosity and hourglass viscosity. The parameters for bulk viscosity are material parameters. The hourglass-viscosity parameters are defined per property.

Bulk Viscosity

Artificial bulk viscosity is used to control the formation of shock waves. Shock waves are the propagation of discontinuities in velocity. The simplest example of a shock wave is a "square wave." An ideal impact between two flat surfaces generates a square wave. Materials that stiffen upon deformation can produce a shock wave from a smooth wave profile. A finite element model of a continuous body cannot numerically represent this propagating discontinuity. When a time integration scheme without algorithmic damping (such as the explicit central difference method) is used to integrate the response, severe oscillations in amplitude trail the shock front. These oscillations can be traced to the limitations imposed by the finite frequency spectrum of the finite element mesh.

To control the oscillations trailing the shock front, artificial bulk viscosity is introduced. Artificial bulk viscosity is designed to increase the pressure in the shock front as a function of the strain rate. The effect on the shock wave is that it will be smeared over approximately five elements. Reducing the coefficients in an attempt to steepen the wave front may result in undesirable oscillations trailing the shock, a condition sometimes referred to as "overshoot."

An artificial viscosity term Q is added to the pressure. An artificial viscosity term can be considered as a modification to the pressure p, which is replaced by:

$$p^* = p + Q$$

The definition of the artificial viscosity term that modifies the pressure:

$$Q = \max\left(\left[-\rho \cdot C_Q^2 \cdot d^2 \cdot \frac{\dot{V}}{V} \cdot \left|\frac{\dot{V}}{V}\right|\right],0\right) + \max\left(\left[-\rho \cdot C_L \cdot d \cdot c \cdot \frac{\dot{V}}{V}\right],0\right)$$

where

C_Q	=	constant = 1.0
C_L	=	constant = 0.0

d is the characteristic element dimension and c is the material speed of sound.

The bulk viscosity equations contain both linear and quadratic terms that are given default values suitable for most situations. The values of the viscosity coefficients, BULKL for the linear viscosity, and BULKQ for the quadratic viscosity, can be changed on the respective fields of the material entries. Using the parameter BULKL, and BULKQ entries results in a global redefinition of the default values.

Hourglass Damping

The solid and shell elements in Dytran have only one integration point at the center of the element. This makes the program very efficient since each element requires relatively little processing, but it also introduces the problem of hourglassing.

For simplicity, consider the two-dimensional membrane action of a CQUAD4 element.

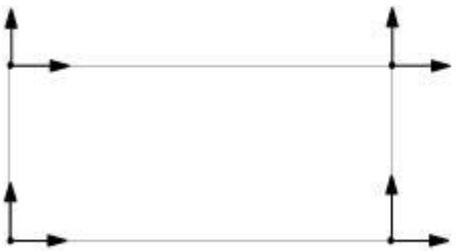

The element has four grid points, each with two degrees of freedom. There are, therefore, a total of eight degrees of freedom and eight modes of deformation. There are three rigid body modes, two translational modes, and one rotational mode.

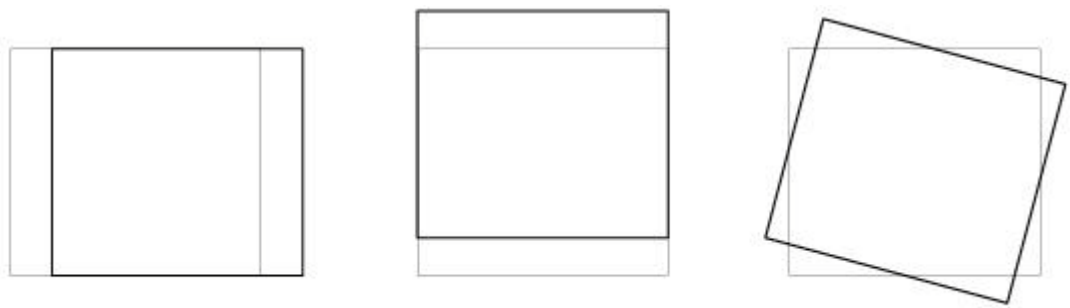

With a single integration point, two direct and one shear stress are calculated at the center of the element. This means that only three modes of deformation have stiffness associated with them.

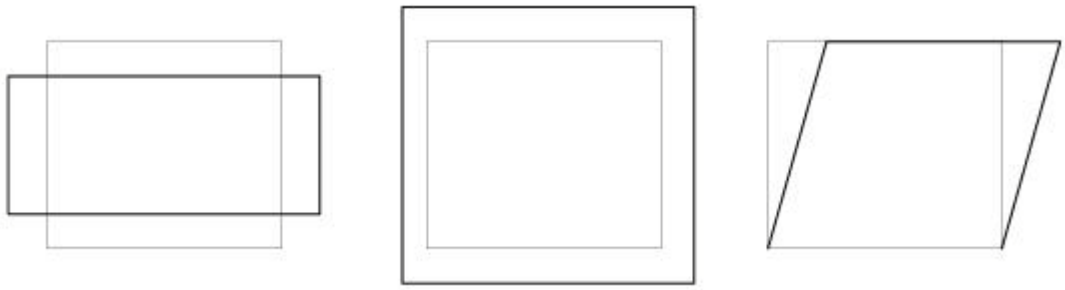

Two modes of deformation remain, that correspond to the linear stress terms. With a single integration point, these have no stiffness associated with them and are called the zero energy or hourglass modes.

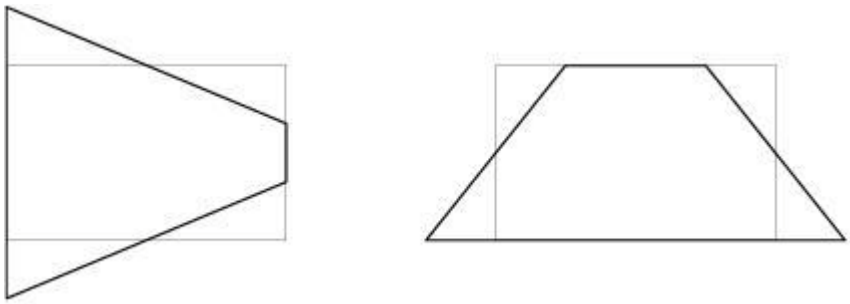

When no measures are taken to stop these modes from occurring, they rapidly spread through the mesh and degrade the accuracy of the calculation (Figure 4-15), reduce the time step, and ultimately cause the analysis to abort when the length of the side of an element becomes zero.

Similar zero energy modes exist for the bending deformation of CQUAD4 elements, in CHEXA and CPENTAelements. CTRIA3 and CTETRA elements do not suffer from hourglassing, since no zero energy modes exist in these elements.

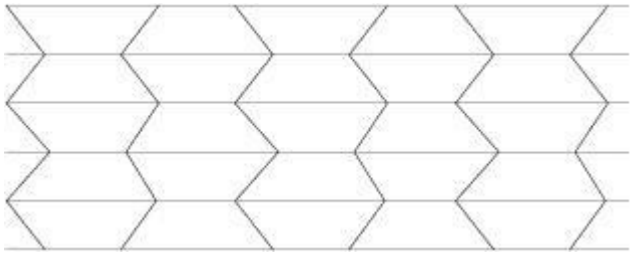

Figure 4-15 Deformation of a Mesh Showing Hourglassing

Sophisticated methods for controlling hourglassing are available in Dytran. There are two forms: viscous and stiffness damping. The viscous form damps out hourglass modes and is carefully tuned so that other modes of deformation are not affected. The stiffness form applies forces to restrict the hourglass deformation by controlling the nonlinear part of the strain field that produces hourglassing. Normally the viscous forms work

well, but, in some instances, are not adequate. The stiffness form is more effective but tends to make the elements overly stiff, depending on the input parameters selected.

Each of the hourglass forms has slightly different characteristics. The default model is efficient and recommended for general use.

The default hourglass type can be reset using the PARAM, HGTYPE, HGSHELL, or HGSOLID option. The hourglass coefficient can also be specified using the PARAM, HGCOEFF, HGCMEM, HGCWRP, HGCTWS, or HGCSOL option. In addition, the hourglass type and coefficient can be specified for each individual property using the HGSUPPR entry.

Careful modeling can help prevent the occurrence of hourglassing in a mesh. Try to avoid sharp concentrations of load and isolated constraints. Rather, try to spread the loading and constraint over as large an area as possible. Some examples of how to avoid hourglassing are shown in Figure 4-16.

In the majority of cases, hourglassing does not cause any problem. In those instances where it does begin to occur, adjustment of the type of hourglass control and the hourglass viscosity should allow the analysis to be completed successfully. Extreme cases of hourglassing are normally caused by coarse meshes. The only solution is to refine the mesh.

Increasing the hourglass coefficient helps prevent hourglassing. However, excessively large values can cause numerical problems. Start with the default value and only increase it if excessive hourglassing occurs.

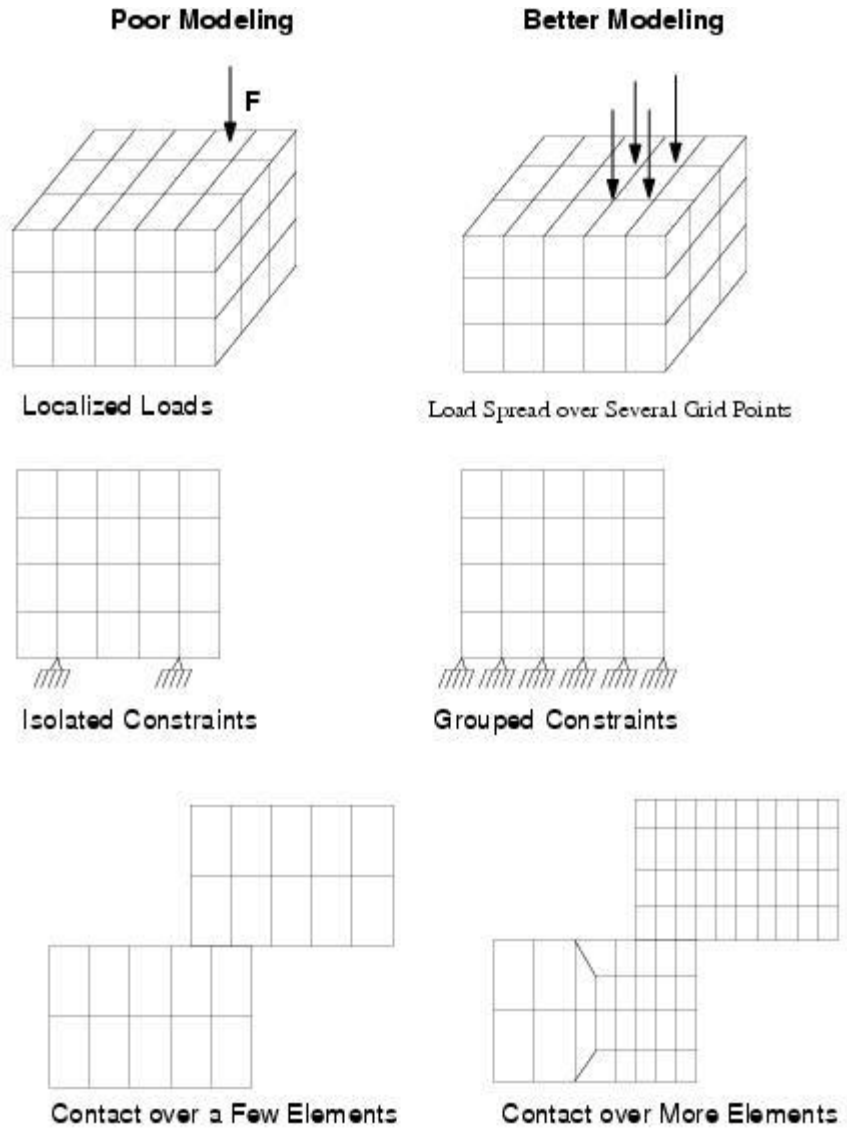

Figure 4-16 Hourglass Promotion and Avoidance

Dynamic Relaxation

Dynamic Relaxation (DR) is a process that uses a damping concept to find the steady-state part of a dynamic solution to a transient response. In general, problems, especially those with highly nonlinear geometric and material behavior, can be treated with an explicit DR method. In many cases, however, the number of iterations needed to reach convergence can be very large.

Dytran offers two possible ways of dynamic relaxation to find a static solution of a structural mechanic problem. The static part of the dynamic solution is found by introducing damping in the iterative solution scheme that is used to solve the equations of motion.

Alpha Damping (VISCDMP)

The Alpha-type of dynamic relaxation uses a single damping parameter that is introduced in the central difference integration scheme of the equations of motion

$$v^{n+1/2} = v^{n-1/2} \cdot (1-\alpha) + a^n \cdot \Delta t^n \tag{4-22}$$

where v denotes the grid-point velocity, a is the acceleration, Δt is the time step, and α is the dynamic relaxation parameter (the damping coefficient). The DR parameter can be individually defined for each available structural element type in Dytran and is input on the VISCDMP entry.

The choice of the DR parameter(s) depends on the natural frequencies of the system. The critical damping α should be taken to be approximately 5/3 times the critical damping (or 5/3 times the natural frequency times the time step).

Global, C-Matrix, or System Damping (VDAMP)

Dynamic relaxation that uses global damping as the damping device is based on a mass-spring-damper system. The equation of motion reads

$$M \cdot a^n + C \cdot v^n + F^n_{int} = F^n_{ext} \tag{4-23}$$

The dynamic relaxation scheme uses the following C-matrix

$$C = \frac{2\beta}{\Delta t} M \tag{4-24}$$

All matrices are diagonal. Thus, each degree of freedom can be written as

$$m_i \cdot a_i + \frac{2\beta}{\Delta t} m_i \cdot v_i^n = (f^n_{ext} - f^n_{\text{int}})_i \tag{4-25}$$

A central difference time integration scheme is applied, yielding

$$a_i^n = \frac{v_i^{n+1/2} - v_i^{n-1/2}}{\Delta t}, \quad v_i^n = \frac{v_i^{n+1/2} + v_i^{n-1/2}}{2} \tag{4-26}$$

Combining Equations (4-25) and (4-26) leads to the following expression for the updated velocity

$$v_i^{n+1/2} = \frac{1-\beta}{1+\beta} \cdot v_i^{n+1/2} + \frac{\Delta t}{1+\beta} \cdot \left\{ \frac{f^n_{exr} - f^n_{\text{int}}}{m_i} \right\}$$

where the parameter β is input on the VDAMP entry.

Equation (4-24) can also be written as

$$m_i \cdot a_i + b_i \cdot v_i = k_i \cdot d_i \tag{4-27}$$

that describes the dynamic motion of a damped, single-degree-of-freedom system. The natural frequency of such a system is found to be

$$\omega_i = \sqrt{\frac{k_i}{m_i}} \tag{4-28}$$

Critical damping is defined by

$$b_i^{crit} = 2m_i \cdot \omega_i = 2\sqrt{km_i} \tag{4-29}$$

Or, in terms of the dynamic relaxation parameter

$$\beta_i^{crit} = \omega_i \cdot \Delta t = \sqrt{\frac{k_i}{m_i}} \cdot \Delta t \tag{4-30}$$

For a system with one degree of freedom, with a constant time step, and with $(f_{ext} - f_{\text{int}}) = -kd$, the dynamic relaxation parameter β can be related directly to a percentage of critical damping. This is shown in the following example. Such a direct relation is not possible for structures that have a lot of different natural frequencies. In those cases, the dynamic relaxation parameter should be set so that it corresponds to the lowest natural frequency. Also, the time step changes during the calculation, making it less easy to relate the relaxation parameter to a natural frequency. See Figure 4-17 and Figure 4-18 for solution for different values of dynamic relaxation parameters α and β.

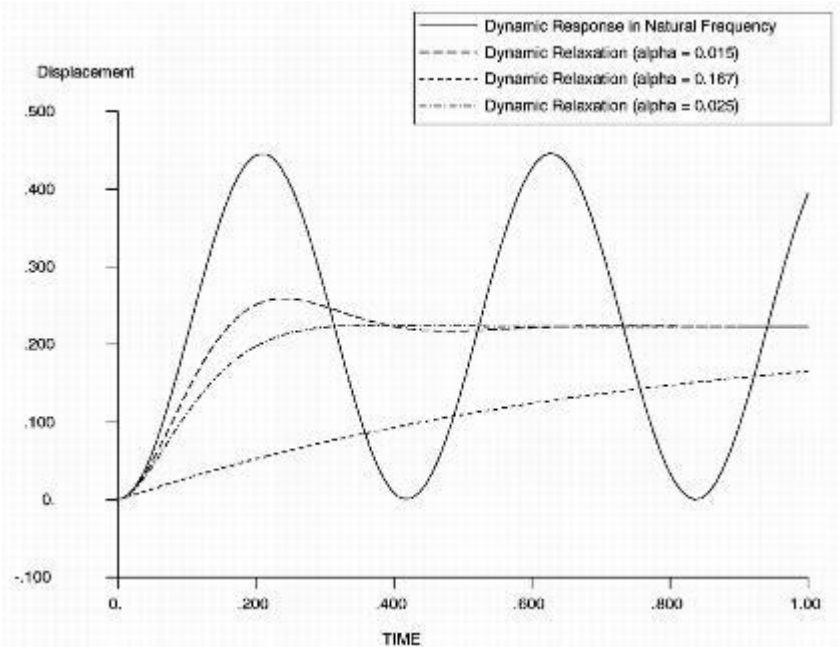

Figure 4-17 Solution for Different Values of the Dynamic Relaxation Parameter (α)

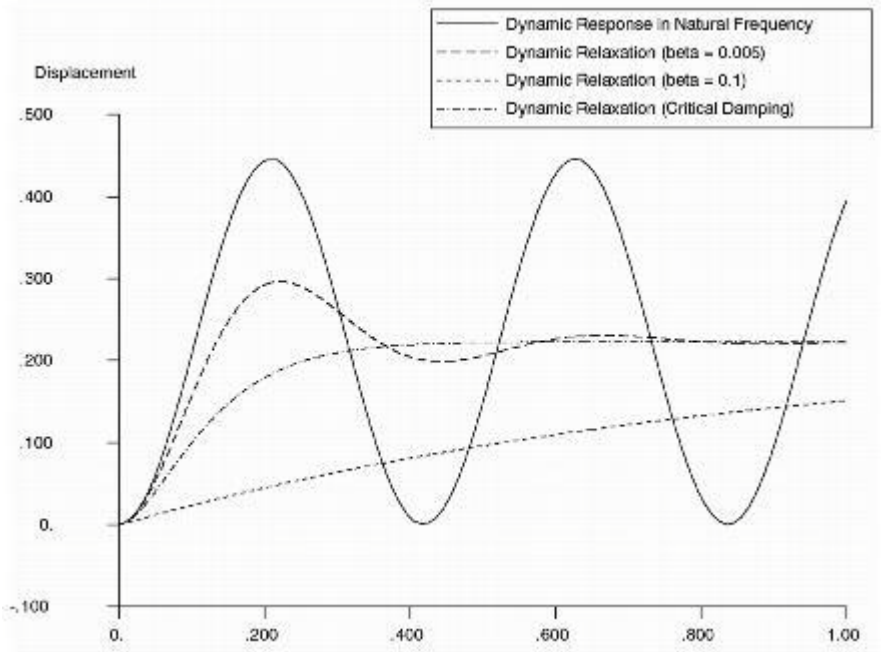

Figure 4-18 Solution for Different Values of the Dynamic Relaxation Parameter (β)

Remarks

Always be very careful when using damping in general, especially if there are large nonlinearities in the solution. Nonlinear solutions are path dependent, and artificially introducing a source of viscosity (damping) might interfere with the solution path.

In regard to the efficiency of the dynamic relaxation, keep in mind that it can require a large number of time steps to reach convergence, as mentioned previously. This is the case in those problems where the ratio between the largest and the smallest natural frequency is large. In such cases, the stable explicit time step is very small compared to the period corresponding to the largest natural frequency. It is very often advantageous to use an implicit code such as MSC.Nastran® in these situations to find the static part of the solution and use this as an initial state. Dytran also supports this capability (NASINIT).

Example

m	=	1 kg
k	=	225 kg/sec^2 (=N/m)
f	=	50 N
Δt	=	1 msec
Natural frequency	$\omega = \sqrt{k/m} = 15$ (rad/sec)	
Period	$T = 2\pi/\omega = 0.4188$ (sec)	
Critical damping	$\beta = \omega\Delta t = 0.015$	

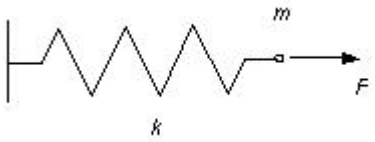

User-defined Porosity Models

A customized porosity model can be defined by a user-defined subroutine in Dytran. By referencing a porosity definition (COUPOR from the coupling definition entry (COUPLE) you can choose several options. There are a number of pre-defined porosity models defined, but when you choose the POREX type on the COUPOR entry, Dytran calls the EXPOR subroutine in every time step. The model must then be programmed into the user subroutine and provide Dytran with required output to continue the computation.

The theory behind the computation of fluxed quantities and the way in which impulse is exerted on the faces is explained below.

The user subroutine is required to return the volume and mass flow through each segment that the coupling surface is constructed from. Dytran then takes the void fraction of the element into account in case there is outflow at the segment:

$$dV = dV_{\text{exp } or} \cdot (1 - f_{void})$$

$$dm = dm_{\text{exp } or} \cdot (1 - f_{void})$$

The sign of the transported volume defines in- and outflow. A positive transported volume means outflow over the segment and a negative volume transport defines inflow over the segment. Given the volume and mass flow, the other fluxed quantities can be computed. The momentum in all three directions is fluxed according to:

$$dI_i = dm \cdot v_i$$

where $i = 1, 2, 3$ for the x-, y- and z-direction and v_i is the velocity component. In case of outflow, the velocity component is taken as the element velocity from the element that the segment is connected to. In case of inflow, the velocity component uses the value as defined by the user in the user subroutine and returned to Dytran through the velocity arrays.

The total energy flux over the segment is computed as

$$dE = E \cdot dm$$

where E is the total energy at the segment. In case of outflow, the total energy is taken to be the total energy in the element that the face is connected to. In case of inflow, the total energy is used from the value returned by the user subroutine.

After the flux computations have been performed, the resulting impulse is computed. The impulse acts on the area of the segment and is computed by taking the porosity factor into account:

$$dI = p \cdot (1 - c) \cdot A \cdot dt$$

where dI is the impulse to be exerted on the segment, p is the pressure at the face, c is the porosity coefficient, A the segment area, and dt the increment in time. The porosity factor must be within the range $0.0 \le c \le 1.0$ where $c = 0$ implies a segment closed for in- or outflow, and $c = 1$ a segment that is fully open to in- or outflow.

Permeability

Permeability is defined as the velocity of gas through a surface area depending on the pressure difference over that area.

On the PERMEAB and PERMGBG entries, permeability can be specified by either a coefficient or a pressure dependent table:

a. Coefficient: Massflow = coeff*pressure_difference

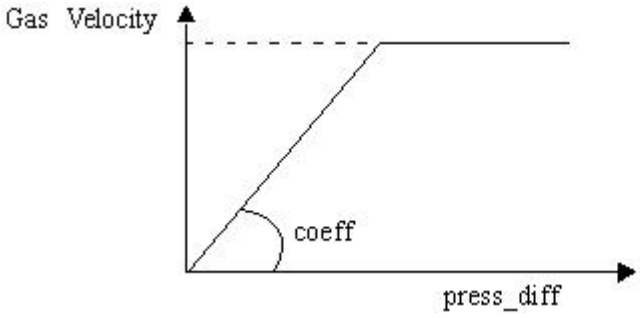

$$coeff = \frac{\delta(massflow)}{\delta(pressdiff)}$$

b. Table:

The velocity of the gas flow can never exceed the sonic speed:

$$V_{max} = V_{sonic} = \sqrt{\gamma R T_{crit}}$$

where γ is the gas constant of in- or outflowing gas, and T_{crit} is the critical temperature.

The critical temperature can be calculated as follows:

$$\frac{T_{crit}}{T_{gas}} = \frac{2}{(\gamma + 1)}$$

where T_{gas} is the temperature of outflowing gas.

Holes

Flow through holes as defined on the PORLHOLE or PORFGBG entries is based on the theory of one-dimensional gas flow through a small orifice. The formulas to calculate the velocity of the gas are the same as for the PORFLOW with the pressure method. The formulas are given in Chapter 2: Principles of the Eulerian and Lagrangian Solvers of this manual.

Flow between coupling surfaces through holes can also be defined by a permeability model by using the PERMCPL entry. The formulas to calculate the velocity of the gas are the same as for PERMEAB.

Hybrid Inflator Model

The hybrid inflator supports the inflow of multiple gases through an inflator subsurface, as well as providing a type of thermally ideal gas for which the specific heat at constant pressure c_p can be dependent on temperature.

In addition, the properties of the gas contained in an air bag will be changed based on the gas composition and temperature. Updating of gas constants is available for use together with INFLATR, IINFLATR1, INFLHYB, and INFLHYB1 inflator definitions, and with PORHOLE, PERMEAB, PERMGBG, and PORFGBG porosity definitions.

Ideal Gas Description

A thermally ideal gas is specified by the specific gas constant and the variation of specific heat at constant pressure with temperature.

The specific gas constant for a gas is defined as:

$$R = R_{uni}/M$$

Where R_{uni} is the universal gas constant and M the gas molar weight.

Using the specific heat as function of temperature, the specific internal energy of a gas as a function of temperature is found as:

$$e(T) = \int_{T_{ref}}^{T} (c_F(T) - R) \cdot dT + e_{ref}$$

We can now define $\bar{c}_v$ so that:

$$e(T) = \bar{c}_v(T) \cdot T$$

Mixture of Gas

A hybrid inflator is specifically meant to give an inflow of several gases with different properties. To account for the properties of these gases, it is necessary to keep track of the composition of a gas at a certain time, not

only for the inflator but also for the gas mixture inside air bag. For use with hybrid inflators, it is assumed that instantaneous mixing takes place. This means the gas composition will be the same throughout the volume.

For an inflator, gas fractions are given as user input. For gas bags and Eulerian, gas fractions are based on the total mass of each gas at a certain time. Gas fractions are defined as follows:

$$mfrac_i(t) = \frac{mass_i(t)}{mass_i(t)}$$

Properties of the gas mixture inside a surface are based upon the principle that a mixture of (thermally) ideal gases is itself an ideal gas. This yields for the properties of the mixture:

$$R^* = \sum_{i=1}^{m} mfrac_i(t) \cdot R_i$$

$$c_v^* = \sum_{i=1}^{m} mfrac_i(t) \cdot c_{v_i}(T)$$

$$c_p^* = c_v^* + R^*$$

$$\gamma^* = \frac{c_p^*}{c_v^*}$$

Here T is the temperature of the gas mixture. This may be the inflow temperature of the inflator, the temperature inside a constant pressure gas bag, or the average temperature of all Eulerian elements that are not covered by the coupling surface. The latter is found as:

$$T_{Euler} = \frac{\sum e_{cell}}{c_{v_{Euler}}}$$

Energy/Work

A formulation for the change of energy in a closed volume can be found when c_p and c_v are a function of temperature and gas composition. This takes into account inflow (by hybrid inflators), outflow (by porosity) and energy loss (through convection and radiation).

We know:

$$dQ = dU + pdV$$

where:

$$dQ = dq_{in} - dq_{loss} - dq_{out}$$

$$dU = m \cdot de + e \cdot dm$$

For inflow of a certain mixture we find:

$$\frac{dq_{in}}{dt} = [\dot{M}_{in}(t) \cdot c^{*}_{p_{in}}(T_{in})] \cdot T_{in}$$

Similarly, for outflow:

$$\frac{dq_{out}}{dt} = [M_{out}(t) \cdot \dot{c}^{*}_{p_{out}}(T_{out})] \cdot T_{out}$$

For the work done by the gas mixture the following holds:

$$p\frac{dV}{dt} = M \cdot (c_p^* - c_v^*) \cdot T \cdot \frac{\dot{V}}{V}$$

Given the expressions above for a thermally ideal gas and a general mixture of these gases, this finally yields for the rate of temperature change in an enclosed volume:

$$\left(1 + \frac{T}{c_v^*}\frac{dc_v^*}{dT}\right) \cdot \frac{\dot{T}}{T} = \frac{1}{M \cdot e} \cdot [\dot{M}_{in} \cdot c_{p_{in}}^*(t, T_{in})] \cdot T_{in} -$$

$$([\dot{M}_{out} \cdot c_{p_{out}}^*(t, T_{out})] \cdot T_{out} - Q_{loss}) - \frac{\sum_i (c_{v_i}(T) \cdot \dot{m}_i)}{M \cdot c_v^*} - (\dot{\gamma} - 1) \cdot \frac{\dot{V}}{V}$$

Air Bag Fabric

Woven Fabric Material Model

This material model is intended for simulating woven materials as used in airbags. This model can only be referred to by triangular shell with one Gauss point when used in airbags. For other applications, it may be referred to by elements with membrane behavior (triangular quadrilateral shell with one Gauss point). Additionally, it can be referred to by the layered composite element property PBCOMP The model is based on a finite strain formulation and tracks the orientation of the fabric tows in both warp and weft direction (that is, warp ends and weft picks) as large shear strains occur.

To allow for an arbitrary orientation of the elements within the finite element mesh, the global warp/weft orientation vector supplied by the user is first transformed into local element system. Each warp/weft tow direction is now tracked with an angle ϕ with respect to the local element system. The strain is a state variable for the tow. Since this is a model which tracks tow directions and uses total tow strain as a state variable, rotation of the stress state from n to $n+1$ is not required. The orientation of the warp and weft tows must be updated instead. The strain rate in the warp ends and weft picks can now be incrementally updated.

$$\varepsilon_i^{n+1} = \varepsilon_i^n + \Delta\varepsilon_i^{n+\frac{1}{2}} \tag{4-31}$$

in which

$$\Delta\varepsilon_i^{n+\frac{1}{2}} = \begin{bmatrix}\Delta\varepsilon_1\\ \Delta\varepsilon_2\end{bmatrix} = \begin{bmatrix}\left(\cos\phi_1^{n+\frac{1}{2}}\right)^2 & \left(\sin\phi_1^{n+\frac{1}{2}}\right)^2 & 2\cos\phi_1^{n+\frac{1}{2}}\sin\phi_1^{n+\frac{1}{2}}\\ \left(\cos\phi_2^{n+\frac{1}{2}}\right)^2 & \left(\sin\phi_2^{n+\frac{1}{2}}\right)^2 & 2\cos\phi_2^{n+\frac{1}{2}}\sin\phi_2^{n+\frac{1}{2}}\end{bmatrix}\begin{bmatrix}\dot{\varepsilon}_{xx}^{n+\frac{1}{2}}\\ \dot{\varepsilon}_{yy}^{n+\frac{1}{2}}\\ \dot{\varepsilon}_{xy}^{n+\frac{1}{2}}\end{bmatrix}\Delta t^{n+\frac{1}{2}} \quad (4\text{-}32)$$

where the subscripts on the strain and angle (ε and ϕ) are used to indicate the warp ends (ϕ_1) and weft picks (ϕ_2). The warp/weft direct stress can be computed from

$$\phi_i^{n+1} = E_{iL}\varepsilon_i^{n+1} + E_{iQ}(\varepsilon_i^{n+1})^2$$

Definition of both linear and quadratic stiffness coefficients (E_{iL} and E_{iQ}) allows for the simulation of fabric slack; that is, increasing stiffness with increasing strain.

Because some types of tow material are not able to carry compressive stresses, the model has a so-called no-compression option. By switching compression off, the stress is zero when the fabric goes into compression and its stress remains zero while the fabric wrinkles. Tensile stress cannot occur until original stress-free flat condition is recovered.

After calculation of the warp/weft direct stresses, the stresses of (4-31) are transformed back into the local element coordinate system.

$$\begin{bmatrix}\sigma_{xx}^{n+1}\\ \sigma_{yy}^{n+1}\\ \sigma_{xy}^{n+1}\end{bmatrix} = \begin{bmatrix}\left(\cos\phi_1^{n+\frac{1}{2}}\right)^2 & \left(\cos\phi_2^{n+\frac{1}{2}}\right)^2\\ \left(\sin\phi_1^{n+\frac{1}{2}}\right)^2 & \left(\sin\phi_2^{n+\frac{1}{2}}\right)^2\\ \cos\phi_1^{n+\frac{1}{2}}\sin\phi_1^{n+\frac{1}{2}} & \cos\phi_2^{n+\frac{1}{2}}\sin\phi_2^{n+\frac{1}{2}}\end{bmatrix}\begin{bmatrix}\sigma_1^{n+1}\\ \sigma_2^{n+1}\end{bmatrix}$$

The shear carrying capacity is based on friction between the warp ends and weft picks. This can be accounted for by calculating the strain increment midway the warp and weft tows; that is,

$$\dot{\varepsilon}_m^{n+\frac{1}{2}} = \dot{\varepsilon}_{xx}^{n+\frac{1}{2}}\left(\cos\phi_m^{n+\frac{1}{2}}\right)^2 + \dot{\varepsilon}_{yy}^{n+\frac{1}{2}}\left(\sin\phi_m^{n+\frac{1}{2}}\right)^2 + 2\dot{\varepsilon}_{xy}^{n+\frac{1}{2}}\cos\phi_m^{n+\frac{1}{2}}\sin\phi_m^{n+\frac{1}{2}}$$

where ϕ_m denotes the angle of the direction vector midway the warp and weft tows with respect to the X-local element axis. The additional midway-stress due to friction can now be incrementally updated

$$\sigma_m^{n+1} = \sigma_m^n + \Delta\sigma_m^{n+\frac{1}{2}}$$

in which

$$\Delta\sigma_m^{n+\frac{1}{2}} = 2G_{12}\dot{\varepsilon}_m^{n+\frac{1}{2}}\Delta t^{n+\frac{1}{2}}$$

where G_{12} is the shear stiffness of the fabric material. The shear stiffness of a woven fabric material is not constant but depends on the shearing angle (see Intraply Shearing Test). At relatively small shearing angles, the initial shear stiffness can be assessed by

$$G_{12} = \frac{\sqrt{E_{1L}E_{2L}}}{2(1+\nu)} \tag{4-33}$$

where the Poisson's ratio ν is taken to be 0.3.

The maximum shear stress is given by a friction coefficient times the RMS value of the direct warp and weft stresses (only if they are not equal to zero). Hence, a cut-off is applied on the midway-stress such that

$$\sigma_m^{n+1} \le \mu\sqrt{\sigma_1^{n+1}\sigma_2^{n+1}} \tag{4-34}$$

where μ is the friction coefficient to be determined by experiments (see Coefficient of Friction Test). In a similar way, the additional stresses due to friction are taken into account which are directed perpendicularly to the midway direction vector and in-plane of the element.

The total additional stress can now be accounted for by first transforming it in the local element coordinate system.

$$\Delta\sigma_{xx}^{n+1} = \sigma_{m}^{n+1} cos 2\phi_{m}^{n+1}$$

$$\Delta\sigma_{yy}^{n+1} = -\sigma_{m}^{n+1} cos 2\phi_{m}^{n+1}$$

$$\Delta\sigma_{xy}^{n+1} = \sigma_{m}^{n+1} sin 2\phi_{m}^{n+1}$$

and subsequently, it must be added to the stresses obtain by (4-33).

Determination of Fabric Material Parameters

This section is aimed at characterizing the mechanical behavior of woven fabric materials by performing experiments. Testing of composites (and particularly fabrics) has always been difficult in comparison to testing more conventional materials. Woven fabrics are well known for their property anisotropy. Moreover, woven fabrics are also dimensionally changeable. Besides simple uniaxial tests, rather unconventional tests should be carried out in order to obtain the material parameters needed for this fabric model.

Uniaxial Tensile Test

The input of nonlinear constitutive constants (E_{iL} and E_{iQ}) allow for fabric slack; that is, increasing modulus with increasing tensile strain. Stress-strain behavior needs to be recorded in a uniaxial tensile test, and the elastic constants along warp and weft direction can be found by using a least-square fitting method.

Tensile test specimens must be cut along both the warp and weft direction as described in ASTM Test D-3039 [Ref. 7.]. Strain gauges should be mounted along longitudinal and lateral directions. The specimens can be tested at a crosshead speed of 1 or 2 mm/min.

Intraply Shearing Test

Characterization of the in-plane shear properties is essential to modeling the mechanical behavior of fabric materials. Numerous shear test methods [Ref. 8.] have been developed to perform shear stiffness measurements for ordinary composite materials: ±45° off-axis tensile test, the Iosipescu test, the 10° off-axis tensile test. However, there are limited studies available directed towards woven fabrics. In the work of Naik [Ref. 8.], the ±45° off-axis test was found to be an excellent test method for the determination of in-plane shear modulus for plain weave fabric. Unfortunately, this simple test method is not applicable to a nonsquare fabric. For nonsquare fabrics in this test, there is no unique relationship between the applied load and the magnitude of shear stress in the test section.

Therefore, the test setup shown in Figure 4-19 can be constructed which is actually derived from the Treloar shear apparatus [Ref. 9.]. The fabric is vertically positioned in the setup by the clamping of two edges (AB and CD). Both clamp edges have to be positioned such that its direction coincides with the warp direction. The

direction of free edges AC and BD must be parallel to the weft direction. The upper clamp is fixed, whereas the lower clamp can freely move in the vertical plane.

The lower clamp is loaded in vertical direction by a weight W (force per unit clamp length). This fabric is forced to shear in its plane (with a shearing angle α) if a force F is applied to point C parallel to clamp edge CD. As soon as a shearing angle is established, an extra force is necessary to compensate the component due to the weight W on the shearing fabric. The restraining force R (per unit length) to overcome the intraply shearing resistance is therefore

$$R = F + minus\left(W\frac{tana}{sin\theta + tan\alpha cos\theta}\right) \tag{4-35}$$

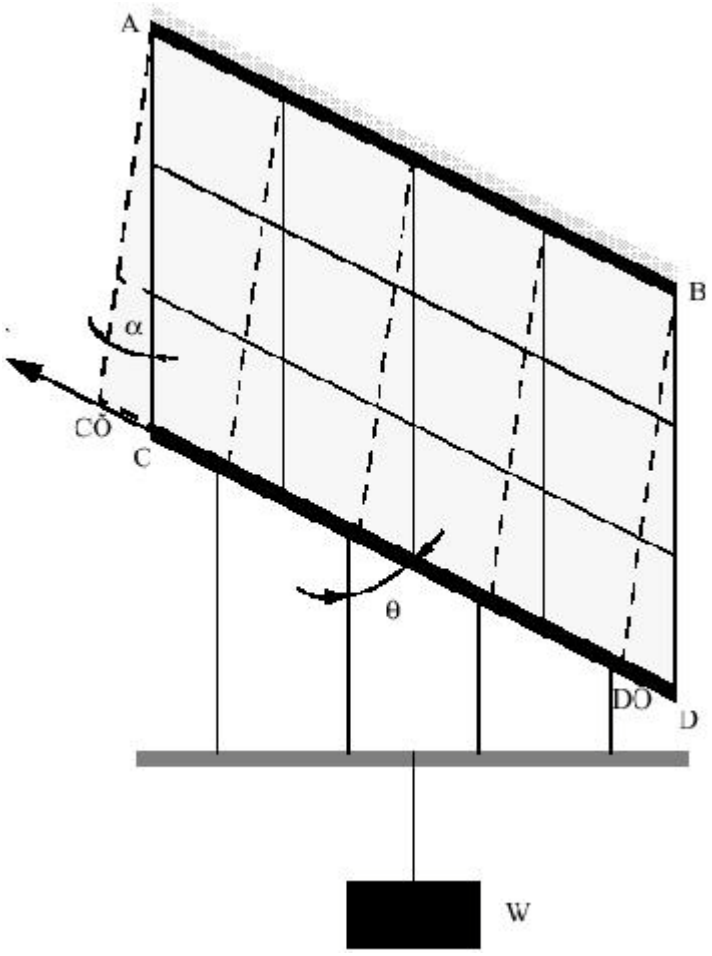

Figure 4-19 Schematic Diagram of Shearing Test Setup for Woven Fabrics

The lower clamp is loaded in vertical direction by a weight W (force per unit clamp length). This fabric is forced to shear in its plane (with a shearing angle α) if a force F is applied to point C parallel to clamp edge CD. As soon as a shearing angle is established, an extra force is necessary to compensate the component due to the weight W on the shearing fabric. The restraining force R (per unit length) to overcome the intraply shearing resistance is therefore

$$R = F + minus\left(W\frac{tana}{sin\theta + tan\alpha cos\theta}\right) \tag{4-36}$$

where θ denotes the constant angle between clamp edge CD and the vertical line BD. During the intraply shearing test, the force F is gradually increased while the shearing angle α must be measured.

A typical output of the shearing text setup is shown in Figure 4-20. It is very likely that the shear deformation is limited by the locking angle α_{lock}. At a certain point during the shearing of a fabric, the force necessary to shear the fabric increases rapidly. At this point, the fabric reaches its locking angle. Note that the initial slope Γ of the curve represents the shear stiffness of the fabric per unit thickness under the condition that relatively small shearing angles occur. Instead of the constant value given by (4-32), the shear stiffness G_{12} as a function of shearing angle α can be obtained from this test.

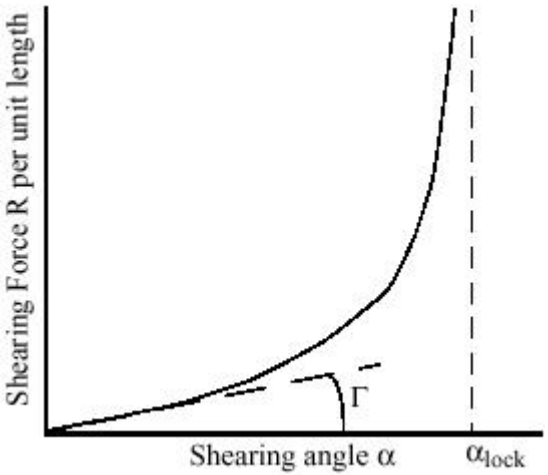

Figure 4-20 Example of the Output of the Shearing Test Setup

For the sake of completeness, the weight W should be varied (for example, 0.1 up to 0.3 N/cm) in order to show its invariance on restraining force R. At least, it should be sufficiently large to prevent wrinkling of the fabric material (otherwise, the strain state is not purely shear anymore).

Coefficient of Friction Test

As mentioned in Uniaxial Tensile Test, this fabric model allows for fabric slack — under loading the woven yarns can be straightened out. Due to the nature of woven fabrics, interlaced fiber bundles always have some degree of plane curvature. The reduction of curvature of the fiber bundles in one direction of a fabric simultaneously increases the curvature of the fiber bundles in the other direction. Stretching in both warp and weft direction results in contact forces between the warp and weft yarns. This is accompanied with friction on the contact surface of the interlacing fiber bundles. Consequently, a fabric in which, for example, the weft picks are stretched, increases the stiffness of the fabric in warp direction — the warp ends are effectively stiffer. It can be imagined that this holds up to a certain extent of straining. Beyond that extent, the friction stresses on the contact surface of the interlacing fibers cannot be sustained anymore.

In order to obtain the coefficient of friction as given in (4-33), the test setup shown in Figure 4-21 is necessary. The fabric (denoted by abcd) is stretched in between four rigid clamps. These clamps can only impose a load in either warp or weft direction. One clamp is fixed in space while the rest can move perpendicularly to its axis. The frame structure may be horizontally positioned.

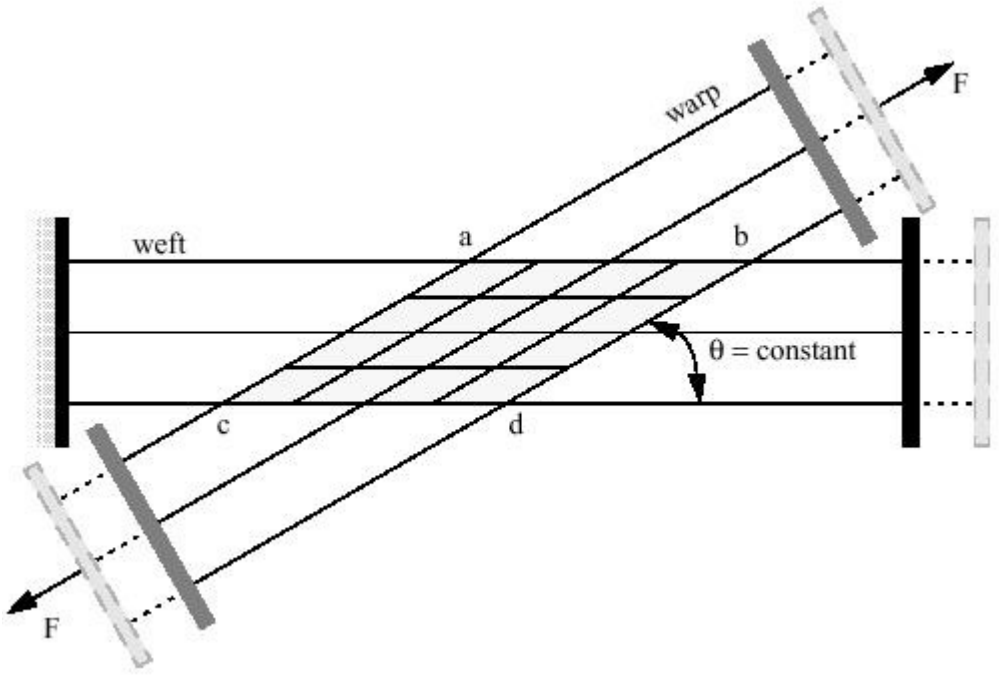

Figure 4-21 Schematic Diagram of Test Setup for Determination of Coefficient of Friction

The test setup is configured such that shearing of the fabric cannot occur during testing. This deliberately establishes a coefficient of friction without mixing it up with the shear deformation as mentioned in Intraply Shearing Test .

The test is initialized by prestraining the fabric in weft direction, such that its corresponding stress σ_2 remains constant throughout the test. Subsequently, imposing a tensile load F on the fabric in warp direction and measuring its corresponding stress σ_1 versus ε_1 strain curve (Figure 4-22). It can be expected that this curve is somewhat higher than the one measured in a uniaxial tensile test (say $\Delta\sigma_t$). In the uniaxial test, σ_2 is zero so that it does not have any contribution to the direct stress in the warp ends. In the case that σ_2 is not equal to zero, the direct stress in the warp ends is increased by $\sigma_2 cos\theta^2$, where θ is the angle between the warp and weft tows (θ is constant here).

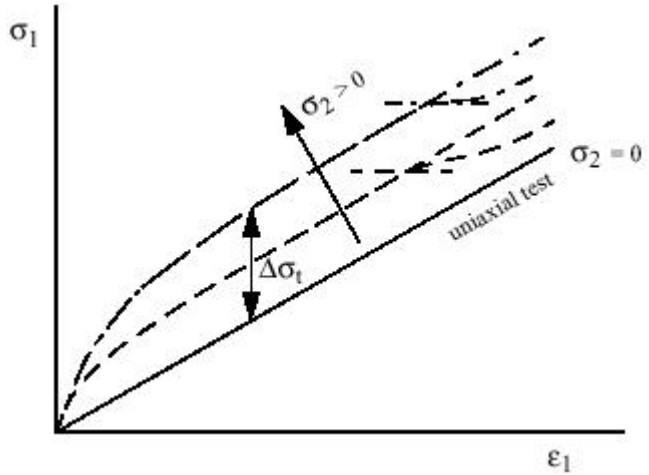

Figure 4-22 Example of the Output of Stress-strain Curves of Fabric in Warp Direction Showing the Effect of Prestraining in Weft Direction

At a certain combination of warp and weft stresses, the additional increase in stress $\Delta\sigma_t$ (see Figure 4-22) cannot be carried anymore by friction forces on the crossover points of the yarns. It becomes smaller than the stress contribution due to prestraining in the weft direction. In formula form

$$\Delta\sigma_t < \sigma_2 cos\theta^2 \tag{4-37}$$

If (4-37) is satisfied for a combination of σ_1 and σ_2, the coefficient of friction can be calculated by using

$$\mu = \frac{\Delta\sigma_t}{cos2\theta\sqrt{\sigma_1\sigma_2}} \tag{4-38}$$

In order to get a consistent coefficient of friction, repeat the preceding procedure by choosing several levels of prestraining in the weft direction (that is, vary σ_2) and take the mean value of μ.

Seat Belts

A seat belt constraint system can be modeled within Dytran using a special belt element. The element has the following characteristics:

- Tension-only nonlinear spring with mass.
- User-defined loading and unloading path.
- Damping is included to prevent high-frequency oscillations.
- Possible to prestress and/or feed additional slack.

A special contact algorithm is available to model the contact between the belt elements and an occupant model.

Seat Belt Material Characteristics

You can specify the following material characteristics on a PBELT entry:

Loading and Unloading Curves

The loading/unloading curves are defined in a TABLED1 entry specifying the force as a function of strain. The strain is defined as engineering strain

$$\varepsilon^n = \frac{l^n - l^o}{l^o}$$

where l^n is the length at time n and l^o is the length at time zero.

The loading and unloading curves must start at (0, 0).

Upon unloading, the unloading curve is shifted along the strain axis until it intersects the loading curve at the point from which unloading commences. An example of a typical load, unload, and reload sequence is shown in Figure 4-23.

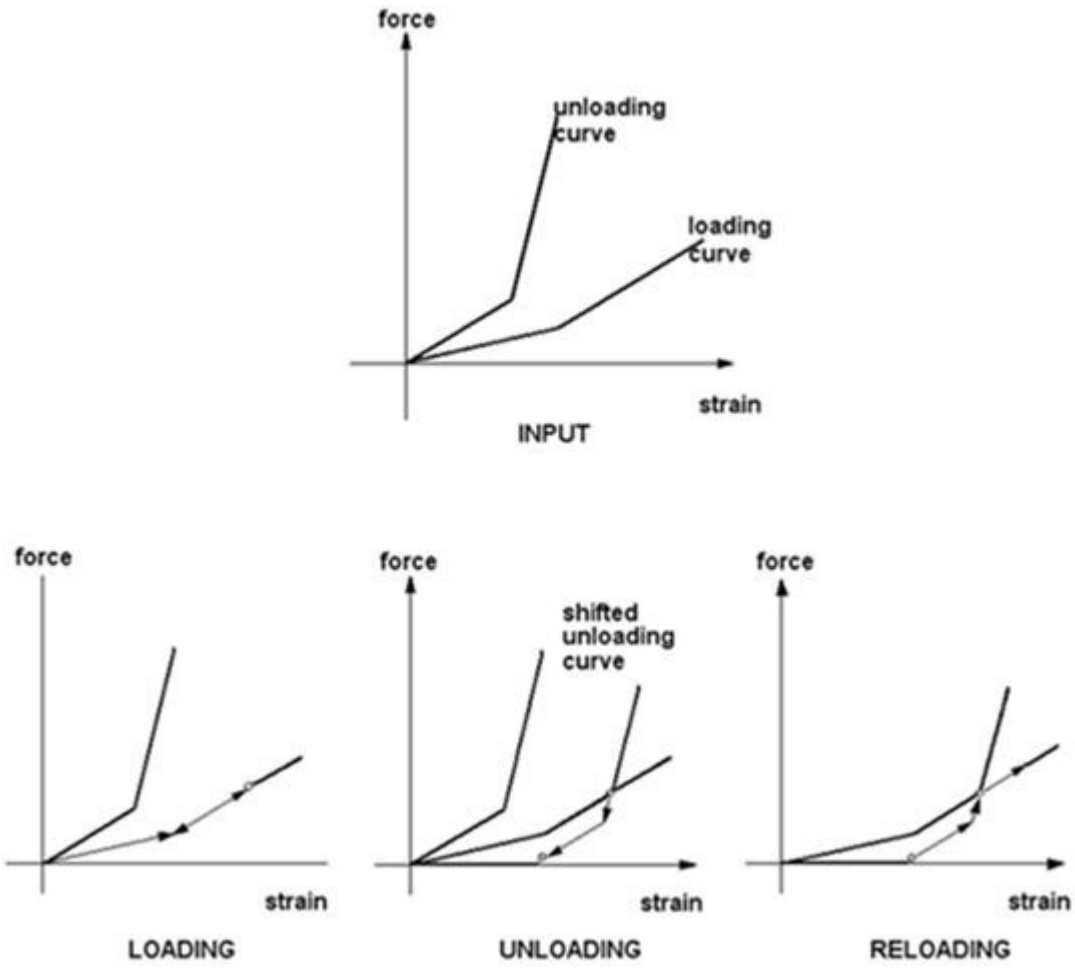

Figure 4-23 Seat Belt Loading and Unloading Characteristics

The unloading table is applied for unloading and reloading until the strain again exceeds the point of intersection. At further loading, the loading table will be applied.

Seat Belt Element Density

The density of the belt elements is entered as mass per unit length. The density is used during initialization to distribute the mass to the grid points. The grid points masses are used to calculate damping and contact forces.

Damping Forces

A damping force is added to the internal force to damp high-frequency oscillations. The damping force $\vec{F}D$ is equal to

$$\vec{F}D = \alpha_1 M \cdot \frac{\vec{V}G1 - \vec{V}G2}{\Delta t}$$

where α_1 is the damping factor CDAMP1 as defined on the PBELT entry, M is the element mass, $\vec{V}G1$ and $\vec{V}G2$ denote the velocity of grid point 1 and grid point 2 of the element, respectively. Δt is the time step.

The damping force $\vec{F}D$ is limited to

$$\vec{F}D = max(\vec{F}D, \alpha_2 \vec{F}S)$$

where α_2 is the damping coefficient CDAMP2 as defined on the PBELT entry, and $\vec{F}S$ is the internal force in the element.

Slack

Additional slack can be fed into the belt elements as a function of time. The slack is specified in the engineering strain and is subtracted from the element strain at time n as

$$\varepsilon^n = \varepsilon^n - \varepsilon^n_{slack}$$

where ε^n_{slack} denotes the slack strain as found from the TABLED1 definition in the input file.

The force in the element is zero until the element strain exceeds the slack.

Prestress

The seat belt elements can be prestressed as a function of time. The prestress strain is specified in the engineering strain and is added to the element strain at time n as

$$\varepsilon^n = \varepsilon^n + \varepsilon^n_{prestress}$$

where $\varepsilon^n_{prestress}$ is the prestress strain as found from the TABLED1 definition in the input file.

As a result, the elements build up a tensile force.

5 Classical Lamination Theory (CLT) for Multilayered Shells

Overview

The problem of shell structure with layered composite materials can be solved using a full integration technique or the classical lamination theory (CLT) (also known as equivalent stiffness method). With Dytran 2001, both methods are available. The full layer integration technique is very general. It can simulate material behavior ranging from a simple linear material to a very complex material with non-linearity and failure mechanism. The newly implemented classical lamination theory is limited in the types of material behavior it can model. It can only analyze a simple linear layered material. The most significant advantage of CLT is the reduction in computational time and the simplicity in introducing the transverse shear stiffness. Therefore, the CLT implementation is very well suited for initial design studies in which not all detail in material behavior is required.

Using CLT, the composite layers are transformed into one equivalent layer with equivalent cross-sectional properties. In this way, there is only one integration point needed across the thickness. Therefore the expected time speed-up in the constitutive routine is about the number of layers times the number of integration points compared to the full layered computation.

During the simulation, the material can fail if certain conditions of failure are met. There are various models of failure criteria for composite materials. Due to the fact the CLT technique only models linear material behavior, the analysis does not take the degradation of the element properties in case of failure into account. Instead, the onset of failure is detected and available for output purposes.

Basic CLT Theory

Classical Lamination Theory is meant for application with shell structures. A structure is assumed to behave like a shell when the thickness is relatively small compared to the other two characteristic lengths. In this way, the cross-sectional kinematics can be assumed to comply with the Kirchhoff or Timoshenko-Reissner-Mindlin constraints.

For the Kirchhoff assumption, the cross-sectional stiffness of the shell consists of Membrane, Bending and Membrane-Bending coupling. The basic derivation of this stiffness is more or less established. The detail derivation of the stiffness can be found in textbooks about mechanical properties of composite materials, for example, see Appendix A, [Ref. 12.]. A brief derivation of the formulation is described below.

The stress strain relations in principal material coordinates for a laminate of an orthotropic material under plane stress are:

$$\begin{Bmatrix} \sigma_1 \\ \sigma_2 \\ \tau_{12} \end{Bmatrix} = \begin{bmatrix} Q_{11} & Q_{12} & 0 \\ Q_{12} & Q_{22} & 0 \\ 0 & 0 & Q_{66} \end{bmatrix} \begin{Bmatrix} \varepsilon_1 \\ \varepsilon_2 \\ \varepsilon_3 \end{Bmatrix} \tag{5-1}$$

The reduced stiffness Q_{ij} is defined in terms of the engineering constants. In any other coordinate system in the plane of the lamina, the stresses are:

$$\begin{Bmatrix} \sigma_x \\ \sigma_y \\ \tau_{xy} \end{Bmatrix} = \begin{bmatrix} \bar{Q}_{11} & \bar{Q}_{12} & \bar{Q}_{16} \\ \bar{Q}_{12} & \bar{Q}_{22} & \bar{Q}_{26} \\ \bar{Q}_{16} & \bar{Q}_{26} & \bar{Q}_{66} \end{bmatrix} \begin{Bmatrix} \varepsilon_x \\ \varepsilon_y \\ \gamma_{xy} \end{Bmatrix} \tag{5-2}$$

In general, the stress-strain relations for the k^{th} layer of a multi-layer laminate can be expressed as follows:

$$\{\sigma_k\} = [\bar{Q}]_k \{\varepsilon\}_k \tag{5-3}$$

Using the assumption of linear strain distribution across the thickness of the shell, the strain at any layer can be defined as a linear combination of the strain in the middle surface and the curvature of the section. The formal equation is given as follows:

$$\begin{Bmatrix} \sigma_x \\ \sigma_y \\ \tau_{xy} \end{Bmatrix}_k = \begin{bmatrix} \bar{Q}_{11} & \bar{Q}_{12} & \bar{Q}_{16} \\ \bar{Q}_{12} & \bar{Q}_{22} & \bar{Q}_{26} \\ \bar{Q}_{16} & \bar{Q}_{26} & \bar{Q}_{66} \end{bmatrix}_k \left\{ \begin{Bmatrix} \varepsilon_x^0 \\ \varepsilon_y^0 \\ \gamma_{xy}^0 \end{Bmatrix} + Z \begin{Bmatrix} \kappa_x \\ \kappa_y \\ \kappa_{xy} \end{Bmatrix} \right\} \tag{5-4}$$

The resultant forces and moments acting on the laminate are obtained by integrating (5-4) through the laminate thickness. The entire collection of force and moment resultants for N-layered laminate depicted in Figure 5-1 can be expressed as follows:

$$\begin{Bmatrix} N_x \\ N_y \\ N_{xy} \end{Bmatrix} = \begin{bmatrix} A_{11} & A_{12} & A_{16} \\ A_{12} & A_{22} & A_{26} \\ A_{16} & A_{26} & A_{66} \end{bmatrix} \begin{Bmatrix} \varepsilon_x^0 \\ \varepsilon_y^0 \\ \tau_{xy}^0 \end{Bmatrix} + \begin{bmatrix} B_{11} & B_{12} & B_{16} \\ B_{12} & B_{22} & B_{26} \\ V_{16} & B_{26} & B_{66} \end{bmatrix} \begin{Bmatrix} \kappa_x \\ \kappa_y \\ \kappa_{xy} \end{Bmatrix} \tag{5-5}$$

$$\begin{Bmatrix} M_x \\ M_y \\ M_{xy} \end{Bmatrix} = \begin{bmatrix} B_{11} & B_{12} & B_{16} \\ B_{12} & B_{22} & B_{26} \\ B_{16} & B_{26} & B_{66} \end{bmatrix} \begin{Bmatrix} \varepsilon_x^0 \\ \varepsilon_x^0 \\ \tau_{xy}^0 \end{Bmatrix} + \begin{bmatrix} D_{11} & D_{12} & D_{16} \\ D_{12} & D_{22} & D_{26} \\ D_{16} & D_{26} & D_{66} \end{bmatrix} \begin{Bmatrix} \kappa_x \\ \kappa_y \\ \kappa_{xy} \end{Bmatrix} \tag{5-6}$$

where

$$\begin{cases} A_{ij} = \sum_{k=1}^{N} (\bar{Q}_{ij})_k (Z_k - Z \\ B_{ij} = \frac{1}{2} \sum_{k=1}^{N} (\bar{Q}_{ij})_k (Z_k^2 - \\ D_{ij} = \frac{1}{3} \sum_{k=1}^{N} (\bar{Q}_{ij})_k (Z_k^3 - \end{cases} \tag{5-7}$$

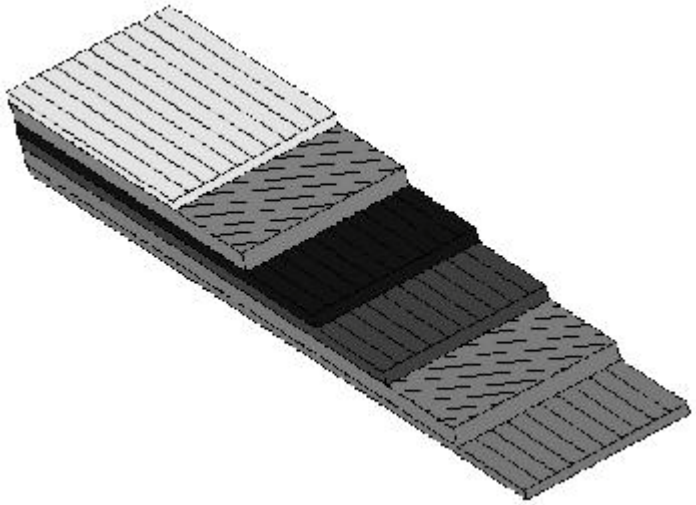

Figure 5-1 Multi-layered Cross Section

The ABD matrices can also be input directly through the MAT2 entry in combination with PSHELL entries. In this way, Dytran will not be able to calculate the stresses and strains at any layers. For input purposes, and to be consistent with MSC Nastran, the ABD matrices are normalized with certain factors. For more detailed descriptions the user should refer to the *Dytran User's Guide*.

Transverse Shear Stiffness

The shell elements in Dytran, namely BLT, BELY, KEYHOFF, Hughes Liu and C0-TRIA, are all based on the Timoshenko-Reissner-Mindlin assumption where there is a transverse shear deformation across the thickness. In the case that the shell structure is very thin, this effect can be neglected. For isotropic material, the transverse shear factor for shell elements is 5/6. For composite shell the evidences say that the transverse shear stiffness is relatively lower than that of the in-plane stiffness. Therefore a "reasonable" transverse shear stiffness prediction is required.

One of the methods mostly used in a general finite element program is the "energy-based" method. Using this technique, the value of 5/6 for isotropic materials is met. One of the variants that is implemented in Dytran is the first order shear theory. The detailed derivation of the formula can be found in Appendix A, [Ref. 13.]. A brief summary of the derivation is described here.

The mean value of the transverse shear modulus $\overline{G}$ for the laminated composite is defined in terms of the transverse shear strain energy, U, through the depth as follows:

$$U = \frac{1}{2}\frac{V^2}{\overline{G}T} = \frac{1}{2}\int\frac{(\tau(Z))^2}{G(Z)} \tag{5-8}$$

A unique mean value of transverse shear strain is assumed to exist for both the x and y components of the element coordinate system, but for ease of discussion, only the evaluation of an uncoupled x component of

the shear moduli is illustrated here. From (5-8) the mean value of transverse shear modulus may be written in the following form:

$$\frac{1}{\overline{G}_x} = \frac{T}{V_x^2} \sum_{i=1}^{N} \int_{Z_{i-1}}^{Z_i} \frac{(\tau_{zx}(Z))^2}{(G_x)_i} dZ \tag{5-9}$$

where $\overline{G}_x$ is the "average" transverse shear coefficient used by the element code and $(G_x)_i$ is the local shear coefficient for layer i. To evaluate (5-9), it is necessary to obtain an expression for $\tau_{zx}(Z)$. This can be accomplished by assuming that the x- and y-components of stress are de-coupled from one another. This assumption allows the desired equation to be deduced through an examination of a beam of unit cross-sectional width, as shown in Figure 5-2.

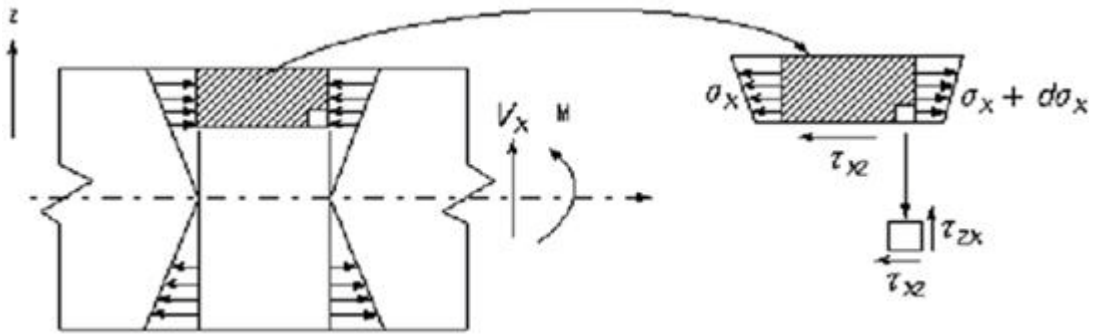

Figure 5-2 Cross-section of beam

The equilibrium conditions in the horizontal direction and for total moment are:

$$\frac{\partial \tau_{xz}}{\partial Z} + \frac{\partial \sigma_x}{\partial X} = 0 \tag{5-10}$$

$$V_x + \frac{\partial M_x}{\partial X} = 0 \tag{5-11}$$

Now, if the location of the neutral surface is denoted by $\bar{z}_x$ and ρ is the radius of curvature of the beam, the axial stress σ_x may be expressed in the form

$$\sigma_x = \frac{E_x(\bar{z}_x - z)}{(\overline{EI})_x} M_x \tag{5-12}$$

(5-12) may be differentiated with respect to x and combined with Equations (5-10) and (5-11). In a region of constant E_x, the result may be integrated to yield the following expression:

$$\tau_{xz} = C_i + \frac{V_x}{(\bar{El})_x}\left(\bar{z}_x z - \frac{z^2}{2}\right)E_{xi} \text{ for } z_{i-1} < z < z_i \tag{5-13}$$

(5-13) is particularly convenient to use in the analysis of N-ply laminates because sufficient conditions exist to determine the constants $C_i \quad (i = 1, 2 \ldots N$ and the "directional bending center" $\bar{z}_x$.

In general for any ply, $z_{i-1} < z < z_i$, the shear stress is:

$$\tau_{xz}(z) = (\tau_{xz})_{i-1} \frac{V_x E_{xi}}{(\bar{El})_x}\left[\bar{z}_x(z - z_{i-1}) - \frac{1}{2}(z^2 - z_{i-1}^2)\right] \tag{5-14}$$

At any ply interface, z_i, the shear is therefore

$$(\tau_{xz})_i = \frac{V_x}{(\bar{El})_x} \sum_{j=1}^{i} E_{xj} T_j \left[\bar{z}_x - \frac{1}{2}(z_j + z_{j-1})\right] \tag{5-15}$$

where $T_j = z_j - z_{j-1}$.

Note that the shear at the top face, $(\tau_{xz})_n$, is zero and therefore

$$(\tau_{xz})_n = \frac{V_x}{(\bar{El})_x}\left[\bar{z}_x \sum_{j=1}^{n} E_{xj} T_j - \sum_{j=1}^{n} E_{xj} T_j \frac{1}{2}(z_j + z_{j-1})\right] = 0 \tag{5-16}$$

(5-16) proves that if $\bar{z}_x$ is the bending center, the shear at the top surface must be zero.

(5-14) could be substituted into (5-9) and integrated. A better form of (5-14), for this purpose, is:

$$(\tau_{xz}(z))_i = \frac{V_x E_{xi}}{(\bar{El})_x}\left[f_{xi} + \bar{z}_x(z - z_{i=1}) - \frac{1}{2}(z^2 - z_{i-1}^2)\right] \tag{5-17}$$

where

$$f_{xi} = \frac{1}{E_{xi}} \sum_{j=1}^{i-1} E_{xj} T_j \left[\bar{z}_x - \frac{1}{2}(z_j + z_{j-1})\right] \tag{5-18}$$

Substituting (5-17) into (5-9) and, after a considerable effort of integrating, the results we obtain

$$\frac{1}{\overline{G}_x} = \frac{T}{(\overline{El})_x^2} \sum_{i=1}^{N} \frac{1}{G_{xi}} R_{xi} \tag{5-19}$$

where

$$(E_{xi})^2 T_i \left[\left\{ f_{xi} + (\bar{z}_x - x_{i-1}) T_i - \frac{1}{3} T_i^2 \right\} f_{xi} \right.$$

$$\left. + \left\{ \frac{1}{3}(\bar{z}_x - 2z_{i-1}) - \frac{1}{4} T_i \right\} \bar{z}_x T_i^2 + \left\{ \frac{1}{3} z_{i-1}^2 + \frac{1}{4} z_{i-1} T_i + \frac{1}{20} \right. \right. \tag{5-20}$$

This expression for the inverse shear modulus for the x-direction may be generalized to provide for the calculation of each term in the two-by-two matrix of shear moduli.

$$[\overline{G}_{kl}] = \left[\frac{T}{(\overline{El})_{kl}^2} \sum_{i=1}^{n} [G_{kl}^i]^{-1} R_{ki} \right]^{-1} \tag{5-21}$$

where $k = 1, 2$, and $l = 1, 2$. The moduli for individual plies are provided through user input. Finally,

$$[G_3] = \begin{bmatrix} \overline{G}_{11} & (\overline{G}_{12})_{avg} \\ (\overline{G}_{12})_{avg} & \overline{G}_{22} \end{bmatrix} \tag{5-22}$$

As an example, let us consider a single layer element. For this case let $z_{i-1} = -\frac{1}{2}T$, $\bar{z} = 0$, $f_0 = 0$, and $\overline{El} = ET^2/12$. Evaluating (5-19) we obtain:

$$R_1 = E^2 T^5 \left[\frac{1}{12} - \frac{1}{8} + \frac{1}{20} \right] = \frac{E^2 T^5}{120} \tag{5-23}$$

and

$$\frac{1}{\overline{G}} = \frac{12^2 T}{E^2 T^6} \cdot \frac{E^2 T^5}{120 G_1} = \frac{6}{5 G_1} \tag{5-24}$$

as expected.

The G_3 matrix can also be input directly through the MAT2 entry in combination with PSHELL entries. In this way, Dytran is not able to calculate the stresses and strains at any layers. For input purposes, and to be

consistent with MSC Nastran, the entries of matrix are normalized with a certain factor. For more detail descriptions, refer to the *Dytran User's Guide*.

Failure Models

As mentioned above, the limitation of the CLT model is that it does not accommodate the after failure behavior, only the onset of failure. Since once the cross-sectional properties are reduced to an equivalent value they are constant throughout the analysis. If a situation happens that failure occurs, this approach is no longer valid. Therefore, to verify whether the analysis is valid or not, the condition of the laminate is checked against failure conditions when these have been defined.

There are various models for failure conditions in composite materials. They are all based on progressive failure criteria where the failure is checked in each layer or lamina. In this case, only the lamina-failure models that are already available in Dytran will be presented. These models are also used if the PCOMP entry (the general integration method) in combination with a MAT8A definition is used to model laminates. The HILL and TSAI models only indicate a layer has failed, but no information about the mode of failure is provided. The STRSS MODTSAI, CHANG, HASHIN indicate both the failure and mode of failure. In Dytran, there are five modes of failure available, namely fiber-tension (FT), fiber-compression (FC), matrix-tension (MT), matrix-compression (MC) and matrix-shear (MS). It is also possible to combine these models using the COMBINAT option.

For a more sophisticated model that does not fit the pre-defined models, the full integration method allows you to use the USER option in combination with an external subroutine. This model is not available in CLT shells.

Maximum stress (STRSS)

This is the simplest model. The failure is only checked against the maximum stress criteria in the principal lamina direction, see Appendix A, [Ref.12.]. There are five stress criteria namely: in-plane shear (S), fiber tensile stress (longitudinal direction, X_T), fiber compressive stress (longitudinal direction, X_c), matrix tensile stress (lateral direction, Y_T), and matrix compressive stress (lateral direction, Y_c).

$$\begin{cases} \text{Fiber tension:} & \dfrac{\sigma_1}{X_T} = 1 & (\sigma_1 > 0 \\ \text{Fiber compression:} & \dfrac{|\sigma_1|}{X_c} = 1 & (\sigma_1 < 0 \\ \text{Matrix tension:} & \dfrac{\sigma_2}{Y_T} = 1 & (\sigma_2 > 0 \\ \text{Matrix compression:} & \dfrac{|\sigma_2|}{Y_c} = 1 & (\sigma_2 < 0 \\ \text{Matrix shear:} & \dfrac{|\tau_{12}|}{S} = 1 \end{cases} \tag{5-25}$$

This model is only valid if the loading is uni-axial. However, the general practical problems involve at least a bi-axial if not tri-axial state of stress. The experimental results showed that for these cases the combination of the uni-lateral strength could predict properly the failure of a lamina. These models are described in the following sections.

Hill model

This model is also called Tsai-Hill one. The failure criteria is based on the following equations:

$$\frac{\sigma_1^2}{X^2} + \frac{\sigma_2^2}{Y^2} - \frac{\sigma_1\sigma_2}{X^2} + \frac{\tau_{12}^2}{S^2} = 1 \tag{5-26}$$

where

$$\begin{cases} X = (\max X_T, \\ Y = (\max Y_T, \end{cases} \tag{5-27}$$

The uni-axial strengths are defined in 0. The present implementation in Dytran is using the relation in (5-27). Therefore, the prediction of failure is not conservative, as there may be significant differences between tensile and compressive strength as can be seen in Figure 2-25 of [Ref. 12.] in Appendix A. Therefore the new logic is implemented now in Dytran. This is based on the sign of the stresses in the material principal direction. The tensile or compressive strengths will be used in (5-26) when the applied stresses are tensile or compressive, respectively.

Tsai model

The Hill model, in 3-D space, is insensitive with the isotropic stresses and has a few shortcomings. While such an assumption may be a good approximation for initial yielding of a metal, it is certainly not valid for isotropic tension of a fiber composite, see References 12. and 14. in Appendix A. Therefore a more general model is needed. This model is normally known as Tsai-Wu theory; see [Ref. 12.]. The failure surface in stress surface is as follows:

$$F_1\sigma_i + F_{ij}\sigma_i\sigma_i = 1 \qquad i,j = 1, \ldots \tag{5-28}$$

For an orthotropic lamina under plane stress conditions, (5-28) can be expressed as follows:

$$F_1\sigma_1 + F_2\sigma_2 + F_6\tau_{12} + F_{11}\sigma_1^2 + F_{22}\sigma_2^2 + F_{66}\tau_{12}^2 + 2F_{12}\sigma_1\sigma_2 = 1 \tag{5-29}$$

where

$$\begin{cases} F_1 = \dfrac{1}{X_T} + \\ F_{11} = -\dfrac{1}{X_T} \\ F_2 = \dfrac{1}{Y_T} + \\ F_{22} = -\dfrac{}{Y_T} \\ F_6 = 0 \\ F_{66} = \dfrac{1}{S^2} \end{cases} \tag{5-30}$$

The determination of the term F_{12} remains. Basically, it cannot be determined from any uni-axial test in the principal material directions. Instead, a bi-axial test must be used. Thus, for example, we can impose a

state of bi-axial tension described by $\sigma_1 = \sigma_2 = \sigma$ and all other stresses are zero. Accordingly, from (5-29), we can derive the following relation.

$$F_{12} = \frac{1}{2\sigma^2}\left[1-\left(\frac{1}{X_T}+\frac{1}{X_C}+\frac{1}{Y_T}+\frac{1}{Y_C}\right)\sigma+\left(\frac{1}{X_T X_C}+\frac{1}{Y_T Y_C}\right)\sigma^2\right] \tag{5-31}$$

The value of F_{12} then depends on the various engineering strengths plus the bi-axial tensile failure stress, σ.

Modified Tsai-Wu

This model only considers the failure of the matrix. Therefore this model should be used in combination with other failure model. The failure criteria is as follows:

$$F_2\sigma_2 + F_{22}\sigma_2^2 + F_{66}\tau_{12}^2 = 1 \tag{5-32}$$

where the constants F_2, F_{22}, and F_{66} are defined in (5-30).

Hashin model

This model is based on the observation of the Tsai-Wu model that in case of isotropic tensile stress, the failure mode will depend on compressive stress. This is physically unacceptable. Moreover, the determination of F_{12} is subject to ambiguity; see Appendix A, [Ref. 14.] for more details.

This model only considers fiber-tension, fiber-compression, matrix-tension and matrix-compression. The tension failure equations are as follows:

$$\begin{cases} \text{Fiber tension:} & \left(\dfrac{\sigma_1}{XT}\right)^2+\left(\dfrac{\tau_2}{S_A}\right)^2 = 1 & (\sigma_1 > 0) \\ \text{Fiber compression:} & |\sigma_1| = X_c & (\sigma_1 < 0) \\ \text{Matric tension:} & \left(\dfrac{\sigma_2}{Y_T}\right)^2+\left(\dfrac{\tau_{12}}{S_A}\right)^2 = 1 & (\sigma_2 > 0) \\ \text{Matrix compression:} & \left(\dfrac{\sigma_2}{2S_T}\right)^2+\left[\left(\dfrac{Y_C}{2S_T}\right)^2-1\right]\dfrac{\sigma_2}{Y_C}+\left(\dfrac{\tau_{12}}{S_A}\right)^2 = 1 & (\sigma_2 < 0) \end{cases} \tag{5-33}$$

Please notice that the ultimate transverse shear is difficult to measure. However, no general failure criterion could avoid inclusion of this quantity. The implementation in Dytran assumes $S_T = S_A$.

Chang model

The original Chang mode, described in Appendix A, [Ref. 15.], only considers fiber breakage or fiber-matrix cracking and matrix cracking. The failure criteria is described as follows:

$$\begin{cases} \text{Fiber breakage:} & \left(\frac{\sigma_1}{X_T}\right)^2 + T = 1 \qquad (\sigma_1 > 0) \\ \text{Matrix cracking:} & \left(\frac{\sigma_1}{Y_T}\right)^2 + T = 1 \qquad (\sigma_2 > 0) \end{cases} \tag{5-34}$$

where

$$T = \left(\frac{\tau_{12}}{S}\right)^2 \frac{1 + \frac{3}{2}\alpha G_{12}\tau_{12}^2}{1 + \frac{3}{2}\alpha G_{12} S^2} \tag{5-35}$$

In Dytran, the matrix compressive failure is added. This model is based on the Hashin criterion that described as follows:

$$\begin{cases} \text{Matrix compression:} & \left(\frac{\sigma_2}{2S}\right)^2 + \left[\left(\frac{Y_C}{2S}\right)^2 - 1\right]\frac{\sigma_2}{Y_C} + T = 1 \qquad (\sigma_2 < 0) \end{cases} \tag{5-36}$$

COMBINAT model

The possible combination of failure mode available in Dytran can be seen in Table 5-1. In case either of the MT or MC has MODTSAI criterion, both of them must be the same.

Table 5-1 Combination of Failure Modes

	NONE	STRSS	MODTSAI	CHANG	HASHIN
FT	x	x		x	x
FC	x	x			x
MT	x	x	x	x	x
MC	x	x	x	x	x
MS	x	x	x		

6 Standard Euler Solver

Introduction

In the Eulerian approach, material is not attached to elements but can move from one Euler element to the other. Mass, momentum, and energy are element averages and are defined in the centers of the elements. This property is called cell-centered.

The equations solved are the conservation laws of mass, momentum and energy as given in equation (6-1). Here, ρ is the material density, u_i are the velocity components, p is the pressure, q is the bulk viscosity, g is gravity and e is the specific total energy. V is a volume and A is its boundary.

$$\begin{aligned}
&\frac{d}{dt}\int_V \rho dV + \int_A \rho(u\cdot n)dA = 0\\
&\frac{d}{dt}\int_V \rho u_i dV + \int_A \rho u_i(u\cdot n)dA = -\int_A (p+q)n_i dA - \rho g e_3 V\\
&\frac{d}{dt}\int_V \rho e dV + \int_A \rho e(u\cdot n)dA = -\int_A u_i p n_i dA
\end{aligned} \tag{6-1}$$

For Eulerian materials with strength, the pressure p is replaced by the stress tensor. The volume integrals represent the total mass, momentum, and energy in the Volume V. The surface integrals on the left signify transport out of the volume through parts of the area A. The surface integrals on the right represent the momentum and energy increase caused by forces acting on the boundary of the volume. The numerical scheme is a finite volume method. It is obtained by applying equation (6-1) to the material inside an Euler element and by specifying how transport terms are computed. The first equation signifies that the decrease of mass in an element equals the loss of mass trough the element boundary. In transporting mass between elements, mass should be conserved globally. This is achieved by looping across the element interfaces and adding the transported mass, momentum, and energy to the acceptor element and subtracting it from the donor element. In this way, the finite volume scheme conserves mass, momentum and energy.

In applying (6-1), it is assumed that density, velocity, and specific energy are constant across an Euler element and only depend on time. In addition, they are constant within one time step. This is consistent with a first-order approach. The evolved time at cycle n will be denoted by t^n. Element density, velocity, and specific total energy inside an element at cycle n is denoted by ρ^n, u^n, and e^n, respectively.

Applying first-order time integration gives equation (6-2). The integration is from t^n to t^{n+1}. Here M denotes the mass inside the element, P momentum, and E energy.

For the surface integrals that represent transport, the forward Euler method is used. Consequently, surface integrals are evaluated at the beginning of the time step. The surface integral with the pressure terms is evaluated using the new density and specific total energy

$$
\begin{aligned}
M^{n+1} - M^n &= -\left[\int_A \rho(u \cdot n) dA \Delta t\right]_{t^n} \\
P^{n+1} - P^n &= -\left[\int_A \rho u_i (u \cdot n) dA\right]_{t^n} \Delta t - \left[\int_A p(\rho, s) n_i dA + \rho g e_3 V\right]_{t^{n+1}} \Delta t \\
E^{n+1} - E^n &= -\left[\int_A \rho e (u \cdot n) dA + \int_A u_i p(\rho, e) n_i dA\right]_{t^n} \Delta t \\
\rho^{n+1} &= \frac{M^{n+1}}{V^{n+1}}, e^{n+1} = \frac{E^{n+1}}{M^{n+1}}, s^{n+1} = e^{n+1} - \frac{1}{2} \sum_{k-1}^{3} u_k^2
\end{aligned}
\tag{6-2}
$$

The transport velocity, $(u \cdot n)$, depends on both the donor as well as the acceptor element and is given by the average of the donor and acceptor velocity. Multiplying the transport velocity with surface area and time step yields the transport volume. This volume is filled up with mass of the donor element. Multiplying this volume with the density of the donor element gives the transported mass. Likewise the transport volume times the donor velocity gives the transported momentum.

Since the fluid-structure interaction forms an integral part of the numerical scheme, we first discuss fluid-structure interaction.

Fluid-structure Interaction

Material in an Euler mesh can interact with Lagrangian structures. Eulerian material can exert forces on a structure causing displacement and deformation. On the other hand, structures provide a barrier to Eulerian material. That is, Eulerian material cannot penetrate the structure and the structural surface determines which Euler element have the capacity to hold mass. Consider, for example, a tank shell surface. Euler Elements that are outside the tank surface cannot hold material and only elements that are partially or completely inside the surface have the capacity to contain mass. This surface defines the effective boundary of the Euler domain and is called the coupling surface. In most cases, the coupling surface consists of Lagrangian Elements. But, the interaction of Eulerian material with a Lagrangian solid is also possible. Then, the coupling surface consists of surface elements that have no Lagrangian model attached but only serve to enable interaction. In the following, we shall assume that the coupling surface is a Lagrangian shell surface. The coupling surface will also be referred to as the structural surface.

The coupling surface consists of shell elements that deform under pressure loads from material inside the Eulerian domain. An explicit finite element solver solves the shell dynamics. An explicit Euler solver solves the fluid dynamics for the inside region of the coupling surface. The interaction between these two solvers occurs in two ways:

- The mass in the Euler elements exerts a pressure load on the Lagrangian elements associated with the structural surface. These loads constitute an additional set of boundary conditions for the finite element solver, resulting in new grid point accelerations and velocities for the structure. From the updated plastic strain or updated stresses of the shell elements, it is determined which elements are failing. Finally the structural grid points are moved using the new velocities

- The structural grid points move giving the Euler mesh a new effective boundary. Consequently, the volume of mass in each element may change. Since density is mass divided by the volume of the mass, densities also change as does the pressures. In the following, we shall assume that the material is inside the coupling surface.

Numerical Scheme

The Euler elements are integrated in time by applying a finite volume method directly to the physical domain, avoiding the use of coordinate transformations. Therefore, the finite volume method is applied to the 3-D object that consists of that part of the Euler element that is inside the coupling surface. This is, in general, not a cube but a multifaceted object. For the 2-D case, this is shown in Figure 6-1.

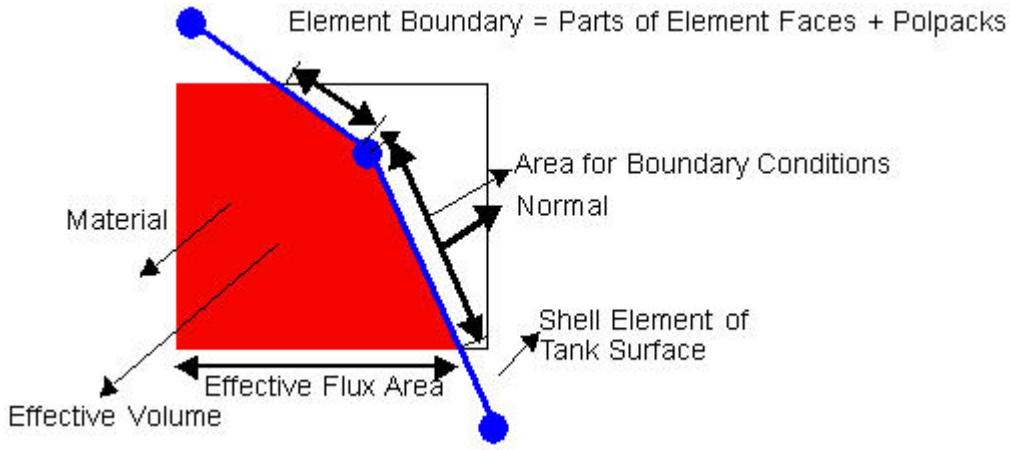

Figure 6-1 The Boundary of an Euler Element

In Figure 6-1, the square represents an Euler element that is intersected by the coupling surface. Only that part of the square that is inside the coupling surface can contain mass. Therefore, this part is the effective volume of material in the element. The boundary of this effective volume consists of two types of surfaces:

- Euler element boundaries that connect two neighboring elements called Euler faces.
- Parts of the coupling surface that are within the Euler element. They are called polpacks (polyhedron packets).

The effective boundary of an Euler element consists of Euler faces and polpacks.

A polpack is the intersection of a coupling surface shell element with an Euler element and is completely inside an Euler element and a coupling surface shell element. In Dytran, an algorithm is available that computes these polpacks for any given, closed 3-D faceted surface and any 3-D Euler domain.

Faces refer to two Euler elements, whereas polpacks refer to only one Euler element. For both faces and polpacks, areas and normals are computed.

In Dytran, the finite volume method results from applying equation (6-2) to these 3-D objects. The volume V^{n+1} in equation (6-2) is the effective volume of the Euler element. Furthermore, the surface integrals are

computed by summing over the faces and polpacks. A contribution of a polpack or a face to integrals signifying transport is called a flux.

When there is more than one material present in the simulation, the mass conservation law applies to each material separately. This means that for each material inside an Euler element, the density has to be monitored. In applying the momentum law, it does not matter whether there are several materials since all materials inside an element are assumed to have the same velocity. The energy equation is also applied to each material separately.

First, consider simulations with only one material present. In the mass conservation law, the mass flux across a face gives:

$$\Delta M_{DONOR} = -\rho_{DONOR}\left|\vec{V}\cdot\vec{A}\right|\Delta t$$

$$\Delta M_{ACCEPTOR} = +\rho_{DONOR}\left|\vec{V}\cdot\vec{A}\right|\Delta t$$

Here, M is the mass in the Euler element, V is the velocity vector, A denotes the area vector of the face, Δt is the time step, $DONOR$ denotes the element supplying mass, and $ACCEPTOR$ denotes the element receiving mass. In most cases, the coupling surface is not permeable, and there will be no transport across the polpacks. However, in case coupling surface shell elements have a porosity model assigned, the flux equations takes that into account.

The momentum in an element can increase by either transport of momentum, or by a pressure load working on the polpacks and faces. The pressure load contribution to this momentum increase is the surface integral $-\int_A pn_i dA\Delta t$. The force contribution of a face to the momentum increase of the element left to the face and right to the face reads:

$$\Delta\vec{P}_{Left} = -p^{Face}\vec{A}\Delta t$$

$$\Delta\vec{P}_{Right} = p^{Face}\vec{A}\Delta t$$

Here P is the momentum of an element, A is the area vector pointing from the left element to the right element and p^{Face} is a weighted average of the pressure in the two elements that are on the left and right of the face. These momentum updates clearly conserve the combined momentum of the left and right element.

For polpacks, the contribution is the same, but now the pressure at the polpack is given by the pressure in the Euler element that contains the polpack. To conserve momentum, the negative of this momentum contribution is put as a force on the coupling surface shell element that hosts the polpack. This is the way boundary conditions are imposed on the Lagrangian element constituting the coupling surface.

The energy equation is applied in a similar way.

The procedure for advancing the Euler domain with one time step is as follows:

1. Do all finite element objects and contact. Move the finite element objects in accordance to their grid point velocities.
2. Using the new position of the finite element structures, compute new polpacks. Using polpacks and faces, compute the volume of the portion that is inside the coupling surface for all Euler elements.
3. Transport mass, momentum, and energy across all faces and permeable polpacks using the conservation laws. The flux velocity is the average of the left and right Euler element velocity. In case no right Euler element is available, the flux velocity is determined from an inflow condition and, in some cases, the velocity of the Euler element. Examples are holes and parts of surfaces that enable flow into the inside region of the coupling surface as a means of filling the inside region of the coupling surface. At the end of this step, element masses are fully updated.
4. For each Euler element, compute density from the new mass and volume and compute pressure from the equation of state using the new density.
5. Compute the effect of Euler element pressures to both structure as well as other Euler elements by going over respective polpacks and Euler faces. This effect contributes to the Euler element momentum. The transport contribution to the momentum increase has already been computed in step 3. At the end of this step, the element momentum and energy are fully updated.
6. Advance the Lagrangian shell elements associated with the coupling surface with one time step using the internal shell element forces, contact forces, and external forces from the Euler domain and compute new velocities on the grid points.
7. Compute a new stable time step based on the mesh size, speed of sound, and velocity. The stability criterion used is the CFL condition and applies to both, the tank surface as well as to the Euler elements.

Time Step Criterion

To maintain stability of the explicit scheme the time step should not exceed:

$$\Delta t_{max} = \frac{\Delta x}{u + c} \tag{6-3}$$

Euler With Strength

Deviatoric stress is a property of mass and is transported along with mass. Deviatoric stress in an element changes because masses with different stresses can enter the element and because strain increments raise stresses. When moving along with a piece of material the change in deviatoric stress denoted by s is given by:

$$\frac{ds_{ij}}{dt} = 2\mu\frac{de_{ij}^{dev}}{dt} = \mu\left(\frac{\partial u_i}{\partial x_j} + \frac{\partial u_j}{\partial x_i} - \frac{1}{3}\frac{\partial u_k}{\partial x_k}\delta_{ij}\right) \tag{6-4}$$

Here the derivative is along the path of the moving mass and (u_k) denotes the velocity in the Euler element. Since the velocity of the moving mass equals the velocity in the Euler element. the total derivative is given by

$$\frac{ds_{ij}}{dt} = \frac{\partial s_{ij}}{\partial t} + \frac{\partial s_{ij}}{\partial x_k}\frac{\partial x_k}{\partial t} = \frac{\partial s_{ij}}{\partial t} + u_k\frac{\partial s_{ij}}{\partial x_k} \tag{6-5}$$

Therefore the change of deviatoric stress in an Euler element is given by

$$\frac{\partial s_{ij}}{\partial t} + u_k\frac{\partial s_{ij}}{\partial x_k} = 2\mu\frac{de_{ij}^{dev}}{dt} \tag{6-6}$$

This equation is not in conservation form and using the equation as it is would require the additional computation of shear stress gradients. By putting the equation in conservation form, gradient computations are not needed and the equation be solved using the divergence theorem.

To enable further use for other quantities like plastic strain consider

$$\frac{\partial \varphi}{\partial t} + u_k\frac{\partial \phi}{\partial x_k} = D \tag{6-7}$$

By using the continuity equation it can be written in conservative form.

$$\begin{aligned}\frac{\partial(\rho\phi)}{\partial t} &= \frac{\partial \rho}{\partial t}\phi + \rho\frac{\partial \phi}{\partial t}\\ &= -\frac{\partial(\rho u_k)}{\partial x_k}\phi + \rho\left(D - u_k\frac{\partial \phi}{\partial x_k}\right)\\ &= -\frac{\partial(\rho u_k\phi)}{\partial x_k} + \rho D\end{aligned} \tag{6-8}$$

This gives

$$\begin{aligned}\frac{\partial(\rho\phi)}{\partial t} + \frac{\partial(\rho\phi u_k)}{\partial x_k} &= \rho D\\ \frac{1}{\rho}\left(\frac{\partial(\rho\phi)}{\partial t} + \frac{\partial(\rho\phi u_k)}{\partial x_k}\right) &= D\end{aligned} \tag{6-9}$$

For stresses this becomes:

$$\frac{1}{\rho}\left(\frac{\partial(\rho s_{ij})}{\partial t}+\frac{\partial(\rho u_k s_{ij})}{\partial x_k}\right) = 2\mu e_{ij}^{dev} \tag{6-10}$$

In this way, transport of stresses can be computed in close analogy to mass and momentum by transporting mass times shear stress. In the same way, transport of plastic strain is carried out.

Strain rates are computed from velocity gradients. They are obtained by use of the divergence theorem as follows:

$$\begin{aligned} V\frac{\partial u_i}{\partial x_j} &= \int\frac{\partial u_i}{\partial x_j}dV = \int div(\vec{e}_j u_i)dV \\ &= \int u_i\vec{e}_j\cdot\vec{dS} = \sum_{Faces} u_i^{Face}S_j^{Face} \end{aligned} \tag{6-11}$$

Pressure can be either computed from density or updated from volume strain rates. The first corresponds to splitting the stress tensor computation into a hydrostatic part and a deviatoric part. The second computes the stress tensor without any splitting and uses the isotropic Hooke's law in terms of strain rates. We show that the two approaches are equivalent. Consider computing pressure from the volume strain rates. Differentiation of the isotropic Hooke's law gives

$$\frac{dp}{dt} = -K\frac{\partial u_i}{\partial x_i} \tag{6-12}$$

with K the bulk modulus. Using the continuity equation in the form

$$\frac{d\rho}{dt} = \frac{\partial\rho}{\partial t}+u_i\frac{\partial\rho}{\partial x_i} = -\rho\frac{\partial u_i}{\partial x_i} \tag{6-13}$$

yields

$$\begin{aligned} \frac{dp}{dt} &= \frac{K}{\rho}\frac{d\rho}{dt} \\ \frac{dp}{dt} &= \frac{d}{dt}(K ln\rho) \end{aligned} \tag{6-14}$$

The pressure in an element can be traced back by using (6-14).

$$p = \int_{\rho_{ref}}^{\rho} d(K ln\rho) = K ln\left(\frac{\rho}{\rho_{ref}}\right) = K ln\left(1+\frac{\rho-\rho_{ref}}{\rho_{ref}}\right) \approx K\left(\frac{\rho-p_{ref}}{\rho_{ref}}\right) \tag{6-15}$$

So to first-order in density Hooke's law and the equation of state give the same pressure. Basing the pressure on the logarithm of the density ratio is expensive and the linearization is sufficiently accurate. Pressures are computed using the linearization. To account for rotation of material, the Jaumann correction is applied.

Multi-material Solver

In simulations with multiple materials, it is important to keep track of the interfaces between materials. For example, in fuel tank sloshing simulations, there is an interface visible between regions filled with fuel and regions filled with air. To handle these interfaces, several extensions of the transport logic and pressure computation are necessary. The extended transport logic is known as preferential transport and tries to maintain interfaces between materials. Consider, for example, the case of a blast wave of air in water. It is important that the interface between water and air during the expansion of the blast wave is maintained and does not deteriorate by the unphysical mixing of water and air.

To enable a multi-material simulation a certain amount of bookkeeping is needed. For every Euler element, the following information is available

- The number of materials inside the Euler elements
- For each material, the volume fraction, the material ID, the density, the mass, the specific energy, the total energy, and volume strain rates are stored. The volume fraction of a material is defined as the fraction of element volume that is filled with that material.

The transport logic for multi-material amounts to:

- Compute the volume that is to be transported. This is $\left|\vec{V}\cdot\vec{A}\right|\Delta t$ and this volume flux gives rise to a mass flux. Had there been only one material, the mass flux would have been the density times the volume flux, but now the donor element has several materials and each material has a distinct density and, therefore, the mass flux is split into several mass fluxes. Each material in the donor element has a distinct mass flux and this material specific mass flux can be easily converted into a volume flux by using the material density. Using this conversion the mass fluxes should give rise to volume fluxes that add up to a total volume flux that equals $\left|\vec{V}\cdot\vec{A}\right|\Delta t$. Materials are transported out of the element until the prescribed total volume flux is reached. The only remaining issue is which materials should be transported first.
- Determine for both donor element as well as acceptor element which materials are present in the element.
- Look which materials are common to both elements.
- First transport any material that is common to both elements. Transport these common materials in proportion to their acceptor material fraction. A material is transported with the material density of the donor element and this material density translates a volume flux into a mass flux and vice versa. Subtract any mass that is transported from the flux volume. If there is sufficient mass of the common materials in the donor element, the whole flux volume is used to transport the common materials.
- If, after transport of the common materials, the flux volume is not fully used yet, transport materials in ratio to their donor material fraction.

To illustrate how this procedure aims at preserving material interfaces, consider two adjacent Euler Elements and assume that flow is from the left element to the right element. The left element is filled with fuel and air and the right one is filled with only air. First, air is transported since air is the only material common to both elements. If there is sufficient air, only air is transported. If, during transport, there is no air left, transport of this common material is not able to use the full flux volume and also fuel is also transported. In both cases, the interface between fuel and air is maintained.

The pressure computation for Euler elements with only one material is straightforward: the pressure readily follows from the equation of state and the density. For elements with more than one material, each material has a distinct equation of state and a distinct density and this results in a distinct pressure for each material. The pressure computation for these elements will be based on the thermodynamic principle of pressure equilibrium. Since masses of materials in Euler elements are only changed by the transport computation, these masses are fixed during the pressure computation. The volume taken up by each material in an Euler element is not known but determines the pressure inside the material. By adjusting the volumes of the materials simultaneously, pressure equilibrium is achieved. Therefore, the pressure computation amounts to an iterative process that iterates on the volumes of the materials inside the Euler element.

To understand the influence of the material volumes, consider an element with fuel and air. Suppose, that at the start of a cycle, there is pressure equilibrium and that during transport air enters the element. Because of the surplus of air, there is no longer pressure equilibrium. Physically, it is expected that the air will very slightly compress the fuel until pressure equilibrium is achieved. The compression of the air is just the adjustment of the material volumes of fuel and air. The material volume of air increases while the material volume of fuel decreases.

Viscosity

Viscous stresses only contribute to the momentum balance:

$$\frac{d}{dt}\int_V \rho u_i dV + \int_A \rho u_i (u \cdot n) dA = -\int_A p n_i dA + \int_A s_{ij} n_j dA \tag{6-16}$$

Here the deviator shear stress tensor s_{ij} is given by

$$s_{ij} = \mu\left(e_{ij} - \frac{1}{3}e_{kk}\right)$$
$$e_{ij} = \frac{1}{2}\left(\frac{\partial u_i}{\partial x_j} + \frac{\partial u_j}{\partial x_i}\right) \tag{6-17}$$

The contribution of viscous dissipation to the energy balance law is small and is not taken into account. Velocity gradients are computed by Gauss's law as given by (6-18). For boundary contributions, the imposed velocity boundary condition is used. Material in one element exerts a viscous force on material in the adjacent elements and leads to changes in momentum. The momentum transferred across an Euler element face is given by

$$\int s_{ij} n_j dA dt = \left(-\frac{2}{3}\mu u_{k,k} n_i + \mu \frac{\partial u_i}{\partial n} + \mu \frac{\partial u_n}{\partial x_i} \right) FaceArea^* \Delta t \tag{6-18}$$

The second term is most significant and requires a special treatment. This term is proportional to the normal velocity derivative at the face. It can be obtained by averaging the normal derivative over the left and right Euler element:

$$\left[\frac{\partial u_i}{\partial n}\right]_{Face} = \frac{1}{2}\left(\left[\frac{\partial u_i}{\partial n}\right]_L + \left[\frac{\partial u_i}{\partial n}\right]_R\right) \tag{6-19}$$

This leads to decoupling. To show this, consider an Euler element and two of its opposing faces. For both opposing faces, a viscous flux that is proportional to equation (6-18) is added to the Euler element. The net contribution is proportional to the difference of equation (6-18) for the two faces. In this subtraction, the normal velocity derivative of the element itself drops out. As a result, the contribution of viscous fluxes to the momentum increase of the Euler elements is only weakly coupled to the velocity gradient in the Euler element. In practice, decoupling will follow. To avoid this decoupling, the gradient is computed directly using the velocity difference between across the face, giving:

$$\left[\frac{\partial u_i}{\partial n}\right]_{Face} = \frac{u_i^R - u_i^L}{\Delta x} \tag{6-20}$$

Also walls exert viscous stress on material and, at the wall, a no-slip condition is applied. Computing these in a specific local system enables a straightforward use of the no-slip condition. In this local system, the x-axis is along the normal of the boundary. The no-slip condition ensures that all tangential velocity derivatives are zero. In addition, normal derivatives are computed directly from the velocity difference between element and wall.

This leads to shear stresses at the wall:

$$s_{xx}^{loc} = \frac{4}{3}\mu\frac{\partial u}{\partial x} = \frac{4}{3}\mu\frac{u^{wall} - u^{element}}{x^{wall} - x^{element}}$$

$$s_{xy}^{loc} = \mu\frac{\partial v}{\partial x} = \mu\frac{v^{wall} - v^{element}}{x^{wall} - x^{element}}$$

$$s_{zx}^{loc} = \mu\frac{\partial w}{\partial x} = \mu\frac{w^{wall} - w^{element}}{x^{wall} - x^{element}} \qquad (6\text{-}21)$$

These shear stresses are added to the momentum balance.

Fluid-structure Interaction with Interactive Failure

Consider a box filled with gas. If a blast wave is initiated inside the box, some parts of the box may fail and gas can escape through ruptures. To simulate this flow, the gas inside the box is modeled by an Euler domain and the box surface by shell elements. These shell elements form the coupling surface for this Euler domain. Once the shell elements of this box have failed, gas flows from the inner domain to an outer Euler domain that models the ambient. The shell surface also forms the coupling surface for this outer Euler domain and is, therefore, able to connect Euler elements inside the shell surface to elements outside the shell surface. Flow from one Euler domain to another is also possible through fully or partly porous segments.

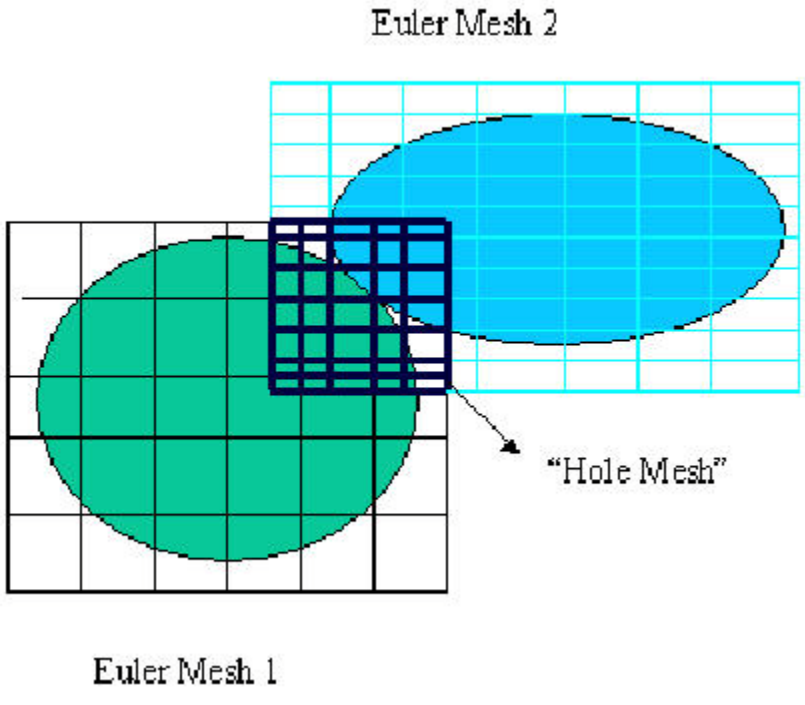

Figure 6-2 The Overlapping Mesh

Flow between Domains

Flow from one Euler domain to another takes place through either shell elements that are porous or that have failed. Flow through a segment can only take place if it is inside both Euler domains. In the following, let us assume that both Euler domains are sufficiently large. In general, a segment can intersect several Euler elements of the first Euler domain and the same applies to the second domain. Therefore, the segment connects several Euler elements in the first Euler domain to several Euler elements in the second domain. For an accurate and straightforward computation of flow through the segment, it is partitioned into subsegments such that each subsegment is in exactly one Euler element of each Euler domain. To carry out this partitioning, an overlapping Euler mesh is created that is the union of both Euler meshes. Then, for each element in this overlapping domain, the intersection with the segment is determined. Each intersection gives one subsegment that refers to both the original segment and to the element in the overlap domain. Since an element in the overlap domain is in exactly one element of both domains, the subsegment connects exactly one element in the first Euler domain to exactly one element in the second domain. Transport across this subsegment is straightforward because it closely resembles transport that takes place between the Euler elements that are within an Euler domain. In computing transport across the subsegment, the velocity of the segment has to be taken into account. If the segment is moving with the same velocity as the material on either side, no material will flow through the segment.

7 Approximate Riemann Euler Solver

The analysis of the physical behavior of fluids and gases is best solved using a Eulerian approach. The nature of the behavior of these types of materials is represented in a natural way using a finite volume description based on the Euler equations of motion. Dytran has an accurate solver available that allows you to analyze the behavior of fluids and gases, coupled to structures if necessary. The solution approach is based on a so-called Riemann solution at the element faces that defines the fluxes of mass, momentum and energy, the conserved problem quantities.

This chapter gives a more detailed explanation of the theory behind the Riemann-based Euler solver, its boundary condition treatment, and accuracy in time and space.

The nonviscous flow of a fluid or a gas is fully governed by the Euler equations of motion. We will use the equations in their conservative form:

$$\frac{\partial q}{\partial t} + \frac{\partial f(q)}{\partial x} + \frac{\partial g(q)}{\partial y} + \frac{\partial h(q)}{\partial z} = 0 \tag{7-1}$$

where q is the state vector and $f(q)$, $g(q)$ and $h(q)$ represent the fluxes of the conserved state variables. They are defined as follows:

$$q = \begin{pmatrix} \rho \\ \rho u \\ \rho v \\ \rho w \\ E \end{pmatrix} \quad f(q) = \begin{pmatrix} \rho u \\ \rho u^2 + p \\ \rho uv \\ \rho uw \\ (E+p)u \end{pmatrix} \quad g(q) = \begin{pmatrix} \rho v \\ \rho uv \\ \rho v^2 + p \\ \rho vw \\ (E+p)v \end{pmatrix} \quad h(q) = \begin{pmatrix} \rho w \\ \rho uw \\ \rho vw \\ \rho w^2 + p \\ (E+p)w \end{pmatrix} \tag{7-2}$$

Equation (7-1) describes the conservation of mass, momentum and energy. In equation (7-2)7-2, ρ is the material density, u, v, and w are the velocity components, p is the pressure and E the total energy. For a gas, we can close the system (note that we have five equations with six unknowns) by adding the equation of state for a calorically perfect gas (the "gamma law equation of state" in Dytran):

$$p = (\gamma - 1) \cdot \rho \cdot e \tag{7-3}$$

In equation (7-3), e denotes the specific internal energy of the gas and γ is the ratio of specific heats. There exist more equations of state for gases, but most gases can be described as calorically perfect gases, in which case equation (7-3) applies.

For a fluid in its simplest form, we may use a so-called "simple bulk" equation of state:

$$p = K\left(\frac{\rho}{\rho_0} - 1\right) \tag{7-4}$$

In (7-4), K is the material bulk modulus and ρ_0 is the reference density at which the material has no pressure.

Also, for fluids there are more equations of state, like a full polynomial or Tait's equation of state. Both are implemented in the approximate Riemann solver that Dytran uses, but the method of implementation is similar to the simple bulk equation of state and is not described in detail here.

Numerical Approach

The conservation laws as described by equation (7-2) are numerically solved by an upwind, cell-centered finite volume method on unstructured 3-D meshes. We briefly describe the solution method here.

When the conservation laws are written in integral form, by integrating over an arbitrary volume, the finite volume (discretized) method becomes apparent when we consider each element in an Eulerian mesh as a finite volume on which we have to solve the conservation laws as described by equation (7-2). The integral form of equation (7-2) when using Gauss's integral theorem:

$$\frac{\partial}{\partial t}\int_V q\,dV + \int_{\partial V} (f(q)\cdot n_x + g(q)\cdot n_y + h(q)\cdot n_z)\cdot dS = 0 \tag{7-5}$$

From equation (7-5), it becomes apparent that the fluxes of mass, momentum, and energy have to be integrated normal to the boundary of the volume or its surface. When we use the rotational invariance of the Euler equations of motion, the integral form can be rewritten using the transformation matrix that describes the transformation of the state variables in a direction normal to the surface:

$$\frac{\partial}{\partial t}\int_V \tilde{q}\,dV + \int_{\partial V} f(\tilde{q})\cdot dS = 0 \tag{7-6}$$

where $\tilde{q}$ denotes the state vector, transformed to a coordinate system with the local x-axis in the direction of the normal to the surface. When we then make the step to a discretized form, by defining the volume as the volume of a finite element (an element of the Euler mesh), and the surface defined by the faces spanning the element, equation (7-6) becomes a local one-dimensional system of equations for each face of the element with the local x-axis in the direction of the normal to the element's face. Note that the fluxes in the local y- and z-direction do not contribute to the change of the state variable. The system of equations to solve for each element face thus becomes:

$$\frac{\partial \tilde{q}}{\partial t} + \frac{\partial f(\tilde{q})}{\partial \tilde{x}} = 0 \tag{7-7}$$

where $\tilde{x}$ defines the x-direction normal to the element's face. Considering the fact that each face has a left and a right element connected to it, we can view the state variables in the left- and right-connected element as initial conditions for the solution of the flux normal to the face:

$$\tilde{q}(\tilde{x},0) = \begin{cases} \tilde{q}^L & \tilde{x} < 0 \\ \tilde{q}^R & \tilde{x} > 0 \end{cases} \tag{7-8}$$

Equations (7-7) and (7-8) describe a so-called Riemann problem. Thus, the solution for the fluxes at the element faces amounts to solving a local 1D Riemann problem for each of the faces of the element, considering the left and right state of the fluid or the gas. The contribution of the face fluxes result in the state change in the element as a function of time as denoted by the first term in equation (7-7). The fluxes on the faces are determined using a flux function, $f_R(q^L,q^R)$ by which, using Equations (7-6), (7-7), and (7-8), the discretization becomes:

$$\frac{dq_i}{dt} = -\frac{1}{V_i}\sum_{n=1}^{6} f_R(q^L,q^R)\cdot A_n \tag{7-9}$$

In equation (7-9), i denotes the element number, V_i the element volume, n the face numbers of the element, and A_n the associated face area.

Using a flux difference scheme, the flux function can be written as:

$$f_R(q^L,q^R) = \frac{1}{2}\{f(q^L)+f(q^R)\} - \frac{1}{2}\{\Delta f^+ - \Delta f^-\} \tag{7-10}$$

The flux difference terms in equation (7-10) are defined as:

$$\begin{aligned}\Delta f^+ &= f_R(q^L,q^R) - f(q^L)\\ \Delta f^- &= f(q^R) - f_R(q^L,q^R)\end{aligned} \tag{7-11}$$

When we use the eigenvectors, the eigenvalues and the wave strengths that can be found from a diagonalization of the Jacobian matrix of the Euler equations, we arrive at a simple definition of the flux function. Note that the shape of the eigenvectors, eigenvalues and the wave strengths depend on the type of equation of state the flux function is constructed for. In general terms, the numerical flux function used in the scheme is defined as:

$$f_R(q^L,q^R) = \frac{1}{2}\{f(q^L)+f(q^R)\} - \frac{1}{2}\left\{\sum_{i=1}^{5}\alpha_i|\tilde{\lambda}|\cdot\tilde{R}_i\right\} \tag{7-12}$$

After some rewriting of equation (7-12), we find:

$$\begin{aligned}f_R(q^L,q^R) = \frac{1}{2}\{&f(q^L)+f(q^R) - [|\tilde{u}|\cdot\Delta q + (|\tilde{u}-\tilde{a}| - |\tilde{u}|)\cdot\tilde{\alpha}_1\cdot\tilde{R}_1\\ &+ (|\tilde{u}+\tilde{a}| - |\tilde{u}|)\cdot\tilde{\alpha}_2\cdot\tilde{R_2}]\}\end{aligned} \tag{7-13}$$

Using the ideal gas equation of state (gamma-law equation of state in Dytran), we find for the wave strengths:

$$\tilde{\alpha}_1 = \frac{\Delta p - \tilde{\rho} \cdot \tilde{a} \Delta u}{2\tilde{a}^2}$$
$$\tilde{\alpha}_2 = \frac{\Delta p + \tilde{\rho} \cdot \tilde{a} \Delta u}{2\tilde{a}^2} \tag{7-14}$$

And for the associated eigenvectors:

$$\tilde{R}_1 = (1 \quad \tilde{u} - \tilde{a} \quad \tilde{v} \quad \tilde{w} \quad \tilde{H} - \tilde{u}\tilde{a})^T$$
$$\tilde{R}_2 = (1 \quad \tilde{u} + \tilde{a} \quad \tilde{v} \quad \tilde{w} \quad \tilde{H} + \tilde{u}\tilde{a})^T \tag{7-15}$$

In the above equations, the quantities denoted by a tilde are weighted quantities according to:

$$\tilde{\phi} = \theta \cdot \phi^L + (1 - \theta) \cdot \phi^R$$
$$\theta = \frac{\sqrt{\rho^L}}{\sqrt{\rho^L} + \sqrt{\rho^R}} \tag{7-16}$$

All quantities are averaged using the above definition, except for the density:

$$\tilde{\rho} = \sqrt{\rho^L \cdot \rho^R} \tag{7-17}$$

The above described flux evaluation scheme is called an approximate Riemann scheme due to the fact a linearization using the weighted quantities at the element faces is applied. As a result, the scheme exhibits an artifact, namely that it does not satisfy the entropy inequality. The entropy inequality states that the entropy of a system can only remain constant or increase. Due to the artifact, the scheme is able to also capture mathematically sound, but physically impossible discontinuities like expansion shocks. This is easily repaired by adding a so-called entropy fix to the scheme as described in the next section.

Entropy Fix for the Flux Difference Riemann Scheme

As described earlier, a so-called entropy fix must be added to the scheme in order to have the scheme correctly decompose a expansion discontinuity into a physically correct expansion fan. The entropy fix amounts to adding some numerical viscosity or dissipation to sonic points, shocks, and contact discontinuities. The dissipation is added only at those points where any one of the system's eigenvalues vanishes.

The entropy fix can be written in terms of a simple function:

$$\Psi(z) = \begin{cases} |z| & |z| \geq \delta_1 \\ \dfrac{(z^2 + \delta_1^2)}{2\delta_1} & |z| < \delta_1 \end{cases} \tag{7-18}$$

The function works automatically on the eigenvalues of the system, represented in (7-18) by z, and is governed by a single parameter δ_1 that depends on the flow field:

$$\delta_1 = \delta \cdot \left(\left| \frac{\tilde{u}}{\tilde{a}} \right| + \left| \frac{\tilde{v}}{\tilde{a}} \right| + \left| \frac{\tilde{w}}{\tilde{a}} \right| + 1 \right) \tag{7-19}$$

Second Order Accuracy of the Scheme

When we consider the flux function as given in general by equation (7-13), it does not say anything about the order of accuracy at which the face fluxes are computed. The accuracy is governed by the way in which the left and the right state variables are determined.

A first order scheme results when the left and the right state variables are taken as the values the state variables have at the left- and the right-element center; a so-called first order extrapolation to the face.

When we increase the stencil by which we determine the left- and right-state variable values at the face by including the left-left and the right-right element, we arrive at a second order accurate scheme in space. A so-called nonlinear limiter that avoids the creation of new minimum or maximum values limits the second order left- and right face values of the state variables. Such a scheme is called total variation diminishing, or TVD. Near sharp discontinuities the scheme reverts to locally first order as to introduce the necessary numerical viscosity to avoid oscillations in the solution near the discontinuity.

The second order approximate Riemann solver in Dytran applies the Superbee limiter. The second order scheme can be formally written as:

$$q^L_{i+1/2} = q_i + \frac{1}{2}\Psi^L \cdot (q_i - q_{i-1}) \tag{7-20}$$

for the left side of the face, with:

$$\Psi^L = \frac{1}{2}\left[(1-\kappa) \cdot \Phi(r^L) + (1+\kappa) \cdot r^L \cdot \Phi\left(\frac{1}{r^L}\right) \right]$$

$$r^L = \frac{q_{i+1} - q_i}{q_i - q_{i-1}} \tag{7-21}$$

For the right side of the face, the second order approximation is defined by:

$$q^R_{i+1/2} = q_{i+1} - \frac{1}{2}\Psi^R \cdot (q_{i+2} - q_{i+1}) \tag{7-22}$$

with:

$$\Psi^R = \frac{1}{2}\left[(1-\kappa)\cdot\Phi(r^R) + (1+\kappa)\cdot r^R \cdot \Phi\left(\frac{1}{r^R}\right)\right]$$
$$r^R = \frac{q_{i+1} - q_i}{q_{i+2} - q_{i+1}} \tag{7-23}$$

The upwind scheme is defined for $\kappa = -1$ and the limiter function Φ is the Superbee limiter:

$$\Phi(r) = max[0, min(2r,1), min(r,2)] \tag{7-24}$$

Time Integration

The set of equations is integrated in time using a multi-stage scheme. For the second order accurate solution, a three-stage time integration scheme is used:

$$\begin{aligned} q^{(0)} &= q_i^n \\ q^{(1)} - q^{(0)} &= -\frac{\alpha_1 \cdot \Delta t}{V_i} \cdot F^{(0)} \\ q^{(2)} - q^{(0)} &= -\frac{\alpha_2 \cdot \Delta t}{V_i} \cdot F^{(1)} \\ q^{(3)} - q^{(0)} &= -\frac{\alpha_3 \cdot \Delta t}{V_i} \cdot F^{(2)} \\ q_i^{n+1} &= q^{(3)} \end{aligned} \tag{7-25}$$

In equation (7-26), $q^{(k)}$ denotes the state variable value in the k-th integration stage, α_k the stage coefficients, and the flux contributions $F^{(k)}$ are defined as:

$$F^{(k)} = \sum_{n-1}^{6} f_R(q_L^{(k)}, q_R^{(k)}) \cdot A_n \tag{7-26}$$

using the state variables at each stage of the integration. The final step then gives the solution of the state variables at the new time level.

A References

1. Sandler, I. S. and Rubin, D., "An Algorithm and a Modular Subroutine for the Cap Model," *International Journal for Numerical and Analytical Methods in Geomechanics*, Vol. 3, 173-186 (1979)
2. Simo, J. C., Ju, J.W., Pister, K. S., and Taylor, R.L., "Assessment of Cap Model: Consistent Return Algorithms and Rate-dependent Extension," *Journal of Engineering Mechanics*, Vol. 114, No. 2, February 1988.
3. Mundl, R., Meschke, G., and Liederer, W., "Friction Mechanisms of Tread Blocks on Snow Surfaces", *Tire Science and Technology*, TSTCA, vol. 25, no. 4, 1997, pp. 245-264.
4. Meschke,G., *A New Visco-plastic Model for Snow at Finite Strains,* 4th International Conference on Computational Plasticity, Barcelona, April 3-6, 1995, Pineridge Press, pp. 2295-2306.
5. DiMaggio, F.L., and Sandler, I.S., "Material Models for Granular Soils", Journal of Engineering Mechanics A.S.C.E., 1971, pp. 935-950.
6. Mahardika, M., *Implementation and Verification of Snow Material in Euler Scheme; Using the type-10 element (hydrodynamic material with strength)*, Hexagon, 2001, to be published.
7. Munjal, A. K. "Test Methods for Design Allowables for Fibre Composites," *ASTM STP* 1003, 1991, pp. 93-110.
8. Naik, N. K. *Woven Fabric Composites*, A Technomic Publishing Company Book, 1994.
9. Treloar, L. R. G. "The Effect of Test-Piece Dimensions on the Behaviour of Fabrics in Shear," *Journal of the Textile Institute*, Vol. 56, 1965, T533-T550.
10. Lee, E.L. and Tarver, C.M., "Phenomenological Model of Shock Initiation in Heterogeneous Explosives," *Physics of Fluids* 23 (12), December 1980, pp. 2362-2372
11. Murphy, M.J, Lee, E.l. et. al., "Modeling Shock Initiation in Composition B," UCRL-JC-111975 LLNL, 10th International Detonation symposium, Boston, Mass., 1993.
12. Jones, Robert M., *Mechanics of Composite Materials*, McGraw-Hill, Tokyo, 1975
13. "Improved Transverse Shear Stiffness Coefficients for the PCOMP Composite Elements", MSC/NASTRAN, Memo No. DNH-40, January 25, 1983 (Revised May 11, 1983)
14. Hashin, Z., "Failure Criteria for Unidirectional Fiber Composite", *Journal of Applied Mechanics*, June 1980, vol. 47, pp. 329-334
15. Fu-Kuo Chang and Kuo-Yen Chang, "A Progressive Damage Model for Laminated Composites Containing Stress Concentrations", *Journal of Composite Materials*, vol. 21, September 1987, pp. 834-855
16. *MSC/DYNA User's Manual*, The MacNeal-Schwendler Corporation.
17. *MSC/PISCES-2DELK User's Manual*, The MacNeal-Schwendler Corporation.
18. Lee, E. L. et al., "Adiabatic Expansions of High Explosive Detonation Products," UCRL-50422, May 1968, Lawrence Livermore National Laboratory, Livermore, California.
19. *MADYMO User's Manual 3-D Version 4.3*, The Dutch Institute of Applied Scientific Research - Road/Vehicles Research Institute, Department of Injury Prevention, October 1988.
20. Obergefell, Louise A., Gardner, Thomas R., Kaleps, Ints, and Fleck, John T., *Articulated Total Body Model Enhancements*, Volume 1: "Modifications," (NTIS No. ADA198726).

21. Obergefell, Louise A., Gardner, Thomas R., Kaleps, Ints, and Fleck, John T.k, *Articulated Total Body Model Enhancements*, Volume 2: "User's Guide," (NTIS No. ADA203566).
22. Obergefell, Louise A., Gardner, Thomas R., Kaleps, Ints, and Fleck, John T., *Articulated Total Body Model Enhancements*, Volume 3: "Programmer's Guide," (NTIS No. ADA197940).
23. Fleck, J. T., F. E. Butler, and N. J. Deleys, "Validation of the Crash Victim Simulator," *Calspan Report* Nos. ZS-5881-V-1 through 4, DOT-HS-806-279 through 282, 1982, Volumes 1 through 4, (NTIS No. PC E99, PB86-212420).
24. Roe, P. L., "Approximate Riemann Solvers, parameter vectors, and difference schemes," *Journal of Computational Physics*, 43, 357-372, 1981.
25. Roe, P. L., and J. Pike, "Efficient construction and utilization of approximate Riemann solutions," *Computing Methods in Applied Sciences and Engineering* (VI), R. Glowinski and J. L. Lions (Editors), Elsevier Publishers B.V. (North Holland), INRIA 1984.
26. van Leer, Bram, Chang-Hsien Tai, and Kenneth G. Powell, *Design of Optimally Smoothing Multi-Stage Schemes for the Euler Equations,* AIAA-89-1933-CP, 1989.
27. Ch. Hirsch, *Numerical Computation of Internal and External Flows, Fundamentals of Numerical Discretization, 1*, Wiley, Chichester, 1988.
28. Ch. Hirsch, *Numerical Computation of Internal and External Flows, Computational Methods for Inviscid and Viscous Flows, 2,* Wiley, Chichester, 1990.
29. Obergefell, Louise A., Cheng, Huaing, Rizer, Annnette L., *Articulated Total Body Model Version V: "User's Manual"*, (NTIS No. ASC-98-0807), 1998.
30. Obergefell, Louise A., Cheng, Huaing, Rizer, Annnette L., *Input Description for the Articulated Total Body Model ATB-V.1*, 1998.
31. Pellettiere, Joseph A., Cheng, Huaing, Rizer, Annnette L., *The Development of GEBOD Version V*, 2000.
32. Tanimura, S., Mimura, K., and Zhu, W.H., "Practical Constitutive Models Covering Wide Ranges of Strain Rates, Strains and Temperatures", *Key Engineering Materials* Vols. 177-180,189-200, 2000.
33. Miller, P. J. and Guirguis, R. H. "Experimental Study and Model Calculations of Metal Combustion in Al/AP Underwater Explosives," *Materials Research Society Symposium Proceedings, Vol. 296, 1993, pp. 299-304.*
34. https://en.wikipedia.org/wiki/Van_der_Waals_equation
35. High-Pressure Burning Rate Studies of Solid Rocket Propellants, A.I. Atwood, K.P. Ford, and C.J. Wheeler, Progress in Propulsion Physics, Volume 4, 2013, DOI 10.1051/eucass/201304003.
36. Representative explosive grain shapes, as with smokeless powder, U.S. Army, Technical Manual TM 9-1300-214, September 1984, p. 9-1.
37. Effect of Propellant Grain Dimension on Progressivity, Kevin J. White, Army Research Laboratory, ARL-TR-1532, October 1997, 19971121 063.
38. The Noble-Abel Equation of State: Thermodynamic Derivations for Ballistics Modelling, Ian A. Johnston, Australian government, department of defense, DSTO.TN.0670, 2005.

39. Barlat, F., & Lian, K. (1989). Plastic behavior and stretchability of sheet metals. Part I: A yield function for orthotropic sheets under plane stress conditions. *International journal of plasticity*, 51-66.

40. Krieg, R. D. (1996). Anisotropic plasticity with anisotropic hardening and rate dependence. *Journal of engineering mechanics*, 316-324.